7-9-2012

# Effect of pH and temperature on the carbonate promoted dissolution of sodium meta-autunite

Ravi Krishna Gudavalli
*Florida International University*, rguda001@fiu.edu

**DOI:** 10.25148/etd.FI12120406

FLORIDA INTERNATIONAL UNIVERSITY

Miami, Florida

# EFFECT OF PH AND TEMPERATURE ON THE CARBONATE PROMOTED DISSOLUTION OF SODIUM META-AUTUNITE

A dissertation submitted in partial fulfillment of the

requirements for the degree of

DOCTOR OF PHILOSOPHY

in

CIVIL ENGINEERING

by

Ravi Krishna Prasanth Gudavalli

2012

To: Dean Amir Mirmiran
College of Engineering and Computing

This dissertation, written by Ravi Krishna Prasanth Gudavalli, and entitled, "Effect of pH and temperature on the carbonate promoted dissolution of sodium meta-autunite", having been approved in respect to style and intellectual content, is referred to you for judgment.

We have read this dissertation and recommend that it be approved.

_____
Leonel Lagos

_____
Kris Jayachandran

_____
Yelena Katsenovich

_____
Shonali Laha

_____
Berrin Tansel, Major Professor

Date of Defense: July 9, 2012

The dissertation of Ravi Krishna Prasanth Gudavalli is approved.

_____
Dean Amir Mirmiran
College of Engineering and Computing

_____
Dean Lakshmi N Reddi
University Graduate School

Florida International University, 2012

ACKNOWLEDGMENTS

It is my pleasure to thank those who made this dissertation possible. I am grateful to my major professor, Dr. Berrin Tansel, who has always been supportive in all stages of this dissertation. I would also like to acknowledge members of my dissertation committee: Dr. Shonali Laha, Dr. Yelena Katsenovich, Dr. Leonel Lagos, and Dr. Krish Jayachandran, whose encouragement, guidance, and knowledge helped me to develop an understanding of the subject, making this dissertation possible. I wish to express my sincere gratitude to Dr. Dawn Wellman (Pacific Northwest National Laboratory/USA) for her valuable guidance, support and encouragement.

I would like to thank my DOE Fellow friends Jose Vasquez, Alexander Henao, Jose Rivera, Lee Brady and Melina Idarraga, for their support with laboratory work that helped me complete experiments presented in this dissertation. I would also like to thank Mr. Kent Parker for his support with surface area analysis and Ms. Peggy Shoffner for her help with reviewing the dissertation document.

None of this would have been possible without the love and patience of my family, who have been a constant source of love, concern, support and strength all these years. I would like to express my heart-felt gratitude to my family for their understanding and loving care.

Finally, I would also like to thank the U.S. Department of Energy's Office of Environmental Management for funding this research under the grant no. DE-EM0000598.

ABSTRACT OF DISSERTATION

EFFECT OF PH AND TEMPERATURE ON THE CARBONATE PROMOTED DISSOLUTION OF SODIUM META-AUTUNITE

by

Ravi Krishna Prasanth Gudavalli

Florida International University, 2012

Miami, Florida
Professor Berrin Tansel, Major Professor

Release of uranium from Na-autunite, an artificial mineral created as a result of polyphosphate injection in the subsurface at the DOE Hanford Site, takes place during slow dissolution of the mineral structure. Stability information of the uranyl-phosphate phases is limited to conditions involving pH, temperature, and a few aqueous organic materials. The carbonate ion, which creates very strong complexes with uranium, is the predominant ion in the groundwater composition.

The polyphosphate technology with the formation of autunite was identified as the most feasible remediation strategy to sequester uranium in contaminated groundwater and soil *in situ*. The objectives of the experimental work were (i) to quantify the effect of bicarbonate on the stability of synthetic sodium meta-autunite created as a result of uranium stabilization through polyphosphate injection, (ii) calculate the kinetic rate law parameters of the uranium release from Na-autunite during dissolution, and (iii) to compare the process parameters with those obtained for natural calcium meta-autunite.

Experiments were conducted using SPTF apparatus, which consists of syringe pumps for controlling flow rate, Teflon reactors and a heating/cooling system. 0.25 grams of

synthetic Na-autunite was placed in the reactor and buffer solutions with varying bicarbonate concentrations (0.0005 to 0.003 M) at different pH (6 - 11) were pumped through the reactors. Experiments were conducted at four different temperatures in the range of 5 - 60$^{o}$C.

It was concluded that the rate of release of uranium from synthetic Na-autunite is directly correlated to the bicarbonate concentration. The rate of release of uranium increased from 1.90 x $10^{-12}$ at pH 6 to 2.64 x $10^{-10}$ (mol $m^{-2}$ $s^{-1}$) at pH 11 at 23$^{o}$C over the bicarbonate concentration range tested. The activation energy values were invariant with the change in the bicarbonate concentration; however, pH is shown to influence the activation energy values. Uranyl hydroxides and uranyl carbonates complexes helped accelerate the dissolution of autunite mineral.

TABLE OF CONTENTS

LIST OF FIGURES

LIST OF TABLES

ABBREVIATIONS

| | |
|---|---|
| AMERI | Advanced Materials Engineering Research Institute |
| DDIW | Distilled De-Ionized Water |
| DOE | Department of Energy |
| EDS | Energy Dispersive X-Ray Spectroscopy |
| EPA | Environmental Protection Agency |
| ICP-OES | Inductively-Coupled Plasma-Optical Emission Spectroscopy |
| IEER | Institute for Energy and Environmental Research |
| KPA | Kinetic Phosphorescence Analyzer |
| LLD | Lower Limit of Detection |
| NPL | National Priorities List |
| ORP | Oxidation Reduction Potential |
| PFA | Perfluroalkoxide |
| PNNL | Pacific Northwest National Laboratory |
| PPB | Parts Per Billion |
| PPM | Parts Per Million |
| SEM | Scanning Electron Microscopy |
| SPFT | Single-Pass Flow-Through |
| TRIS | Tris (hydroxymethyl) aminomethane |
| XRD | X-Ray Diffraction |

CHAPTER ONE

## Effect of bicarbonate on the dissolution of sodium meta-autunite

ABSTRACT

Release of uranium from Na meta-autunite, a mineral frequently found in contaminated sediments as the long-term controlling phase of uranium, takes place during slow dissolution of the mineral structure. Single-pass flow-through (SPTF) experiments were conducted to estimate the rate of release of uranium from Na meta-autunite, $Na_2[(UO_2)_2(PO_4)_2]\cdot 3H_2O$, as a function of bicarbonate (0.0005 - 0.003 M) in the pH range of 6 - 11 and a temperature range of 5 - 60$^{o}$C. The rate of uranium release from Na meta-autunite in the presence of low bicarbonate concentrations increased over 300 fold when compared to the rate of release of uranium in the absence of bicarbonate. At a constant pH, the rate of release of uranium showed little increase with an increase in bicarbonate concentration.

# INTRODUCTION

Uranium is a naturally occurring radioactive element that is commonly found in very small quantities in rocks (2 - 4 ppm), soil, seawater (3.3 ppb) and plants. Weakly radioactive by nature, uranium contributes to low levels of natural background radiation in the environment (EPA, 2011). Significant concentrations of uranium occur in some substances such as phosphate rock deposits and minerals such as uraninite in uranium-rich ores. Refined silvery white uranium is weakly radioactive and is 65% denser than lead. Uranium is found naturally as three different isotopes U-238, U-235, and U-234, and has half-lives of 4.46 billion years, 704 million years and 245,000 years, respectively (IEER, 2005). Uranium can be released into the environment via wind and water erosion and volcanic eruptions. Industries involved in mining, milling and processing of uranium are also contributors of uranium released into the environment (Keith, 2011). In air, uranium exists as dust; very small dust-like particles fall out onto water, plants and land. Uranium deposited on land can be reincorporated into soil, washed into surface water, or adsorbed onto plant roots. Uranium in the surface water can be transported large distances. Alpha particles emitted by uranium-238 are less penetrating than the gamma rays and, as long as the uranium remains outside of the body, it poses little health hazard. However, radioactivity from uranium poses increased risks of lung and bone cancers when inhaled or ingested. At high concentrations, uranium is chemically toxic and can damage internal organs such as kidneys (EVS, 2011). Depleted uranium is used as shielding material to protect army tanks and also in parts of missiles and bullets. The enriched uranium is used to power nuclear propelled ships, submarines and in nuclear weapons. Uranium's ability to undergo fission, splitting into smaller parts when

bombarded with neutrons releasing energy, is the important property for nuclear weapons and nuclear power production. As shown in Figure 1, uranium-235 has the ability to absorb a neutron and fissions into two new atoms (krypton and barium) while releasing two neutrons and a large amount of energy. These neutrons help sustain the chain reaction so that the fission process in maintained without external source of neutrons (Makhijani et al., 2004). As shown in Figure 2, uranium-238 absorbs one of the neutrons released during the fission of uranium-235 and converts into uranium-239; uranium-239 releases a β-particle and converts into neptunium-239 which releases a β-particle and converts into plutonium-239 (Settle, 2009) that was used in the first atomic bomb tested and dropped on Nagasaki.

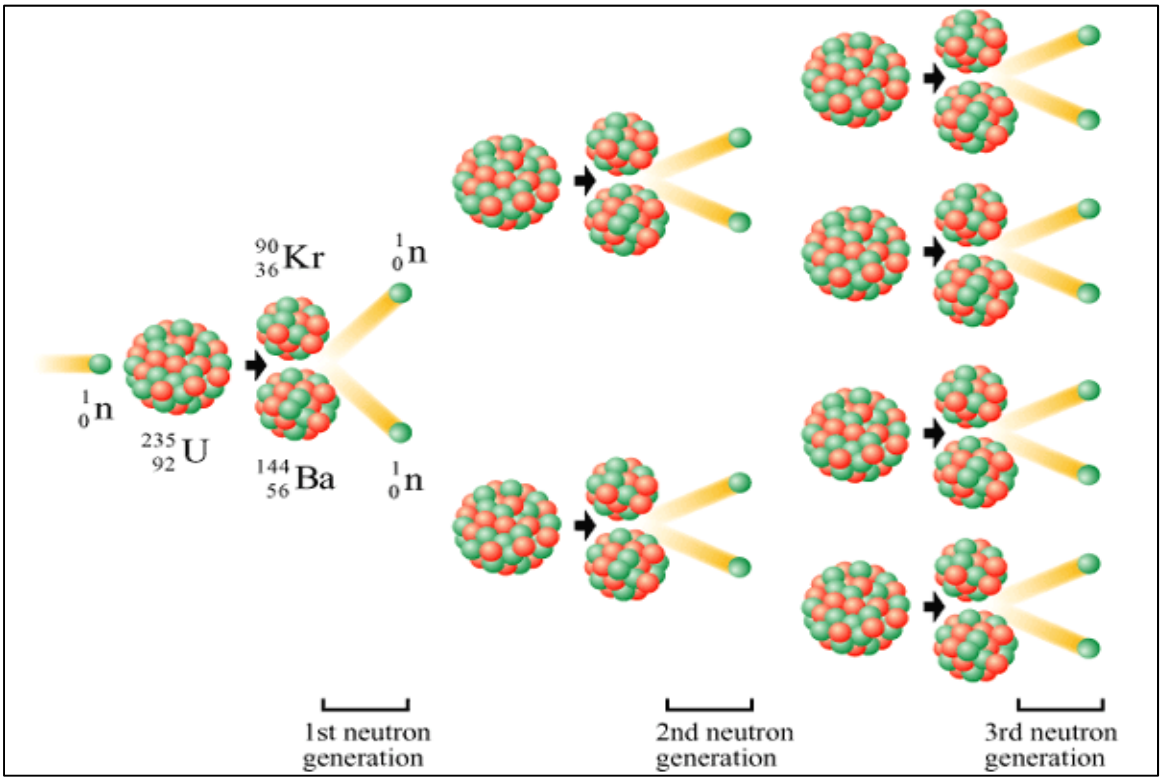


**Figure 1 Uranium-235 chain reaction (Source www.hk-phy.org)**

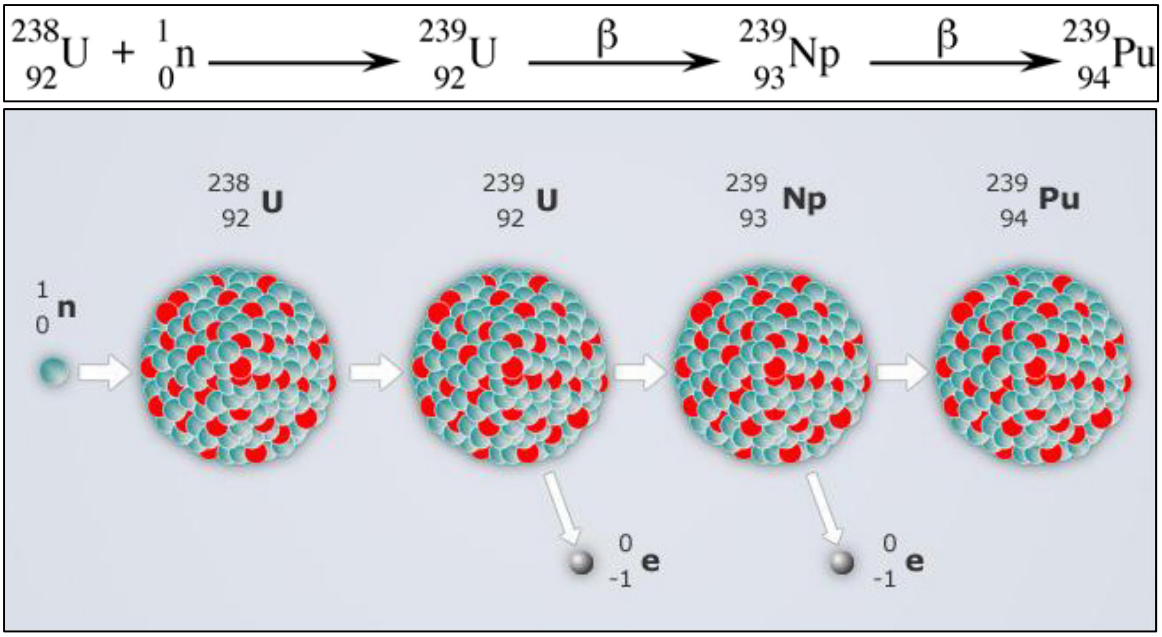


**Figure 2 Production of plutonium-239 from uranium-238**

Uranium occurs in high concentrations at several contaminated sites in the United States (Eisenbud et al., 1997) and is an important risk-driving contaminant at the Hanford Site (Zachara, 2007). Due to the potential threat on human health, the U.S. Environmental Protection Agency (USEPA) has set a maximum contaminant level of 30 μg $L^{-1}$ for uranium concentration in groundwater (EPA, 2011).

DOE's Hanford Site covers approximately 586 square miles and was established to produce nuclear material for national defense (EPA, 2011). The Hanford Site was placed on the National Priorities List (NPL) in 1989 and was divided into 4 NPL sites, including the 100 Area, 200 Area, 300 Area, and 1100 Area (Figure 3). The 300 Area of the Hanford Site consists of a 0.52 square-mile industrial complex area that was used for uranium fuel fabrication as well as research and development activities. After operations at the 300 Area began in 1943, these activities led to the contamination of streams, soil and groundwater, primarily with 58,967 kg of uranium. Furthermore, waste from the

operations was disposed of in designated landfills/burial grounds and discharged to unlined surface ponds and trenches. The primary cleanup activities that have taken place in the 300 Area include removal of contaminated soils and debris, treatment of the material to reduce the toxicity and mobility of the contaminants, and disposal of the material in an appropriate long-term waste management facility. Currently, the contaminated groundwater in the 300 Area is being monitored to ensure that the contamination levels are decreasing through natural processes. The uranium concentration is associated with contamination remaining in the deep vadose zone and smear zone, where the smear zone is the area where free product occurred in the soil and was then smeared across the soil when the water table fluctuated between historic high and low water table elevations. Uranium in its soluble form is of concern because of its chemical toxicity and risk of radiological exposure, even though the concentrations in groundwater for chemical toxicity are lower than those associated with exceeding radiological dose standards. Currently, elevated uranium concentrations are entering the Columbia River along the shoreline and enter the riparian and river biota through seeps. Figure 4 shows the concentrations of uranium in the 300 area of the Hanford Site.

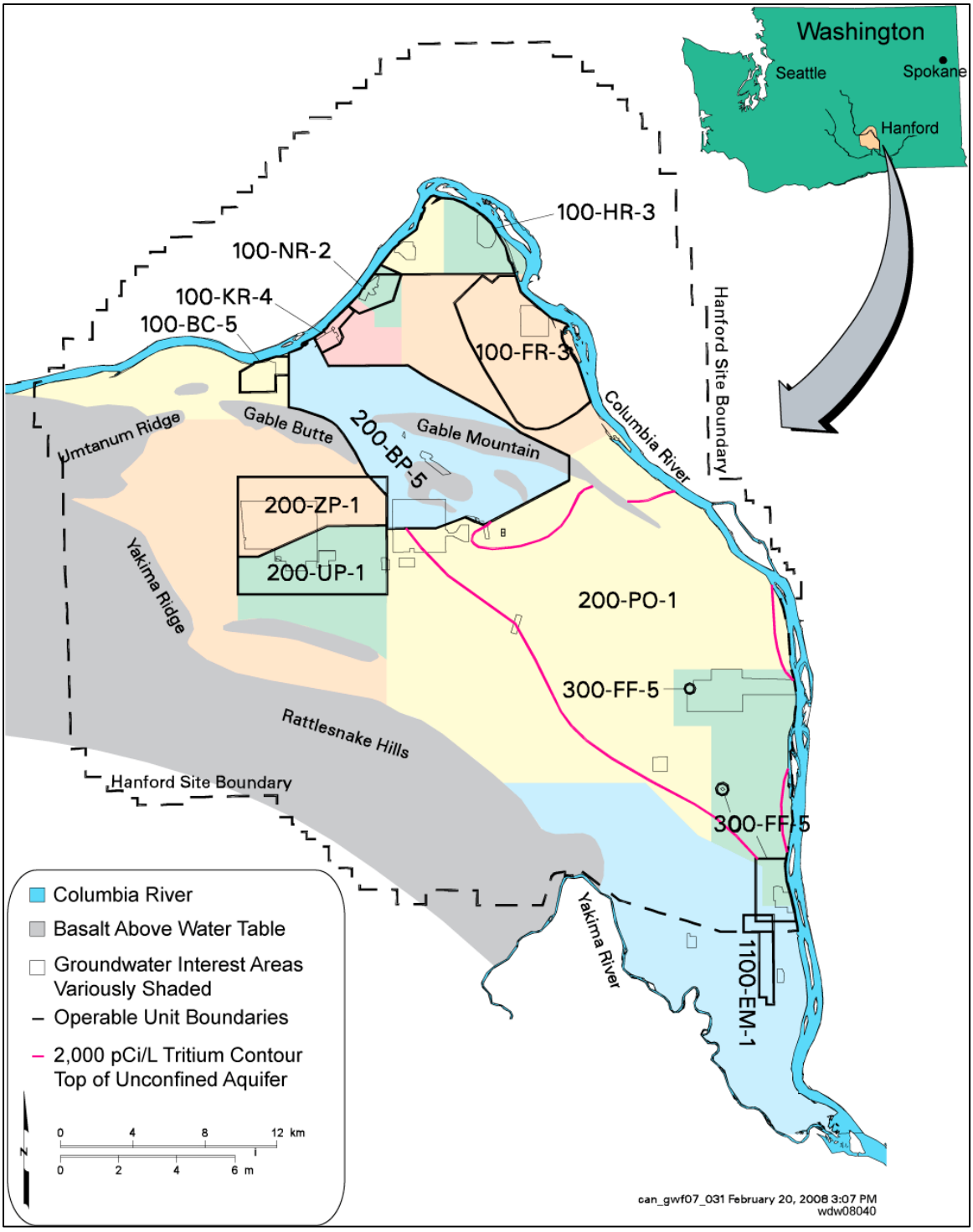


**Figure 3 Hanford Site water monitoring areas**

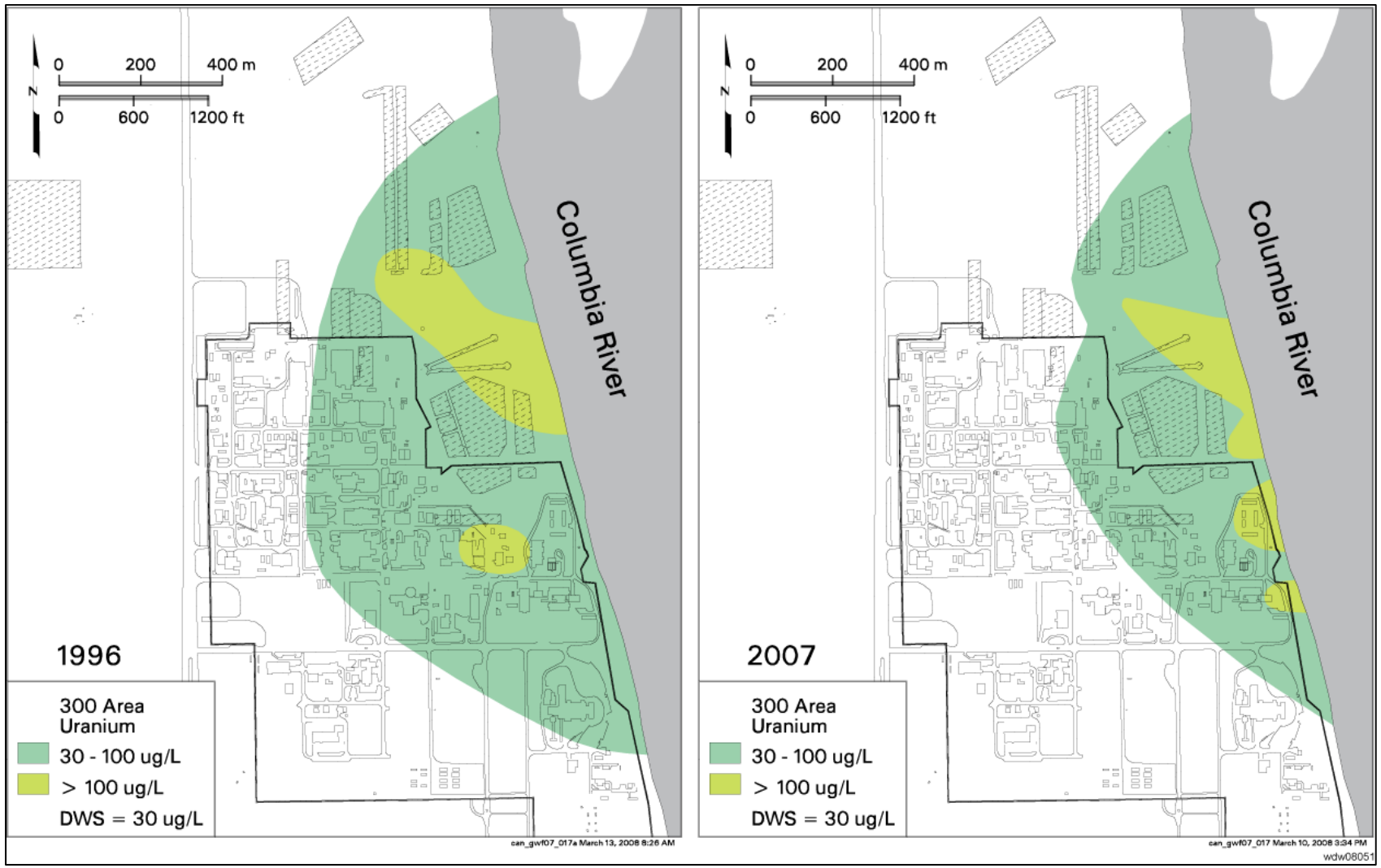


**Figure 4 Uranium plume at the 300 Area of the Hanford Site**

# LITERATURE REVIEW

## 1.1 Uranium Geochemistry

Solubility of uranium in the aqueous system is controlled by oxidation-reduction potential (ORP), pH and dissolved carbonate (Giammar, 2001). Uranium in the aqueous environment can exist in various oxidation states such as +III, +IV, +V and +VI; however, under environmental conditions, only two oxidation states (+IV and +VI) are stable. The reduction half-reactions and associated potentials for all of the uranium oxidation states are given in Table 1 (Grenthe, 1992). Uranyl (VI) species are predominantly found in oxidizing environments, and uranium (IV) prevails in reducing environments. Both of these species have a strong tendency towards complexation with other chemicals and are greatly affected by aquifer characteristics such as pH, redox status, and concentrations of dissolved constituents (Merkel et al., 2005; Zhang et al., 2002). The thermodynamic properties of uranium minerals and aqueous species govern reactions that may control U concentrations and its mobility in the subsurface. The major contributors to uranium geochemistry have been made by publications of the Nuclear Energy Agency's (NEA) database for uranium (Grenthe, 1992) and updates for uranium databases published by Lemire et al., (1980). Langmuir (1997) published several important corrections and additions to the thermodynamics data. The term pe is a measure of the oxidation-reduction capacity of natural water. Natural water with a high pe (low electron activity) would be considered to be oxidizing, and water with a low pe (high electron activity) would be considered to be reducing. Just as pH is important to mineral solubility and the speciation of acid-base pairs, pe is important to the solubility of

minerals containing elements with variable oxidation states, and the speciation of redox pairs. $E_h$ is the potential of a solution relative to the standard hydrogen electrode. High values of $E_h$ or pe correspond to oxidizing conditions, and low values of $E_h$ or pe correspond to reducing conditions. A pe-pH plot showing the domains of stability of dissolved and solid uranium species is given in Figure 5. At high pe and high pH, uranium tends to form complexes with carbonate.

**Table 1 Reduction potentials of uranium half reactions**

| Reaction | $E_h$ (V) | pe | logK |
|---|---|---|---|
| $U^{4+} + e^- = U^{3+}$ | -0.553 | -9.35 | -9.35 |
| $4H^+ + UO_2^{2+} + 2e^- = 2H_2O_{(l)} + U^{4+}$ | +0.267 | 4.51 | 4.51 |
| $UO_2^{2+} + e^- = UO_2^+$ | +0.088 | 1.49 | 1.49 |
| $UO_2^{2+} + 2e^- = UO_{2(s)}$ | +0.411 | 6.95 | 13.89 |
| $U_4O_{9(s)} + 2H^+ + 2e^- = 4UO_{2(s)} + H_2O_{(l)}$ | +0.456 | 7.71 | 15.41 |
| $4\beta\text{-}U_3O_{7(s)} + 2H^+ + 2e^- = 3U_4O_{9(s)} + H_2O_{(l)}$ | +0.517 | 8.74 | 17.48 |
| $U_3O_{8(s)} + 2H^+ + 2e^- = \beta\text{-}U_3O_{7(s)} + H_2O_{(l)}$ | +0.565 | 9.55 | 19.10 |

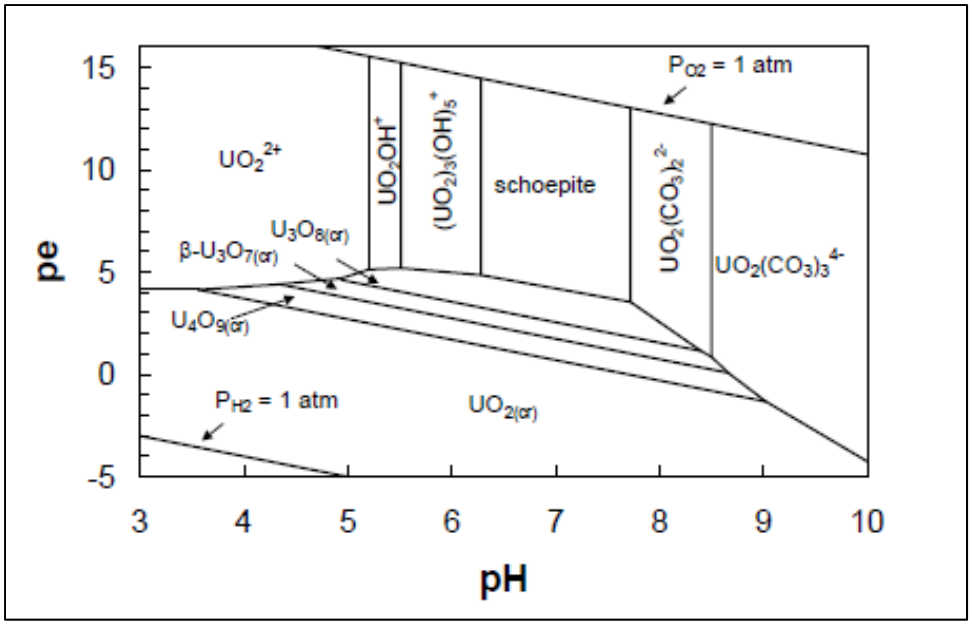


**Figure 5 pe-pH diagram for aqueous species and solids in the U-$O_2$-$CO_2$-$H_2O$ system**

Takeno (2005) reported intercomparison of thermodynamic databases by means of $E_h$-pH diagrams for understanding geochemical behavior of uranium. The $E_h$-pH diagram (Figure 6 and Figure 7) depicts the dominant aqueous species and stable solid phases in the absence of ligands predicted by different geochemical models. The solid stability area in the $E_h$-pH diagram provides essential understanding of solute and radionuclide transport in groundwater which is related to the saturation condition. The dominant aqueous species gives fundamental information on sorption and colloid phenomena as well as surface characteristics of materials. Figure 8 shows the aqueous complexes of uranium in the presence of sulfate, carbonate, and uranium (Krupka et al., 2002).

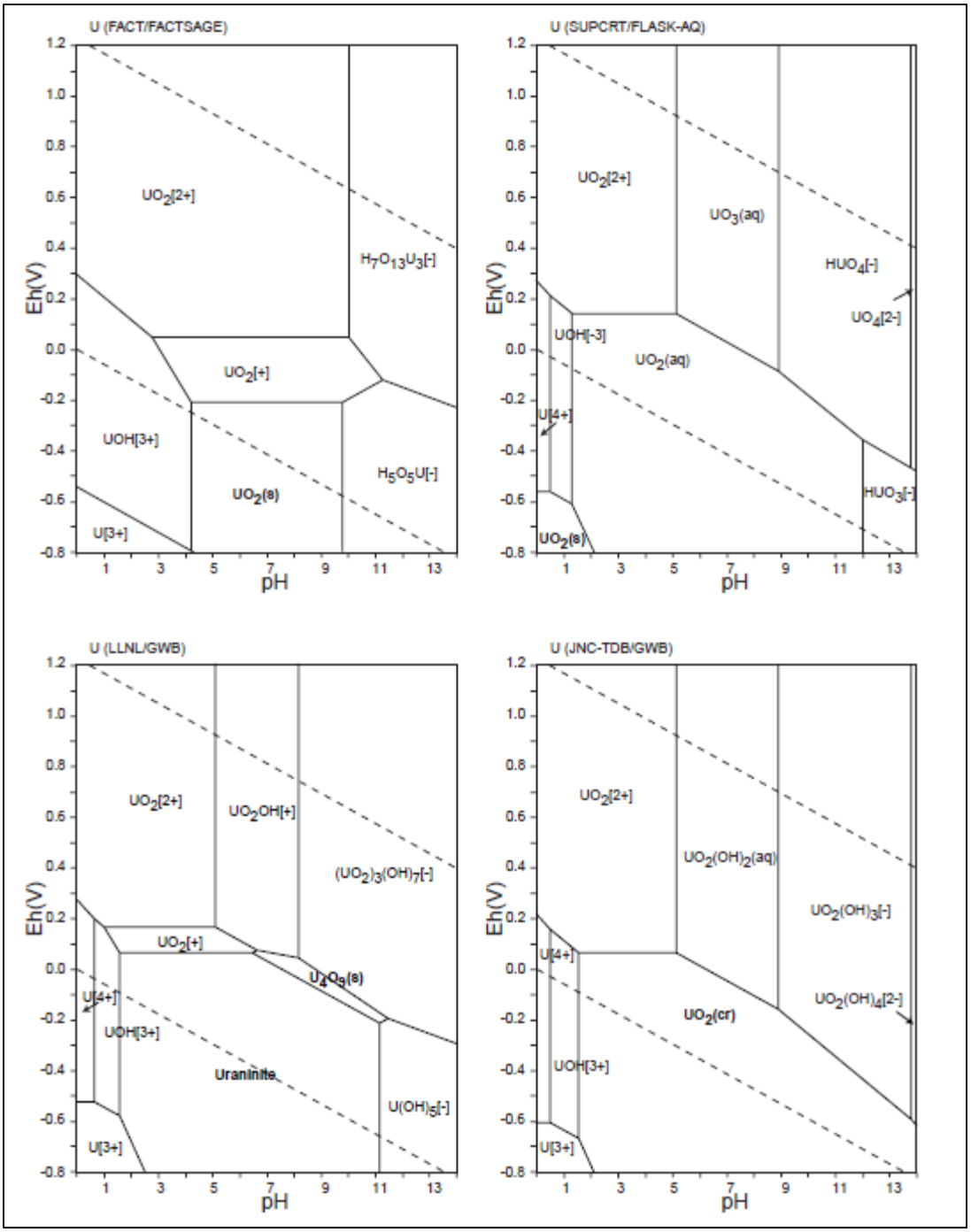


**Figure 6 Eh-pH diagrams of the system U-O-H**

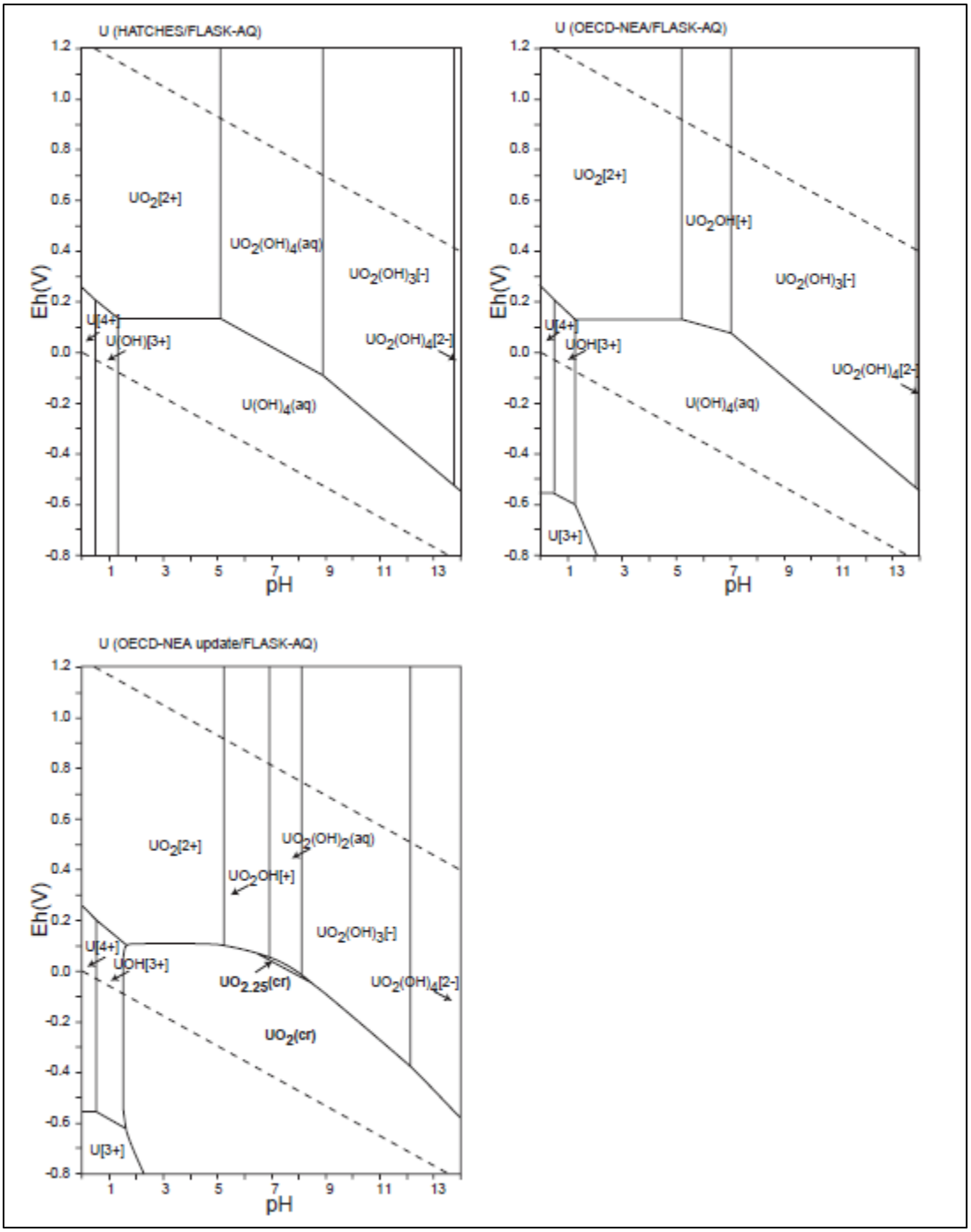


**Figure 7 Eh-pH diagrams of the system U-O-H**

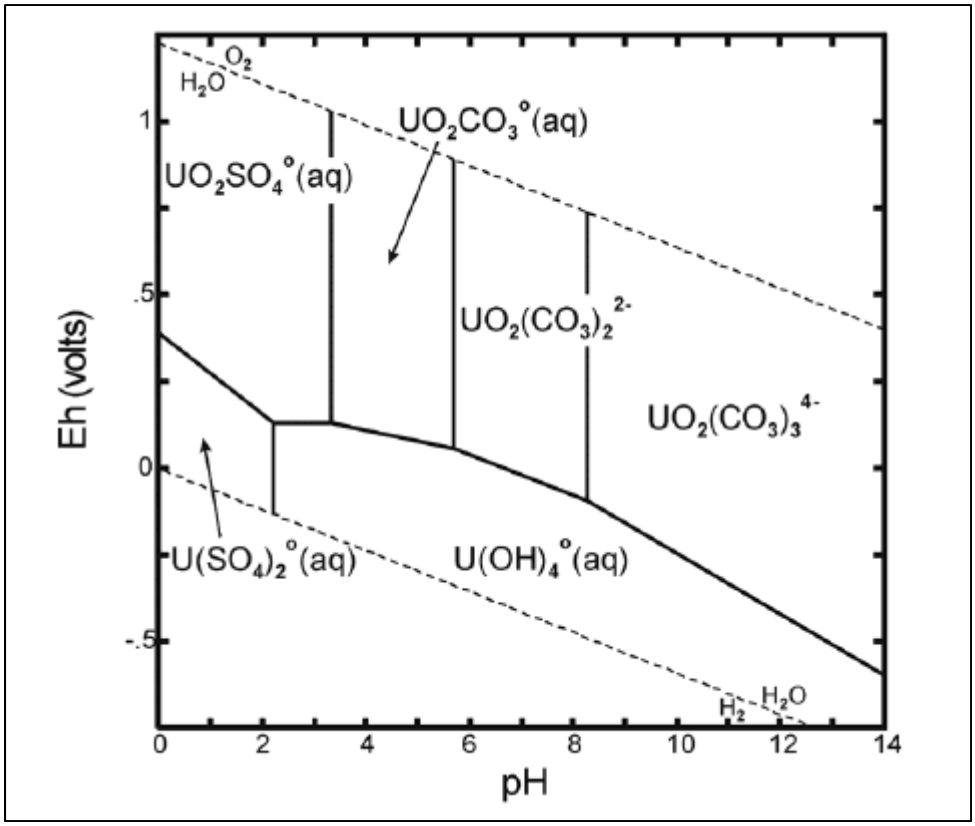


**Figure 8 Dominant aqueous complexes of uranium in the presence of ligands**

Uranium(IV) complexes with hydroxide or fluoride are the only dissolved species under reducing conditions (Gascoyne, 1992), while the precipitation of uranium(IV) under reducing conditions is the dominant process leading to naturally enriched zones of uranium in the subsurface (Osmond et al., 1992). In oxidizing aqueous environments, uranium (VI) is present as the linear uranyldioxo ion ($UO_2^{2+}$) and an array of mononuclear and polynuclear hydrolysis species. With increasing carbonate concentrations, mononuclear uranyl carbonate species become increasingly important. In oxidizing groundwater conditions, soluble uranyl ion ($UO_2^{2+}$) creates strong complexes with carbonate. Wellman et al., (2008) reported that at pH of ~8.5, uranyl ion form carbonate complexes: 27% as $UO_2(CO_3)_2^{2-}$ and 68% as $UO_2(CO_3)_3^{4-}$, 3% as $UO_2(OH)_2^0$ and 2% as $UO_2(OH)_3^{1-}$. The highly water soluble uranyl carbonate complexes can greatly

increase the solubility of uranium minerals and facilitate uranium desorption reactions from soil and sediments (Langmuir, 1997). Serne (2002) reported that the uranium adsorption $K_d$ values ranged from 7 to 2 mL $g^{-1}$ in the presence of bicarbonate concentrations between 0.9 to 2.2 mM; however, $K_d$ values were reduced from 0.3 to 0 mL $g^{-1}$ when bicarbonate concentrations increased to 2.5 - 13 mM.

## 1.2 Polyphosphate Remediation Technology

By changing the chemical speciation, toxic and mobile species can be converted to nontoxic and immobile species (Knox, 2008). Uranium has a high affinity to form strong and the most stable complexes with phosphate amongst oxygen-containing ligands (Giammar, 2001; Sowder et al., 2000). The presence of phosphate in groundwater can limit the mobility of the uranyl cation ($UO_2^{2+}$) in the subsurface due to the formation of sparingly insoluble autunite minerals.

Water soluble phosphate compounds can be injected into contamination plumes by using strategically placed wells as chemical stabilizers for uranium and other heavy metals. Soluble amendments allow treatment of plumes situated deep within the subsurface and act to sequester uranium by precipitating insoluble uranium minerals. Arey (1999) and Shi (2009) used water soluble phosphate compounds to sequester uranium but with little success. Wellman et al., (2007) demonstrated that the compounds such as tribasic sodium phosphate will rapidly form phosphate phases, occluding ~30% of the fluid-filled pore space and reducing hydraulic conductivity. However, the use of soluble long-chain polyphosphate compounds has been demonstrated to delay the precipitation of phosphate phases (Figure 9). Precipitation of phosphate minerals occur when the phosphate

compounds degrade in water, due to the hydrolysis, to yield orthophosphate molecules ($PO_4^{3-}$). The longer the polyphosphate chain, the slower the hydrolysis reaction leading to orthophosphate products (Shen et al., 1973) Figure 10. Hence, the drastic change in the hydraulic conductivity of the system will not occur due to the use of long-chain polyphosphate.

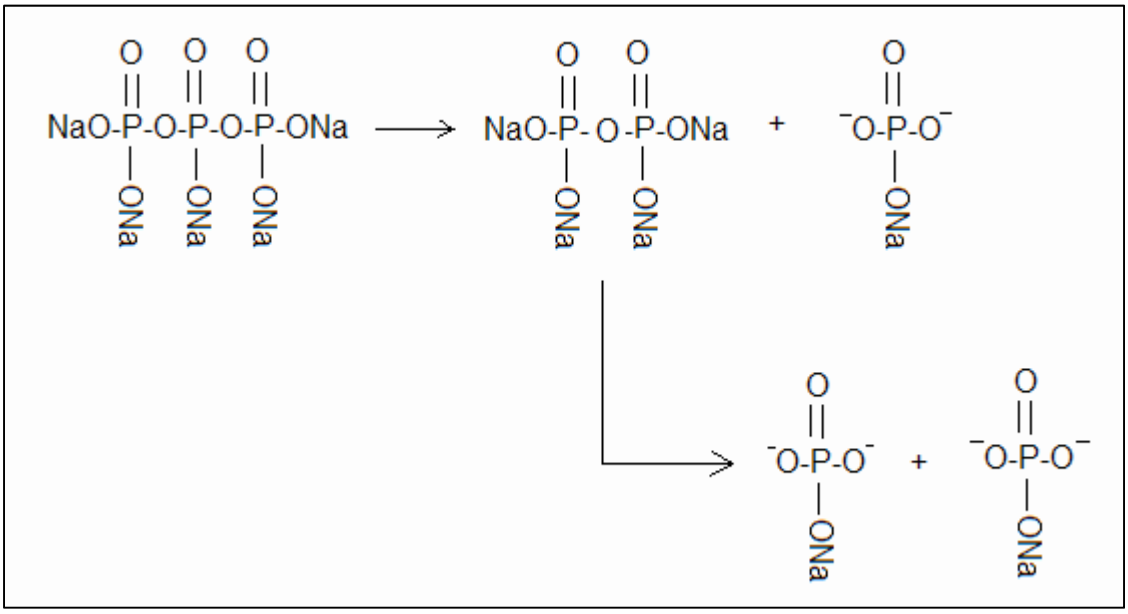


**Figure 9 Schematic showing the step-wise hydrolysis of sodium tri-polyphosphate**

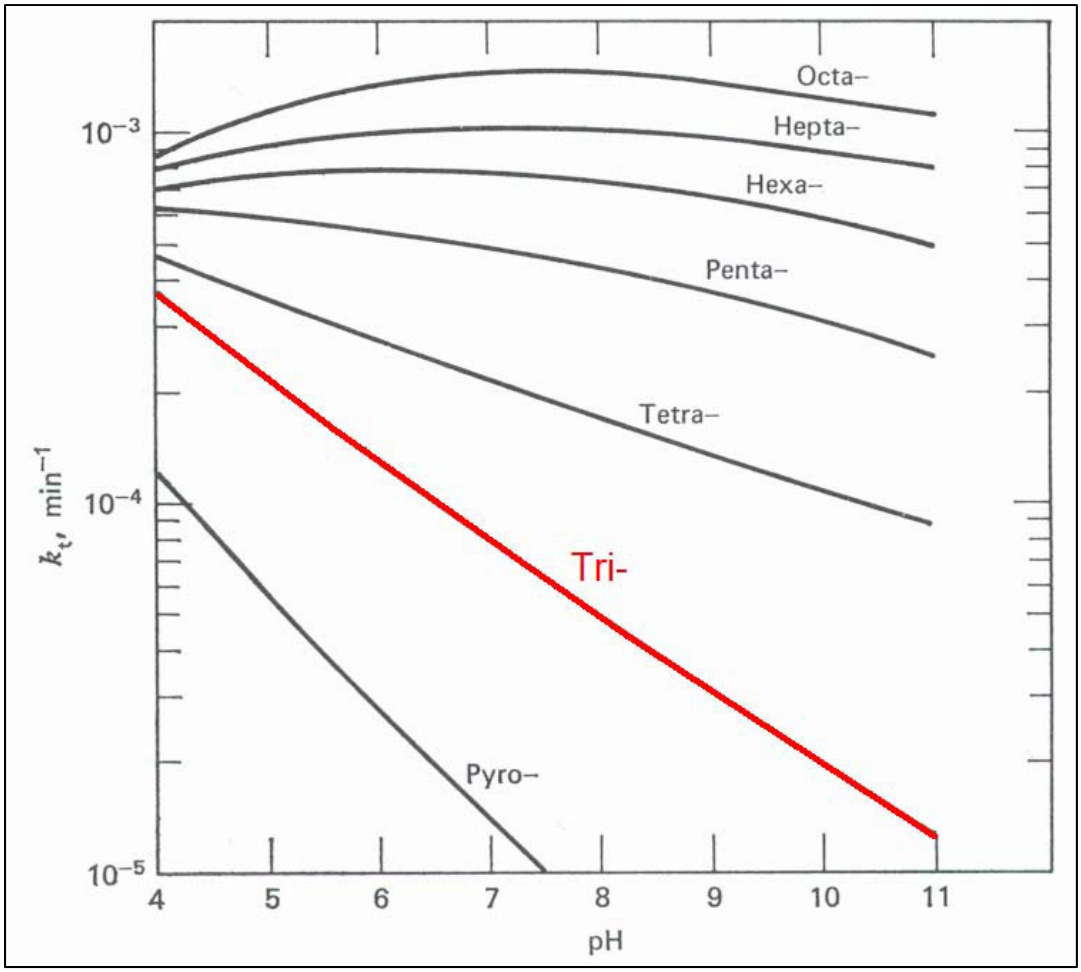


**Figure 10 Hydrolysis of polyphosphate as a function of pH**

*In situ* stabilization of uranium by polyphosphate amendments has gained popularity at some of the DOE sites contaminated with uranium (Knox, 2008; Wellman et al., 2007). Injection of a soluble sodium tripolyphosphate amendment into the uranium contaminated groundwater and soil have been shown to effectively sequester uranium through the formation of insoluble uranyl phosphate minerals. The uranyl phosphates are a large family of minerals, $X_{1\text{-}2}[(UO_2)(PO_4)]_{2\text{-}1}{\cdot}nH_2O$, where X is any monovalent of divalent cation (Vermeul, 2008). Table 2 lists several of the most commonly observed uranyl phosphate minerals (Finch et al., 1999) that can be formed due to the polyphosphate injection.

**Table 2 Environmentally significant uranyl phosphate minerals**

| Name | Composition |
|---|---|
| autunite | $Ca(UO_2)_2(PO_4)_2 \cdot 10H_2O$ |
| meta-autunite | $Ca(UO_2)_2(PO_4)_2 \cdot (2\text{-}6)H_2O$ |
| uranyl orthophosphate | $(UO_2)_3(PO_4)_2 \cdot 4H_2O$ |
| chernikovite | $(H_3O)_2(UO_2)_3(PO_4)_2 \cdot 4H_2O$ |
| sodium meta-autunite | $Na_2(UO_2)_2(PO_4)_2 \cdot 8H_2O$ |
| meta-ankoleite | $K_2(UO_2)_2(PO_4)_2 \cdot 6H_2O$ |
| phosphuranylite | $Ca(UO_2)_3(PO_4)_2(OH)_2 \cdot 6H_2O$ |
| saleeite | $Mg(UO_2)_2(PO_4)_2 \cdot 10H_2O$ |

## 1.3 Chemical Weathering

Chemical weathering is one of the dominating processes controlling the hydrogeochemical cycle of elements. It involves complex chemical reactions that alter the structure of minerals through dissolution, hydration, oxidation and hydrolysis. Soil pore water and groundwater rich in dissolved carbon dioxide, mineral cations and organic molecules are the primary agents in the dissolution reactions. Chemical weathering takes place in soils and groundwater and mainly depends on the nature of the minerals material, water acidity, and temperature (Langmuir, 1997).

Release of uranium from autunite takes place during slow dissolution of the mineral structure. The solubility products of uranyl phosphate, log $K_{sp}$, reported in the literature have been measured from 49 to 53 (Table 3) (Grenthe, 1992; Sandino et al., 1992) which is slightly less soluble then other autunite phases such as calcium (log $K_{sp}$ = 45) or sodium (log $K_{sp}$ = 48) (Langmuir, 1997). Gorman - Lewis et al., (2009) reported in their recent solubility study on well- characterized natural Ca-U-P and uranyl orthophosphate stability constant values, log $K_{sp}$, of -48.36 and -49.36, respectively. Environmental

factors, such as pH, temperature, dissolved organic matter, and redox potential, have tremendous effects on both uranium and polyphosphates. For example, hydrolysis of polyphosphates has been found to take place at lower pH ranges (Henk-Jan, 1998), which in turn can influence its reaction rate with uranium. Similarly, pH and redox potential can also have influence on these chemicals, either by changing their oxidation states (uranium) or by influencing hydrolysis (polyphosphates).

Information on the stability of uranyl-phosphate phases is limited to pH, temperature, and a few aqueous organic materials (Wellman et al., 2006). Kinetic dissolution studies of autunite conducted in the wide range of pH and temperatures in flow-through and batch experiments illustrated a strong dependency of dissolution rates on pH but were relatively insensitive to temperature variations (Wellman et al., 2006, 2007). Yet, limited data is available about autunite stability as it relates to complexation with ligands. The ability of ligands to form complexes tends to increase the solubility of minerals. Sowder (1998) investigated the dissolution of meta-autunite in a variety of leaching solutions. Dissolution in 100 mM EDTA and acetic acid resulted in release of 5 - 25% of the total uranium after 2 weeks. Dissolution of meta-autunite was rapid with 100% recovery after only 8 hours with 100 mM sodium bicarbonate.

As shown in other studies (Davis, 2003 & 2004; Curtis, 2004), U(VI) sorption to soil and sediments is extremely sensitive to the alkalinity value due to aqueous carbonate complexation. However, the effect of carbonate complexation on uranyl phosphate (Na-autunite) dissolution has not been evaluated. The dissociation reactions of some of the

uranyl phosphate minerals along with the solubility product constants are listed in Table 3.

**Table 3 Dissociation reactions and associated solubility products**

| Reaction | Log $K_{sp}$ |
|---|---|
| $(UO_2)_3(PO_4)_2 \bullet 4H_2O_{(s)}$ -----> $4H_2O_{(l)} + 2PO_4^{3-} + 3UO_2^{2+}$ | -49.37[1],-53.32[2] |
| $UO_2HPO_4 \bullet 4H_2O_{(s)}$ -----> $4H_2O_{(l)} + H^{+} + PO_4^{3-} + UO_2^{2+}$ | -24.20[1] |
| $Ca(UO_2)_2(PO_4)_2 \bullet xH_2O_{(s)}$ -----> $xH_2O_{(l)} + Ca^{2+} + 2PO_4^{3-} + 2UO_2^{2+}$ | -44.70[3] |
| $Na_2(UO_2)_2(PO_4)_2 \bullet xH_2O_{(s)}$ ----> $\bullet xH_2O_{(l)} + 2Na^{+} + 2PO_4^{3-} + 2UO_2^{2+}$ | -47.409[4] |

1-Grenthe et al, (1992), 2- Sandino and Bruno (1992), 3-Van Haverbeke et al. (1996), 4-Visual MINTEQ

Carbonate/bicarbonate leaching solutions are traditionally used to extract uranium from contaminated soils. Manson (1997) examined carbonate leaching of uranium from contaminated soil at the Fernald Site, Ohio. The leach solution of $KHCO_3/K_2CO_3$ at 1:1 ratio and the total concentration of $CO_3^{2-}$ 0.5 M effectively removed 80% of uranium from soil within 48h and an additional 5% over the next 288h in column experiments. Increases in the reaction temperature often enhance the solution reaction rate. However, no appreciable changes were noted in the removal rate at temperatures of 25, 45, and 65$^{o}$C using 0.5 M $HCO_3^{-}$ as a leaching solution (Manson, 1997).

### 1.4 Surface-controlled Ligand Promoted Dissolution Mechanism of Minerals

The dissolution transforms minerals to solutes through several steps which involve mass transport, adsorption, surface chemical reactions, and desorption processes (Stumm et al., 1990). Recent studies using surface spectroscopy of the mineral dissolution reactions by ligands have revealed that the overall reaction is surface-controlled. In these reactions, the concentrations of solutes close to the surface are equal to the bulk solution

concentration. The dissolution kinetics is zero-order if steady-state conditions exist on the surface (Stumm et al., 1990 & 1996):

$$r = \frac{dC}{dt} = kA \quad (1)$$

Where:

$r$ = the dissolution rate (M $s^{-1}$),

A = the surface area of the mineral $A$ ($m^{-2}$), and

$k$ =the reaction rate constant (mol $m^{-2}$ $s^{-1}$)

The important reactants in the dissolution process are $H_2O$, $H^+$, $OH^-$, ligands, and reductants and oxidants in case of reducible or oxidizable minerals. The latter is not the case for the uranyl ion sequestrated into the stable uranyl phosphate minerals under the aerobic groundwater conditions that are typically present at the Hanford Site.

There are two important mechanisms in the surface-control reactions (Stumm et al., 1990; Sparks 1999):

i. Fast bonding of the reactants to the surface sites, and
ii. Slow and rate-limiting detachment of metal species from the surface into solution.

$$\text{Surface site + Reactants (Ligands)} \xrightarrow{Fast} \text{Surface Species} \quad (2)$$

$$\text{Surface Species} \xrightarrow{Slow\ \text{det}achment\ of\ metal} \text{M (aq)} \quad (3)$$

The dissolution reaction begins with the surface complexation with ligands that tend to weaken metal bonds, causing detachments of the metal cation into the solution phase. Since detachment of metal from the surface is rate limiting, the rate law of the dissolution reaction depends on the concentration of the surface species, *Cj* (mol $m^{-2}$):

$$R = kCj \tag{4}$$

Where:

*k* = the rate constant for ligand-promoted dissolution ($time^{-1}$), and

*Cj* = the surface concentration of the ligand (mol $m^{-2}$)

### 1.5 Hanford's 300 Area Uranium Plume Characterization

The aqueous bicarbonate system is important in the environment because of the high abundance of carbon dioxide and carbonate containing minerals (Clark et al., 1995). Aqueous carbonate at a common groundwater $CO_2$ pressure of $10^{-2}$ to $10^{-3.5}$ atmosphere is the predominant species affecting the dissolution of actinides and facilitating uranium desorption reactions from soil and sediments, thus increasing uranium mobility in natural waters (Langmuir, 1997). The composition of groundwater collected at several locations within the uranium contaminated area at the Hanford Site has revealed relatively constant concentrations for the major anions, cations, and pH. The groundwater ionic strength ranging 3 - 8 mmol $L^{-1}$ was dominated by $Ca^{2+}$, $Na^{+}$, $Mg^{2+}$, $HCO_3^{-}$, and $SO_4^{2-}$. Zachara (2005) reported that computerized speciation model (MINTEQA2) indicated that 300 Area groundwater was supersaturated with $CO_{2(g)}$ and $Ca_2UO_2(CO_3)_3^{0}$ and $UO_2(CO_3)_2^{2-}$ are the predominant U(VI) aqueous species. The concentration of uranium exceeds the

maximum contaminant level for drinking water of 30 mg $L^{-1}$ required by EPA as shown in Figure 4. Table 4 lists the groundwater composition collected from various excavations of the 300 Area uranium plume.

The Columbia River total inorganic carbon concentration is about 0.5 mM; concentrations in the range of 1.2 - 2.7 mM were determined in the groundwater at the 300 Area, and more than 10 mM were detected in the vadose zone porewater.

**Table 4 Composition of 300 area groundwater collected from various excavations**

| Parameter | Range |
|---|---|
| pH | 7.71 - 8.11 |
| Ionic strength, (mmol $L^{-1}$) | 3.50 - 8.20 |
| Ca, (μmol $L^{-1}$) | 0.60 - 1.31 |
| K, (μmol $L^{-1}$) | 0.06 - 0.20 |
| Na, (μmol $L^{-1}$) | 0.77 - 2.65 |
| Inorganic carbon, (mmol $L^{-1}$) | 1.2 - 2.71 |
| U(μmol $L^{-1}$) | 0.3 - 4.96 |

OBJECTIVES

The objective of the experimental work was to quantify the effect of bicarbonate on the stability of synthetic meta-autunite created as a result of uranium stabilization through polyphosphate injection. The polyphosphate technology with the formation of autunite was identified as the most feasible remediation strategy to sequester uranium in contaminated groundwater and soil *in situ*. The experimental work helped to quantify the dissolution kinetics of meta-autunite minerals in the presence of bicarbonate.

This was accomplished through a series of dissolution experiments conducted in a single-pass flow-through (SPFT) reactor using a mixture of carbonate and TRIS as a buffer solution subjected to various temperatures.

The parameters that were tested are as follows:

i. Carbonate concentration: 0.5, 1.0, 2.0, and 3.0 mmol $L^{-1}$

ii. pH: 6 - 11

iii. Temperature: 5 - 60$^{o}$C

## 1.6 Research Hypothesis

Bicarbonates' ability to complex with uranium yields highly soluble and mobile species in the subsurface environment. The presence of bicarbonate ions in the solution are expected to enhance the solubility of uranium-bearing minerals by complexation reactions with carbonate.

METHODOLOGY

## 1.7 Synthesis of Uranyl Phosphates Mineral

Several published methods have described procedures for synthesis of synthetic autunite salts (Zheng, 2006; Sowder et al., 2000). A review of literature revealed two main approaches to synthesize uranium phosphate minerals by using direct and indirect precipitation. Wellman et al., (2005) described the direct precipitation method modified from (Vochten et al., 1980) for synthesis of Na-autuntie. The precipitation of Na-autunite was accomplished by mixing uranyl nitrate, $UO_2(NO_3)_2{\cdot}6H_2O$, solution and sodium phosphate dibasic, $Na_2HPO_4{\cdot}7H_2O$, in a volumetric ratio of 1:7.5 while stirring at 70$^oC$. The overall reaction is as follows:

$$Na_2HPO_4{\cdot}7H_2O + UO_2(NO_3)_2{\cdot}6H_2O \text{ ----> } Na[UO_2PO_4]{\cdot}nH_2O + NaNO_3 + HNO_3 \quad (5)$$

Heating was terminated after a yellowish green precipitate was formed rapidly and stirring was continued until the solution returned to room temperature. The solids were allowed to cure at room temperature for 24 hours without stirring. Solids were recovered from solution using vacuum filtration with a 0.45 µm disposable Nalgene filter; the solids were then washed with DI water heated to 70$^oC$ followed by rinsing with isopropyl alcohol. Solids were dried at room temperature until a constant weight was achieved (Wellman et al., 2005).

## 1.8 Characterization of Sodium Meta-Autunite

The synthesized and partially reacted autunite solids were characterized by JSM-5900-LV low vacuum scanning electron microscope (SEM) at 15kV for identification of

particle size. Energy Dispersive X-Ray Spectroscopy (EDS) was used to determine the composition and purity of the solids. The composition of the particles was analyzed using a Noran System Six Model 200 SEM Energy Dispersive X-Ray Spectroscopy (EDS). Pre-experimental surface area analysis was conducted following the $N_2$-adsorbtion BET method (Brunauer et al., 1938) by using a micromeritics ASAP 2020 surface and porosity analyzer at Pacific Northwest National Laboratory (PNNL) and compositional analysis using Bruker 5000D XRD instruments.

### 1.8.1 Scanning Electron Microscopy (SEM)

SEM with EDS analysis was performed in the Advanced Materials Engineering Research Institute (AMERI) at Florida International University (FIU) by using a JSM-5900-LV low vacuum SEM at 15kV. The sample was mounted on a double-sided carbon tape as the mineral has a very low electrical conductivity and can be electrostatically charged during imaging. Initial analysis of the sample showed that the mineral has impurities, shown as non-uniform colored areas in Figure 11. The solids were washed with DI water heated to $70^{o}$C to remove impurities, followed by washing with isopropyl alcohol to reduce aggregation. Repeated SEM analysis showed that the impurities were washed out, showing a uniform color in Figure 12.

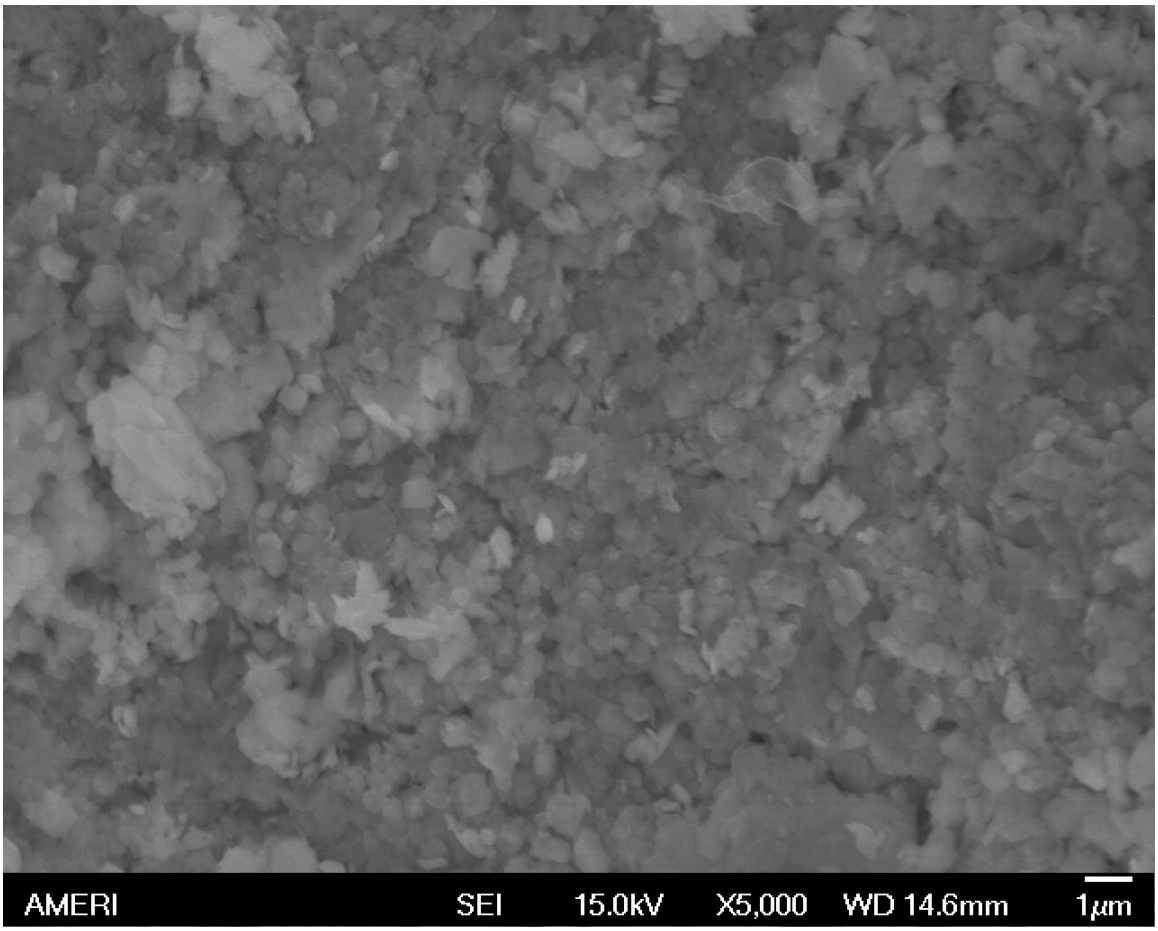


**Figure 11 Photomicrograph of synthetic sodium meta-autunite before washing**

The compositional analysis was performed on both samples using EDS; composition of the solids was conducted at three (3) locations for sodium (Na), oxygen (O), phosphorous (P), nitrogen (N), and uranium (U), and the data is presented in Table 5, Figure 13 and Table 6, Figure 14. Presence of N is shown in Figure 13 before washing and Figure 14 shows absence of N after washing. Average compositions of the elements were divided by molecular weight of the element to obtain molar quantities of the elements. Molar quantities of elements were divided with the lowest molar quantity to obtain the chemical formula of the mineral. Based on the data shown in Table 5, the chemical formula of the synthesized mineral's atomic ratio does not match that of autunite. However, after

washing, the mineral matches the atomic ratio of autunite (Table 6) and the chemical formula of the synthesized mineral is Na $[UO_2\ PO_4]$.

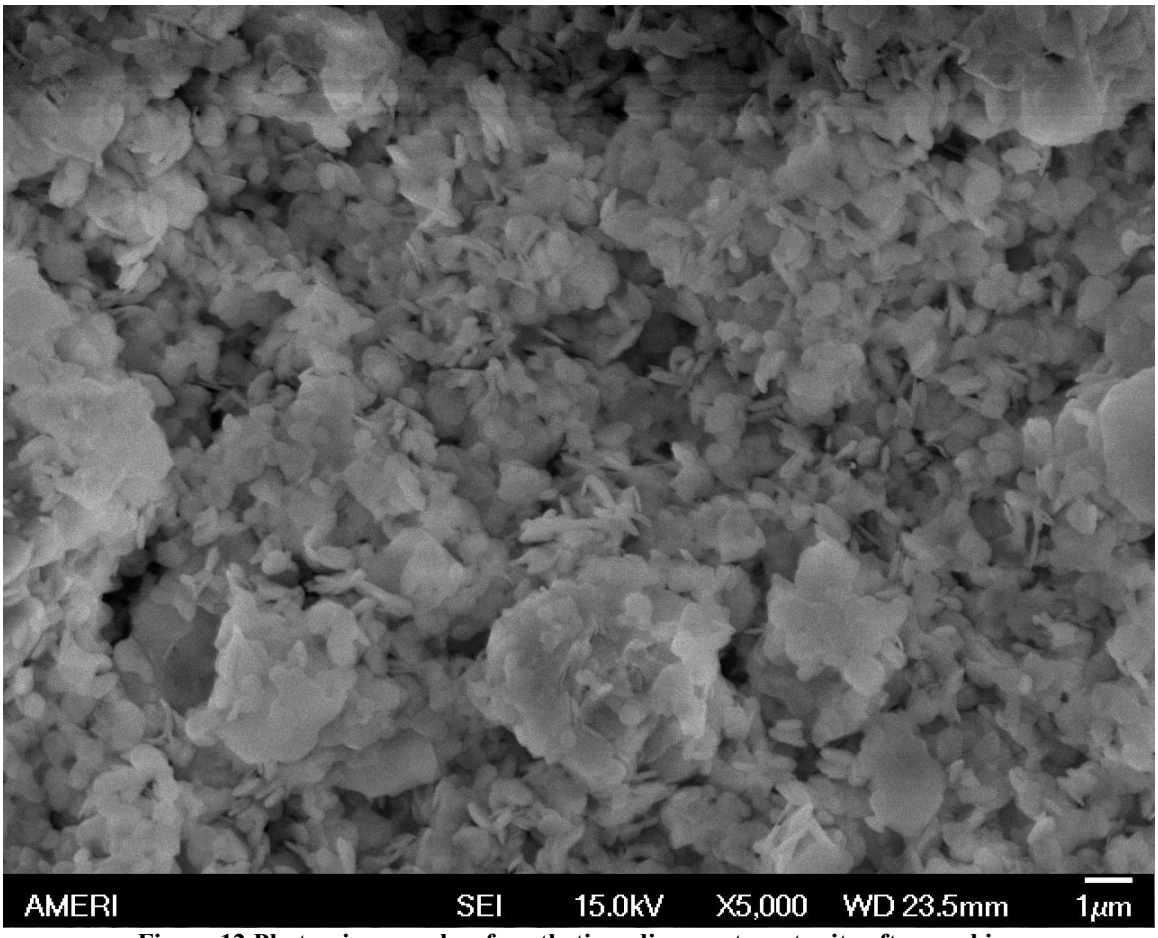


**Figure 12 Photomicrographs of synthetic sodium meta-autunite after washing**

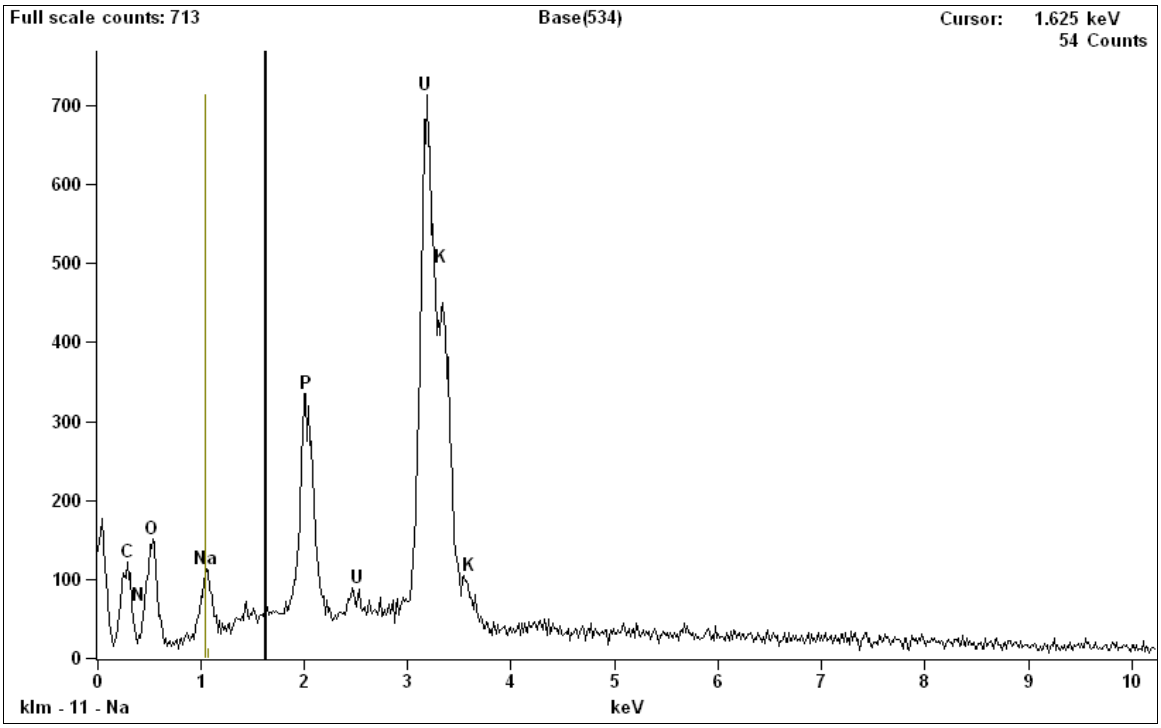


**Figure 13 Compositional peaks of elements before washing**

**Table 5 Elemental composition of sodium meta-autunite before washing**

| Element | Sample 1 | Sample 2 | Sample 3 | Average | Molecular wt. | Molar Quantity | Atomic Ratio |
|---|---|---|---|---|---|---|---|
| **Na** | 0.89 | 1.36 | 0.79 | 1.01 | 23 | 0.04 | 1.00 |
| **O** | 10.94 | 12.96 | 6.71 | 10.20 | 16 | 0.64 | 14.47 |
| **P** | 8.74 | 8.68 | 7.38 | 8.27 | 31 | 0.27 | 6.05 |
| **U** | 75.97 | 74.01 | 82.26 | 77.41 | 238 | 0.33 | 7.38 |
| **N** | 3.27 | 2.97 | 2.74 | 2.99 | 14 | 0.21 | 4.85 |

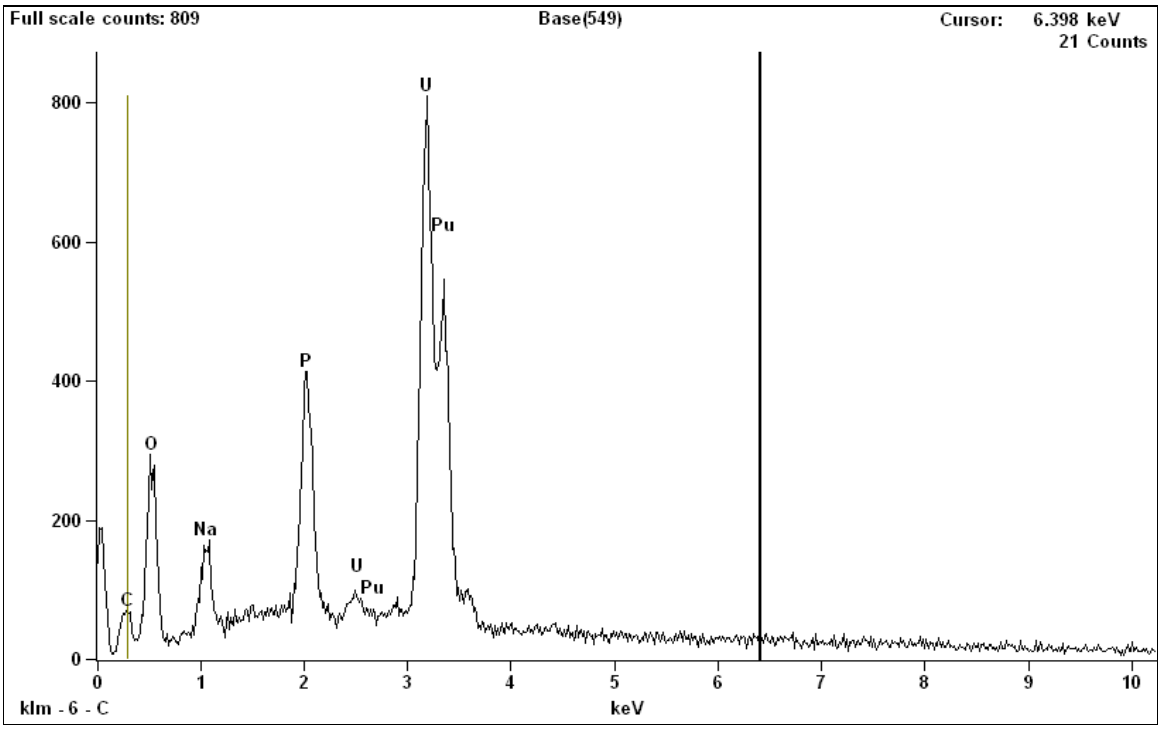


**Figure 14 Compositional peaks after washing**

**Table 6 Elemental composition of sodium meta-autunite after washing**

| Element | Sample 1 | Sample 2 | Sample 3 | Average | Molecular Wt. | Molar Quantity | Atomic Ratio |
|---|---|---|---|---|---|---|---|
| **Na** | 5.14 | 6.29 | 6.91 | 6.11 | 23 | 0.27 | 1.08 |
| **O** | 20.37 | 21.93 | 25.11 | 22.47 | 16 | 1.40 | 5.69 |
| **P** | 7.3 | 7.77 | 7.87 | 7.65 | 31 | 0.25 | 1.00 |
| **U** | 65.25 | 62.1 | 56.54 | 61.30 | 238 | 0.26 | 1.04 |

### 1.8.2 X-Ray Diffraction (XRD)

X-ray diffraction analysis was performed on the synthesized autunite mineral at 40 kV and 40 mA using a Bruker 5000D XRD instrument. Diffraction patterns were obtained using a copper radiation source with a tungsten filter. The sample was analyzed in the range of 2 to 35$^{o}$ for the 2-theta (2□) with 0.04$^{o}$ step increment and a two-second count time at each step. As shown in Figure 15, XRD patterns obtained for synthesized autunite

matched, but at higher intensity, the diffraction patterns of the known autunite PDF obtained from PNNL for comparison.

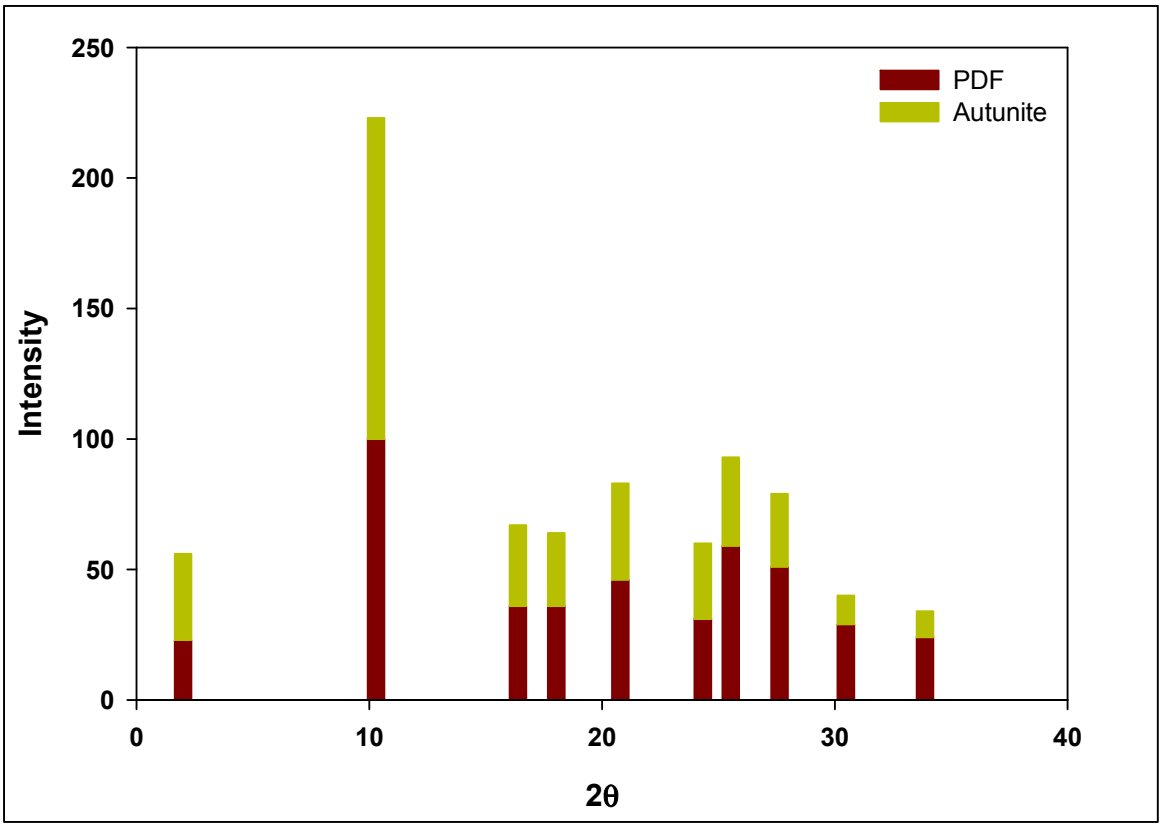


**Figure 15 X-Ray diffraction patterns of synthetic Na-autunite mineral**

## 1.9 Carbonate Buffer Solutions

Buffer solutions prepared with distilled de-ionized water (DDIW) at 23°C consisting of 0.05 M *tris (hydroxymethyl) aminomethane* (TRIS, $(HOCH_2)_3CNH_2$) buffer and aqueous bicarbonate concentration in the range of 0.0005 to 0.003 M were used to investigate the uranium release from synthetic autunite mineral over a pH interval of 6 to 11. The pH of the buffer solutions was adjusted using 0.1 M hydrochloric (HCl) acid and potassium hydroxide (KOH) and composition of the buffer solutions are shown in Table 7.

**Table 7 Composition of solutions of bicarbonate concentrations used**

| Solution | Composition | pH @ 23°C |
|---|---|---|
| 1 | 0.05 M Tris + 0.0005 M $HCO_3^-$ + 0.01096 M HCl | 5.96 |
| 2 | 0.05 M Tris + 0.0005 M $HCO_3^-$ + 0.0103M HCl | 7.00 |
| 3 | 0.05 M Tris + 0.0005 M $HCO_3^-$ + 0.00779 M HCl | 8.01 |
| 4 | 0.05 M Tris + 0.0005 M $HCO_3^-$ + 0.00256 M HCl | 9.01 |
| 5 | 0.05 M Tris + 0.0005 M $HCO_3^-$ + 0.000147 M HCl | 10.02 |
| 6 | 0.05 M Tris + 0.0005 M $HCO_3^-$ + 0.00083 M KOH | 11.00 |
| 7 | 0.05 M Tris + 0.001 M $HCO_3^-$ + 0.0112 M HCl | 6.01 |
| 8 | 0.05 M Tris + 0.001 M $HCO_3^-$ + 0.0103 M HCl | 7.02 |
| 9 | 0.05 M Tris + 0.001 M $HCO_3^-$ + 0.00654 M HCl | 8.00 |
| 10 | 0.05 M Tris + 0.001 M $HCO_3^-$ + 0.00265 M HCl | 9.01 |
| 11 | 0.05 M Tris + 0.001 M $HCO_3^-$ + 0.000147 M HCl | 10.00 |
| 12 | 0.05 M Tris + 0.001 M $HCO_3^-$ + 0.00116 M KOH | 11.00 |
| 13 | 0.05 M Tris + 0.002 M $HCO_3^-$ + 0.0118 M HCl | 6.01 |
| 14 | 0.05 M Tris + 0.002 M $HCO_3^-$ + 0.0108 M HCl | 6.99 |
| 15 | 0.05 M Tris + 0.002 M $HCO_3^-$ + 0.00798 M HCl | 7.99 |
| 16 | 0.05 M Tris + 0.002 M $HCO_3^-$ + 0.00267 M HCl | 9.01 |
| 17 | 0.05 M Tris + 0.002 M $HCO_3^-$ + 0.00006 M KOH | 10.00 |
| 18 | 0.05 M Tris + 0.002 M $HCO_3^-$ + 0.00192 M KOH | 11.00 |
| 19 | 0.05 M Tris + 0.003 M $HCO_3^-$ + 0.0125 M HCl | 6.01 |
| 20 | 0.05 M Tris + 0.003 M $HCO_3^-$ + 0.01077 M HCl | 7.01 |
| 21 | 0.05 M Tris + 0.003 M $HCO_3^-$ + 0.00784 M HCl | 8.01 |
| 22 | 0.05 M Tris + 0.003 M $HCO_3^-$ + 0.00240 M HCl | 9.01 |
| 23 | 0.05 M Tris + 0.003 M $HCO_3^-$ + 0.000379 M KOH | 9.99 |
| 24 | 0.05 M Tris + 0.003 M $HCO_3^-$ + 0.002747 M KOH | 11.00 |

## 1.10 Single-Pass Flow-Through (SPFT) Experiments

The SPFT test was designed to conduct experiments under controlled pH and temperature conditions with constant fresh water flowing through a reaction cell filled with a mineral sample. The well-mixed batch type reactor was used in the current study to measure the dissolution rates of autunite minerals under strictly controlled conditions. The most important feature of this test was to remove the ions released into solution as a result of autunite dissolution by continuously flowing fresh water into the system. This test has been widely used to measure reaction rates of minerals and could be easily adapted to operate with various flow rates, solution composition, and sample mass, temperature variations to ensure accurate rate determinations (McGrail, 1997; Wellman et al., 2006).

The SPFT system, shown in Figure 16, includes a programmable Kloehn V6 syringe pump (55022) that transferred carbonate buffered fresh solution from an influent reservoir (R) via Teflon lines into two-port (1/4") 60 mL capacity *perfluoroalkoxide* (PFA) Teflon reactor vessels (Re) obtained from Savillex (Minnetonka, MN). The transport of the influent solution from the reservoir to the reactors was accomplished via 1/16-inch Teflon tubing and the effluent solution was transported via 1/32-inch Teflon tubing. The reactors were kept in an oven and refrigerator under the temperature controlled conditions during continuous system operation to maintain them at a specific temperature in the range of 5 to 60$^{o}$C. A thin sample solids layer resting at the bottom of the reactor interacted with solution flowing through the reactor.

The solution flow rate was in the range of 1 - 2.5 L $d^{-1}$. A blank solution sample was collected prior to the addition of Na-autunite. The effluent solution was continuously

collected until steady state conditions were attained, which occurred after the transfer of ~8 reactor volumes; aliquots samples were retained for pH measurements and concentrations analysis of the dissolved elements (mainly U, P and Na). The concentrations of Na and P were determined by inductively coupled plasma mass spectroscopy (ICP-MS) and the total uranium concentration was measured using a kinetic phosphorescence analyzer (KPA).

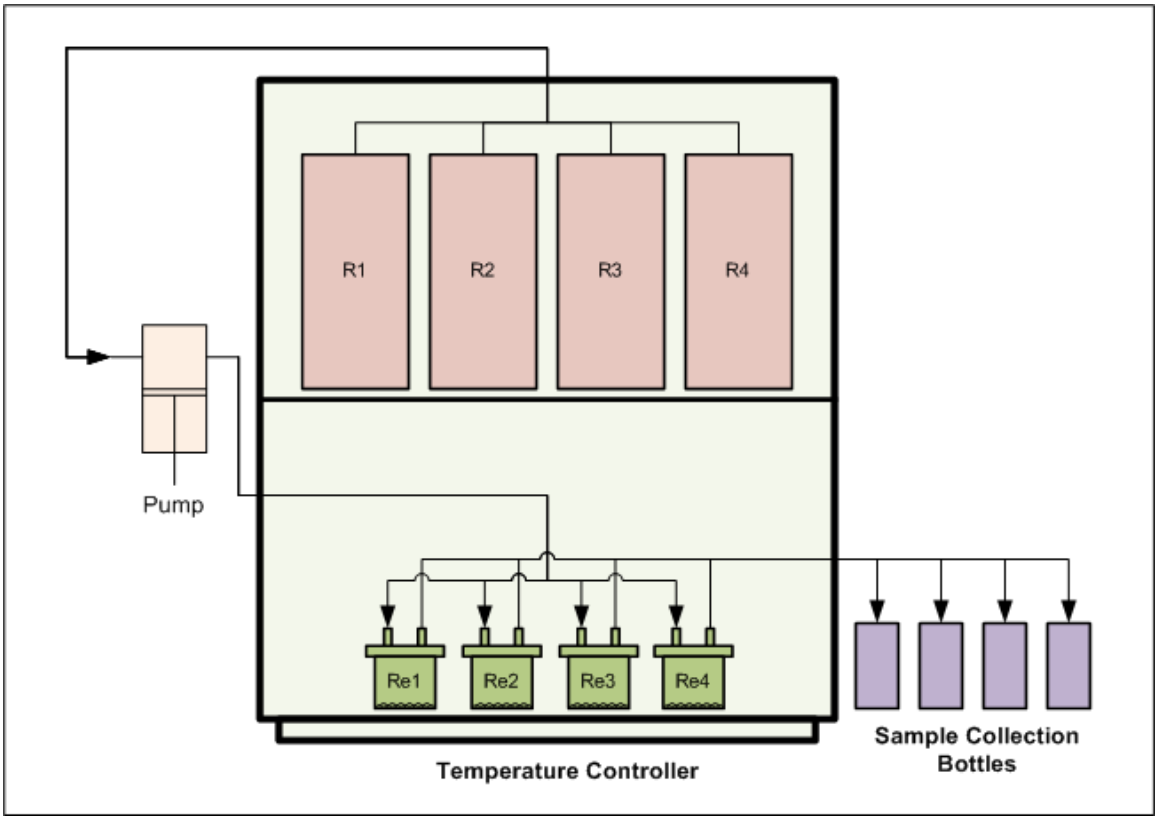


**Figure 16 Graphical representation of experimental setup**

### 1.10.1 Dissolution Rate Calculations

Surface area measurements of autunite solids were carried out at PNNL by using the $N_2$-adsorption BET method (Brunauer et al., 1938). A micromeritics surface and porosity analyzer, Model ASAP 2020, was used to measure the surface area of the synthetic

autunite samples. After the surface area was determined, the normalized dissolution rate was calculated for each component and at each sampling interval using the following formula

$$R_i = (C_i - C_{ib})\frac{q}{f_i S} \quad (6)$$

Where:

$R_i$ = the normalized dissolution rate for element $i$ (g $m^{-2}$ $d^{-1}$),

$Q$ = flow rate, (L $d^{-1}$),

$C_i$ = concentration of component $i$ in the effluent (g $L^{-1}$),

$C_{ib}$ = mean background concentration of component i (g $L^{-1}$),

$f_i$ = the mass fraction of the element in the metal (dimensionless), and

S = the surface area of the sample ($m^2$).

Flow rates, $q$, were determined gravimetrically by measuring fluid collected upon the sampling event. The background concentration of metals, $C_{ib}$, was determined by triplicate analyses of the influent solution. The value of $f_i$ was calculated from the sample chemical composition.

SPFT experiments were designed to limit the accumulation of reaction products using a sufficient ratio of the flow rate to the surface area of the mineral sample (q/S) to ensure that maximum dissolution rate or forward rate was achieved. By varying the flow rate and surface area (either increasing the flow rate or decreasing the surface area), the value

of q/S can be increased, consequently increasing the difference in chemical potential between the solid phase and the solution. This allowed achievement of the dissolution plateau, which is equated to the forward rate of dissolution.

### 1.10.2 Error Analysis

The lower limit of detection (LLD) of the instrument was used for the element where the element concentration is below the detection limit. The LLD of the instrument for an element is the lowest concentration of calibration standards that is reproducible within ±10% error.

The standard deviation of the dissolution rate is determined according to the uncertainty associated with each parameter shown in Equation 6. Standard deviation for uncorrelated random errors is given by:

$$\sigma_f = \sqrt{\sum_{i=1}^{n} \left( \frac{\partial f}{\partial x_i} \right)^2 \sigma_i^2} \tag{7}$$

Where:

$\sigma_f$ = standard deviation of the function *f*;

$x_i$ = parameter *i*, and

$\sigma_i$ = standard deviation of parameter *i*.

Substituting Equation 6 into 7 and converting to relative standard deviations, $\hat{\sigma}_r = \sigma_f / \bar{x}$, gives the following equation:

$$\hat{\sigma}_r = \sqrt{\frac{\left(\hat{\sigma}_c C_i^{out}\right)^2 + \left(\hat{\sigma}_b C_i^{in}\right)}{\left(c_i^{out} + c_i^{in}\right)^2} + \hat{\sigma}_{fi}^2 + \hat{\sigma}_s^2 + \hat{\sigma}_q^2} \quad (8)$$

Relative errors include:

$\hat{\sigma}_c$ = final concentration 10%,

$\hat{\sigma}_b$ = background concentration 10%,

$\hat{\sigma}_{fi}$ = mass distribution error 5%,

$\hat{\sigma}_s$ = surface area error 15%, and

$\hat{\sigma}_q$ = flow rate error 5%.

Wellman et al., (2006) reported that this error analysis results in typical $2\sigma$ uncertainties of approximately ±35% for SPFT-measured dissolution rates (or ±0.2 log units). The conservative evaluation of errors assigned to parameters in Equation 8, in addition to the practice of setting detection threshold values to background concentrations, results in typical uncertainties of nearly ±35% on the dissolution rate (Wellman et al., 2009).

### 1.11 Groundwater Modeling

Steady state concentrations were used to determine the aqueous speciation and saturation state of the effluent solution with respect to solid and liquid phases by using geochemical modeling Visual MINTEQ version 3.0, (maintained by Jon Petter Gustafsson at KTH Royal Institute of Technology, Sweden). Visual MINTEQ is a geochemical equilibrium speciation model capable of computing equilibria among the dissolved, adsorbed, solid,

and gas phases in an environmental setting. Visual MINTEQ uses the well-developed thermodynamic database of the U.S. Geological Survey's WATEQ3 model and can be used to calculate the mass distribution between the dissolved, adsorbed, and multiple solid phases under a variety of conditions including a gas phase with constant partial pressure. MINTEQ has an extensive thermodynamic database that is adequate for solving a broad range of problems.

### 1.12 Sample Preparation

The presence of organic content in the leach solutions interfered with KPA; hence, samples collected during the experiments were pre-processed by wet ashing followed by dry ashing. A modified ashing technique described by John, et al., (2000) was used to wet and dry ash samples.

***Wet ashing:*** To a 20 ml scintillation vial, 1 ml of sample, 0.5 ml of concentration of nitric acid and 0.5 ml of 34% hydrogen peroxide were added. The contents were mixed and placed on a hot plate and dried slowly until white precipitate was obtained. Occasionally, some samples turned yellow while ashing; 0.5 ml of peroxide was added to those samples and the process was continued until a white precipitate was obtained.

***Dry ashing:*** After wet ashing was completed, samples were placed in a muffle furnace preheated to 450$^{o}$C for about 15 - 20 minutes to dry ash the samples.

Samples were allowed to cool after the wet and dry ashing and 1 ml of 2 M nitric acid was added to bring the sample to the original volume; aliquots from the sample were used for analysis.

# RESULTS AND DISCUSSION

## 1.13 Steady-State Concentrations

Concentrations used to calculate the dissolution rates were obtained when the system reached equilibrium. The results presented in Figure 17 are representative of the observations for all experiments and illustrate that steady-state conditions are met for different aqueous bicarbonate concentrations (0.0005 - 0.003 M) at the four temperatures (5, 23, 40, and 60°C) studied. For the pH range of 6 - 11, the graph shows the achievement of steady-state conditions, illustrated by the plateau region, after approximately eight reactor volumes where the concentrations of uranium released from synthetic Na-autunite are invariant with respect to time. This figure also depicts the strong effect of pH in the dissolution rate of autunite, increasing uranium release as a function of pH; this is consistent with previous studies on dissolution rate of autunite minerals (Wellman et al., 2006).

## 1.14 Effect of Bicarbonate Concentrations

Bicarbonate concentrations ranging from 0.0005 to 0.003 M in 0.1 M TRIS buffer solutions were used to investigate the effect of bicarbonate, pH and temperature on the dissolution rate of synthetic Na-autunite. The solutions pH values were varied from 6 to 11 at temperatures of 5, 23, 40, and 60$^{o}$C. Even though the temperature of the groundwater at the Hanford Site is 22$^{o}$C (Schalla et al., 2001) and it would be impractical to raise groundwater temperature to 60$^{o}$C, experiments were conducted up to 60$^{o}$C to examine the effects of a broader temperature range.

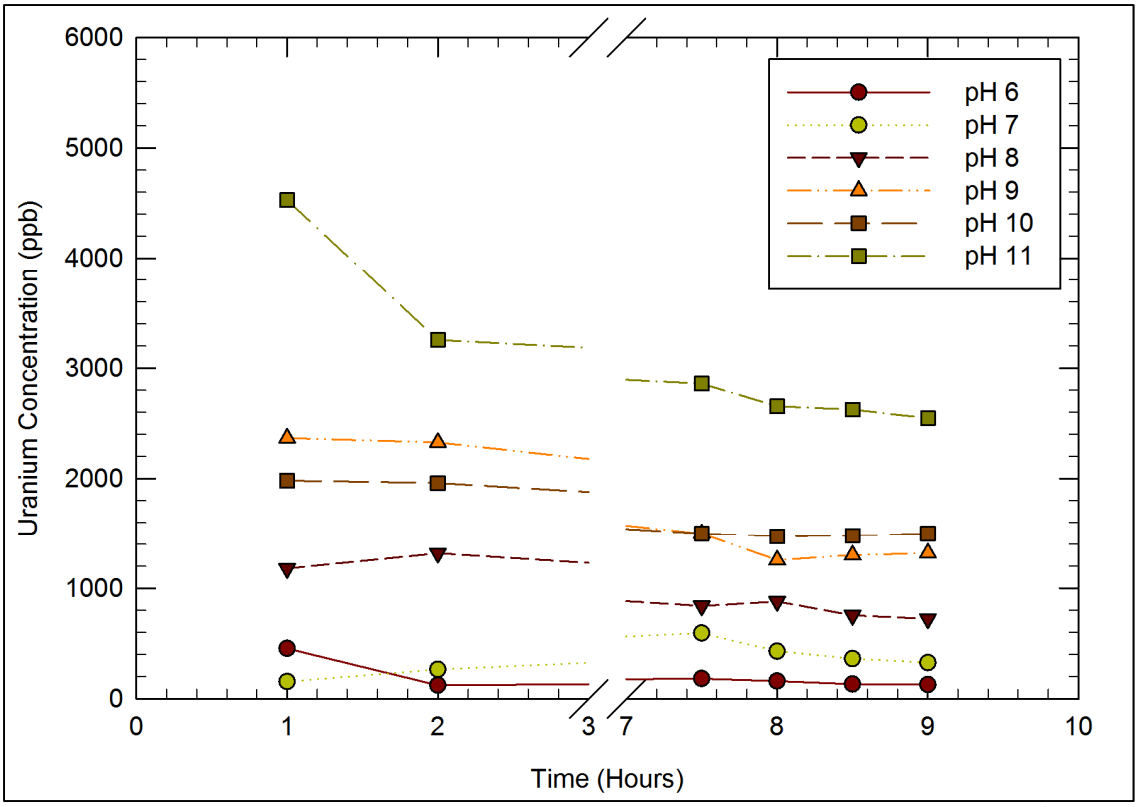


**Figure 17 Change in the uranium concentration over time for 3mM bicarboante at 23°C**

A normalized dissolution rate was calculated for each component and at each sampling interval using the following formula (effluent concentrations of uranium, dissolution rate are presented in appendix):

$$R_i = (C_i - C_{ib})\frac{q}{f_i S} \tag{9}$$

Where:

$R_i$ = the normalized dissolution rate for element $i$ (g $m^{-2}$ $d^{-1}$),

$q$ = Flow rate, (L $d^{-1}$),

$C_i$, $C_{ib}$ = concentration of component $i$ in the effluent, mean background concentration (g $L^{-1}$),

$f_i$ = the mass fraction of the element in the metal (dimensionless), and

S = the surface area of the sample ($m^2$).

From the experimental results, the dissolution rate of Na-autunite in bicarbonate solution was derived using:

$$R = k[HCO_3^-]_T^{\eta} \quad (10)$$

Where:

R = the dissolution rate (mol $m^{-2}$ $s^{-1}$),

*k* = the intrinsic rate constant (mol $m^{-2}$ $s^{-1}$),

$[HCO_3^-]_T$ = the total bicarbonate concentration (mol $L^{-1}$), and

□ = the power law coefficient (dimensionless).

A non-linear regression was performed at each temperature to determine the slope (power law coefficient), □. The resulting regression coefficient over the entire data helped to determine the intrinsic rate constant, k (mol $m^{-2}$ $s^{-1}$).

Figure 18 shows the rate of uranium release from synthetic Na-autunite at pH 6 across aqueous bicarbonate concentrations from 0.0005 to 0.003 M and temperature values of 5, 23, 40 and 60°C. Under these conditions, the increase in the rate of uranium release from Na-autunite increased from 2.74 x $10^{-12}$ (mol $m^{-2}$ $s^{-1}$) at 0.0005 M and 5°C to 4.58 x $10^{-11}$ (mol $m^{-2}$ $s^{-1}$) at 0.003 M and 60°C. It is evident that there is 16.7 fold increase in the uranium release with an increase in the bicarbonate concentration at a constant slope (η) value of 0.66 ± 0.08. However, the rate constant (k) showed dependency on the temperature with a shift in the values at 40 and 60°C when compared to the values at 5 and 23°C; the average rate constant was estimated as 4.82 x $10^{-10}$ (mol $m^{-2}$ $s^{-1}$). Figure 19 presents the rate of uranium release as a function of bicarbonate concentration from

synthetic Na-autunite at pH 7; the rate of release of uranium increase was in the range of 1.7 - 2.7. The rate of uranium release increased from 3.60 x $10^{-12}$ (mol $m^{-2}$ $s^{-1}$) at 0.0005 M and 5°C to 6.00 x $10^{-11}$ (mol $m^{-2}$ $s^{-1}$) at 0.003 M and 60°C. On average, the uranium release increased by 3.4 fold at pH 7 when compared to the release of uranium at pH 6. The nonlinear regression of the data at pH 7 was performed for temperatures 23, 40 60°C; resulting regression coefficients were determined as □= 0.03 ± 0.02 and k = 3.85 x $10^{-10}$ (mol $m^{-2}$ $s^{-1}$). Geochemical modeling results based on steady state effluent concentrations for Na-autunite are presented in Table 8. At pH 6 - 7, the system is under-saturated with Schoepite and β-$UO_2(OH)_2$ at all bicarbonate concentrations tested and $(UO_2)_3(PO_4)_2$(s) is saturated at pH 6 and 7; therefore, there is a potential for a secondary phase formation with respect to $(UO_2)_3(PO_4)_2$(s). This potential formation indicates that the concentration of uranium is not attributed only to the dissolution of Na-autunite, but also to the secondary phase controlling the net uranium concentrations.

**Table 8 Saturation indices of uranyl compounds from geochemical model**

| pH | Bicarbonate (M) | $(UO_2)_3(PO_4)_2$(s) | Schoepite | β-$UO_2(OH)_2$ |
|---|---|---|---|---|
| 6 | 0.0005 | 5.079 | -0.11 | -0.338 |
| | 0.001 | 4.902 | -0.206 | -0.435 |
| | 0.002 | 4.572 | -0.382 | -0.61 |
| | 0.003 | 4.305 | -0.522 | -0.75 |
| 7 | 0.0005 | 3.388 | 0.189 | -0.039 |
| | 0.001 | 2.799 | -0.114 | -0.342 |
| | 0.002 | 1.846 | -0.595 | -0.824 |
| | 0.003 | 1.224 | -0.907 | -1.136 |
| 8 | 0.0005 | 0.963 | 0.368 | 0.139 |
| | 0.001 | -0.094 | -0.163 | -0.391 |
| | 0.002 | -1.265 | -0.748 | -0.976 |
| | 0.003 | -1.962 | -1.096 | -1.324 |
| 9 | 0.0005 | -1.583 | 0.58 | 0.352 |
| | 0.001 | -2.377 | 0.183 | -0.045 |
| | 0.002 | -3.543 | -0.399 | -0.627 |
| | 0.003 | -4.242 | -0.747 | -0.975 |
| 10 | 0.0005 | -4.609 | 0.569 | 0.341 |
| | 0.001 | -4.738 | 0.505 | 0.277 |
| | 0.002 | -5.147 | 0.302 | 0.074 |
| | 0.003 | -5.678 | 0.037 | -0.191 |
| 11 | 0.0005 | -8.669 | 0.342 | 0.112 |
| | 0.001 | -8.739 | 0.32 | 0.09 |
| | 0.002 | -8.948 | 0.254 | 0.024 |
| | 0.003 | -9.285 | 0.144 | -0.086 |

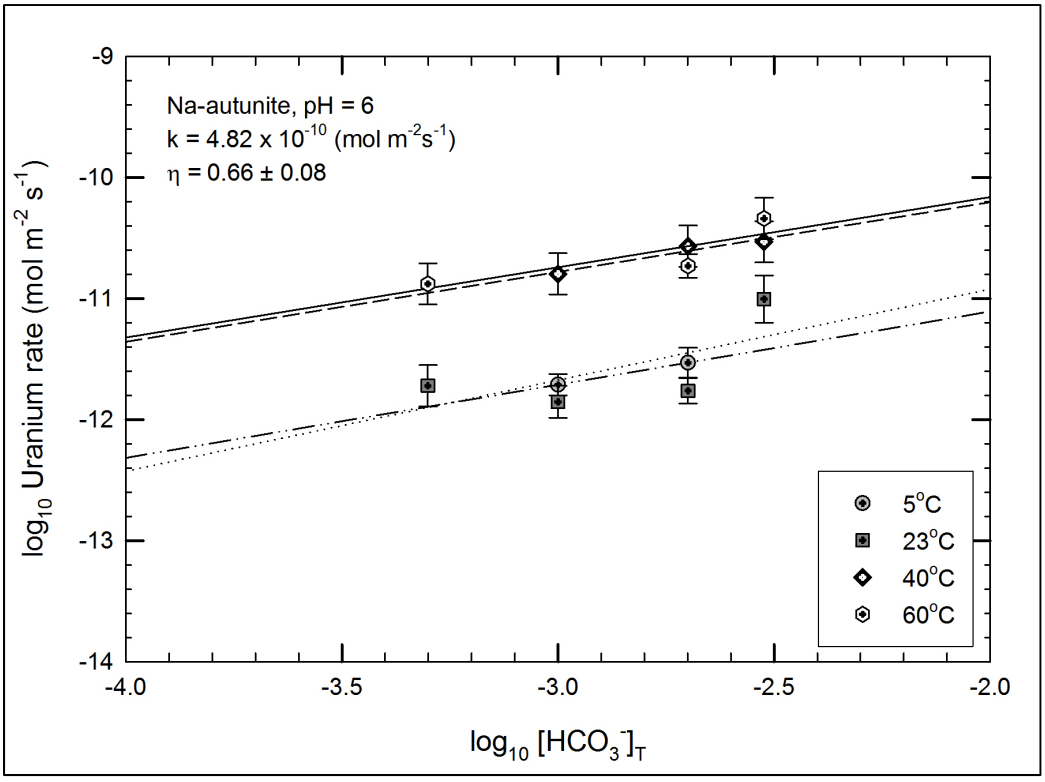


**Figure 18 Uranium rate of release as a function of bicarbonate concentration at pH 6**

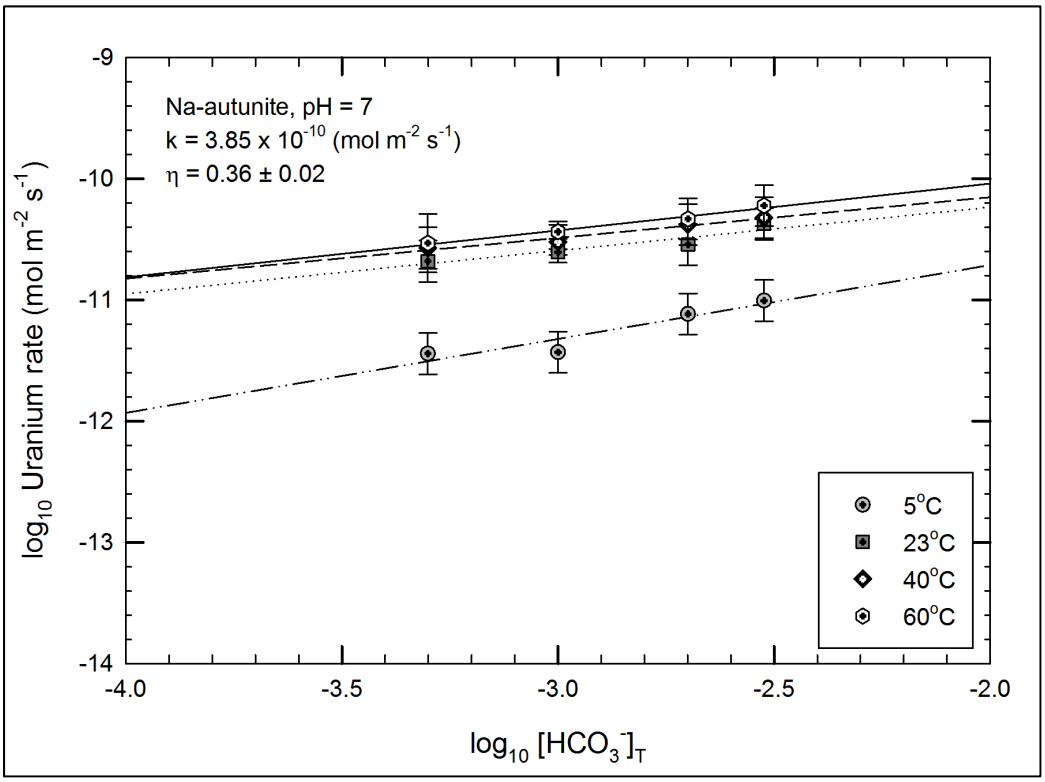


**Figure 19 Uranium rate of release as a function of bicarbonate concentration at pH 7**

The increase in the rate of uranium release over the bicarbonate concentrations tested at pH 8 was in the range of 3.2 - 5.6 (Figure 20). The rate of uranium release at pH 8 amplified by ~1.7 fold from 7.02 x $10^{-12}$ to 6.89 x $10^{-11}$ (mol $m^{-2}$ $s^{-1}$) when compared to the rate at pH 7. The nonlinear regression of data at pH 8 provided regression coefficient values of k = 1.48 x $10^{-9}$ (mol $m^{-2}$ $s^{-1}$) and □ = 0.56 ± 0.03. According to the geochemical modeling data (Table 8), Schoepite, β-$UO_2(OH)_2$, and $(UO_2)_3(PO_4)_2$(s) were saturated at low bicarbonate concentration 0.5mM while they remained under-saturated at bicarbonate concentrations higher than 1mM. This suggests that the concentrations of uranium are solely attributed to dissolution of autunite.

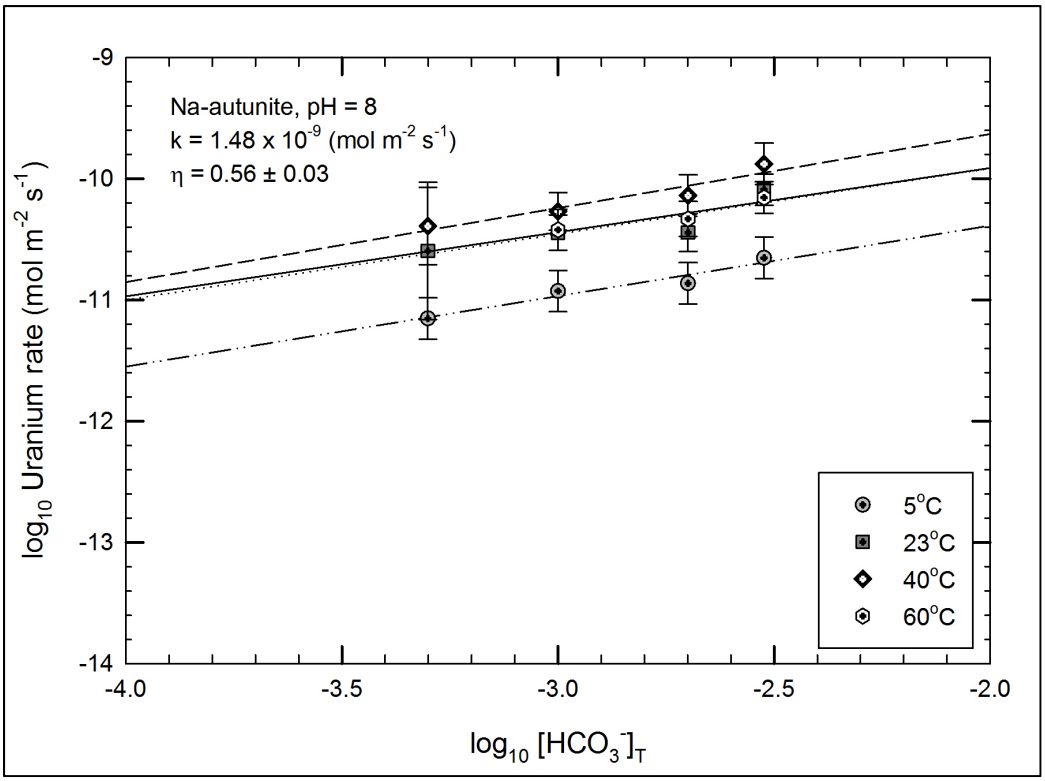


**Figure 20 Uranium rate of release as a function of bicarbonate concentration at pH 8**

The rate of release of uranium from synthetic Na-autunite at pH 9 is shown in Figure 21. The dissolution of uranium at 5°C showed only a minor variation with the change in the

bicarbonate concentration; however, at other temperatures, the rate of dissolution varied at a constant slope (□) of 0.61 ± 0.04 and the k value was estimated as 3.19 x $10^{-9}$ (mol $m^{-2}$ $s^{-1}$). The rate of dissolution shown to improve at ~3.3 fold over the range of bicarbonate concentrations tested at pH 8. At pH 9, the effect of bicarbonate resulted in 1.8 - 4.7 times increase in the rate of uranium release for all bicarbonate concentrations tested. The value of uranium release at 5°C and 0.0005 M bicarbonate was estimated to be 3.66 x $10^{-11}$ and increased to 2.04 x $10^{-10}$ (mol $m^{-2}$ $s^{-1}$) at 60°C and 0.003 M bicarbonate concentration. Geochemical modeling data at pH 9 (Table 8) predicted that $(UO_2)_3(PO_4)_2$(s) was under-saturated at all bicarbonate concentrations tested and Schoepite was found under-saturated at 0.002 - 0.003 M of bicarbonate. At 0.0005M of bicarbonate, Schoepite was saturated, resulting in secondary mineral formation that controls the net concentration of uranium in the system.

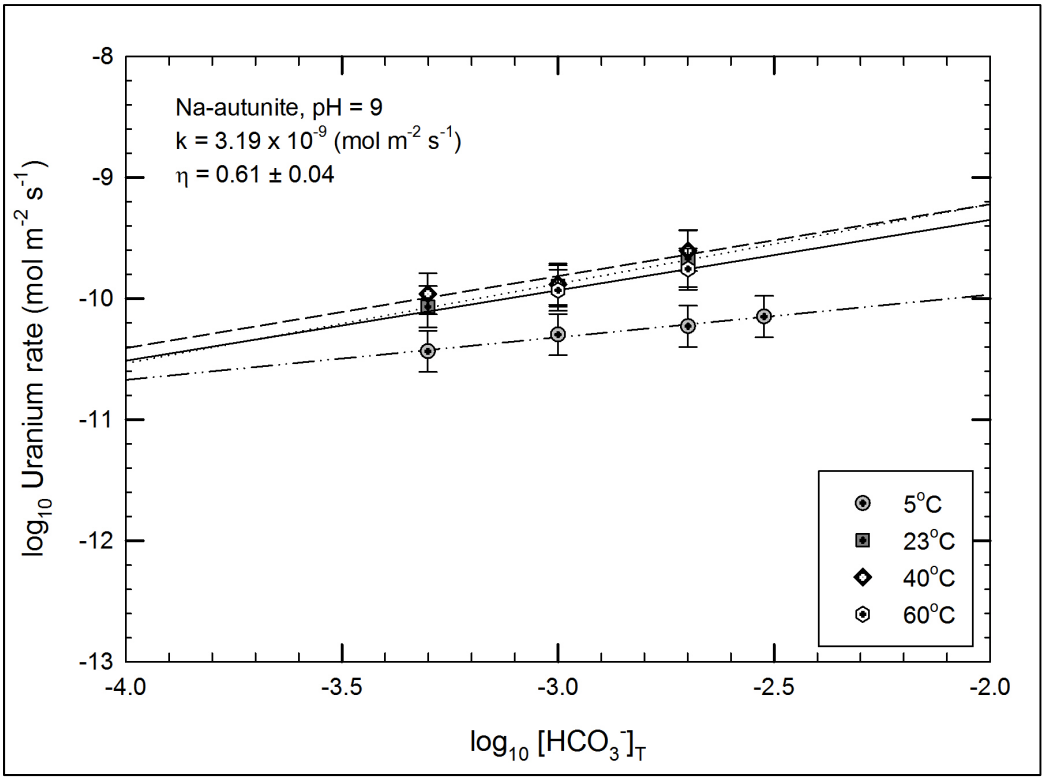


**Figure 21 Uranium rate of release as a function of bicarbonate concentration at pH 9**

Figure 22 and Figure 23 show the rate of release of uranium from Na-autunite at pH 10 and pH 11 over the conditions tested. At pH 10 and pH 11, temperature showed on influence on the dissolution of uranium from Na-autunite. The regression coefficient values of k and □ at pH 10 and 11 were evaluated to be k = 4.25 x $10^{-9}$ and 5.80 x $10^{-9}$ (mol $m^{-2}$ $s^{-1}$) and □ = 0.39 ± 0.02 and 0.51 ± 0.02, respectively. The increase in the dissolution at pH 10 - 11 was found to be in the order of ~ 1.5 - 2.0 times and 2.0 - 2.7 times, respectively. Schoepite and β-$UO_2(OH)_2$ became saturated at pH 10 – 11 creating a possibility for secondary phase formation which controls the concentration of uranium in the solution.

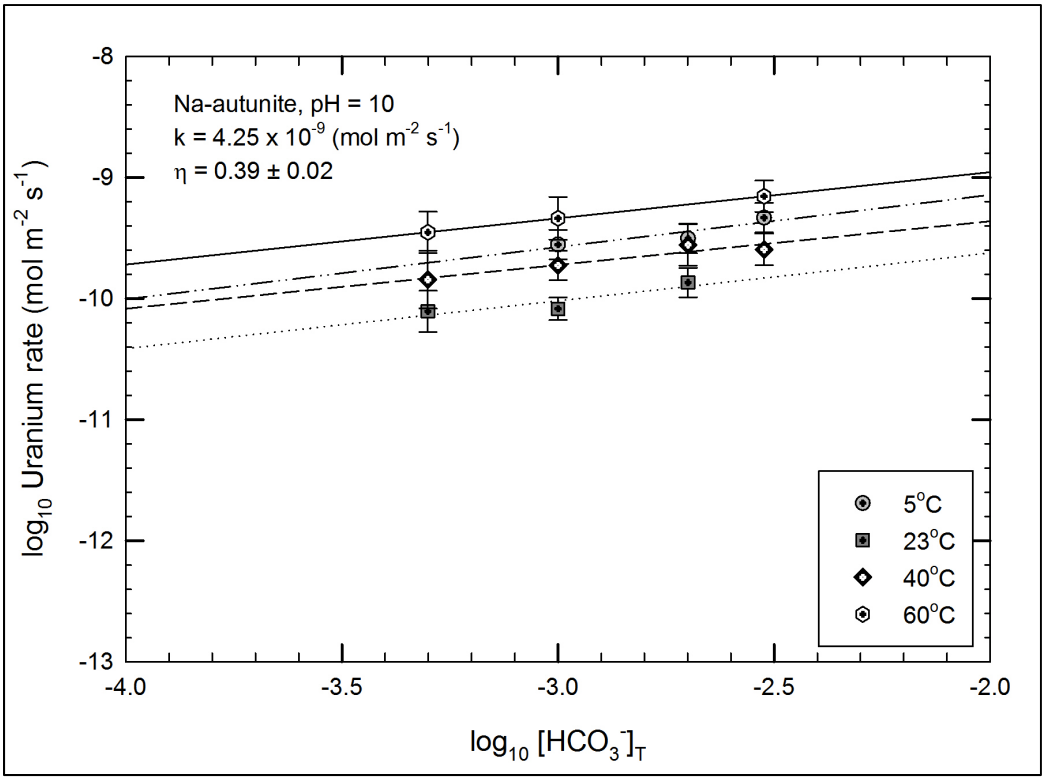


**Figure 22 Uranium rate of release as a function of bicarbonate concentration at pH 10**

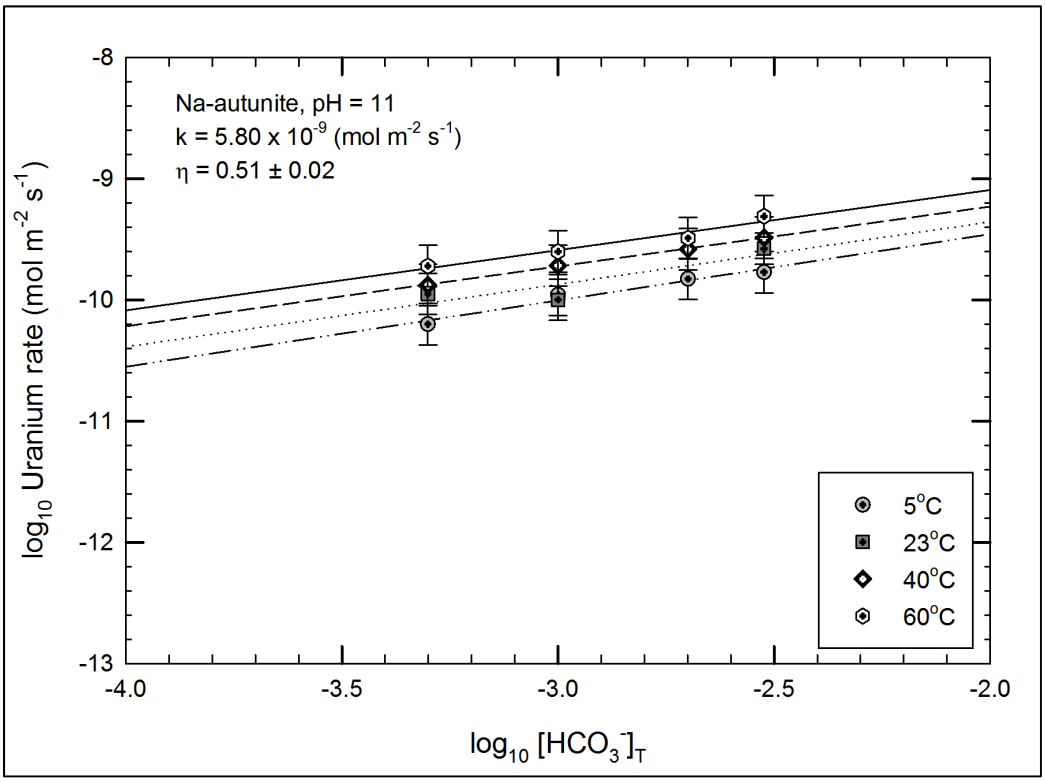


**Figure 23 Uranium rate of release as a function of bicarbonate concentration at pH 11**

3D graphs were constructed with bicarbonate concentrations, pH and the rate of release of uranium along the X, Y, and Z-axes, respectively. 2D graphs show the change in the release of uranium with one variable (bicarbonate concentration) at constant pH whereas 3D graphs provide insight into how the rate of release of uranium changed within the system with the change in bicarbonate concentration and pH.

Figure 24 shows the change in the rate of uranium release from Na-autunite at different temperatures (5 - 60$^{o}$C) with the change in the bicarbonate concentration (0.0005 - 0.003 M) and pH (6 - 11) on a 3D plot. It is evident from the figures that at low pH values, 6 - 8, the rate of uranium release increases with an increase in the bicarbonate concentration; however, at high pH values, 9 - 11, the effect of pH dominates the system and the addition of bicarbonate shows a modest quantifiable increase in the uranium release. At lower pH values, the increase in the rate of uranium release increased with the change in the bicarbonate concentrations; the amount of dissolution at high bicarbonate concentrations is much higher compared to the dissolution at low bicarbonate concentration at the same pH values. At high pH values, the effect of bicarbonate was reduced considerably at all bicarbonate concentrations tested.

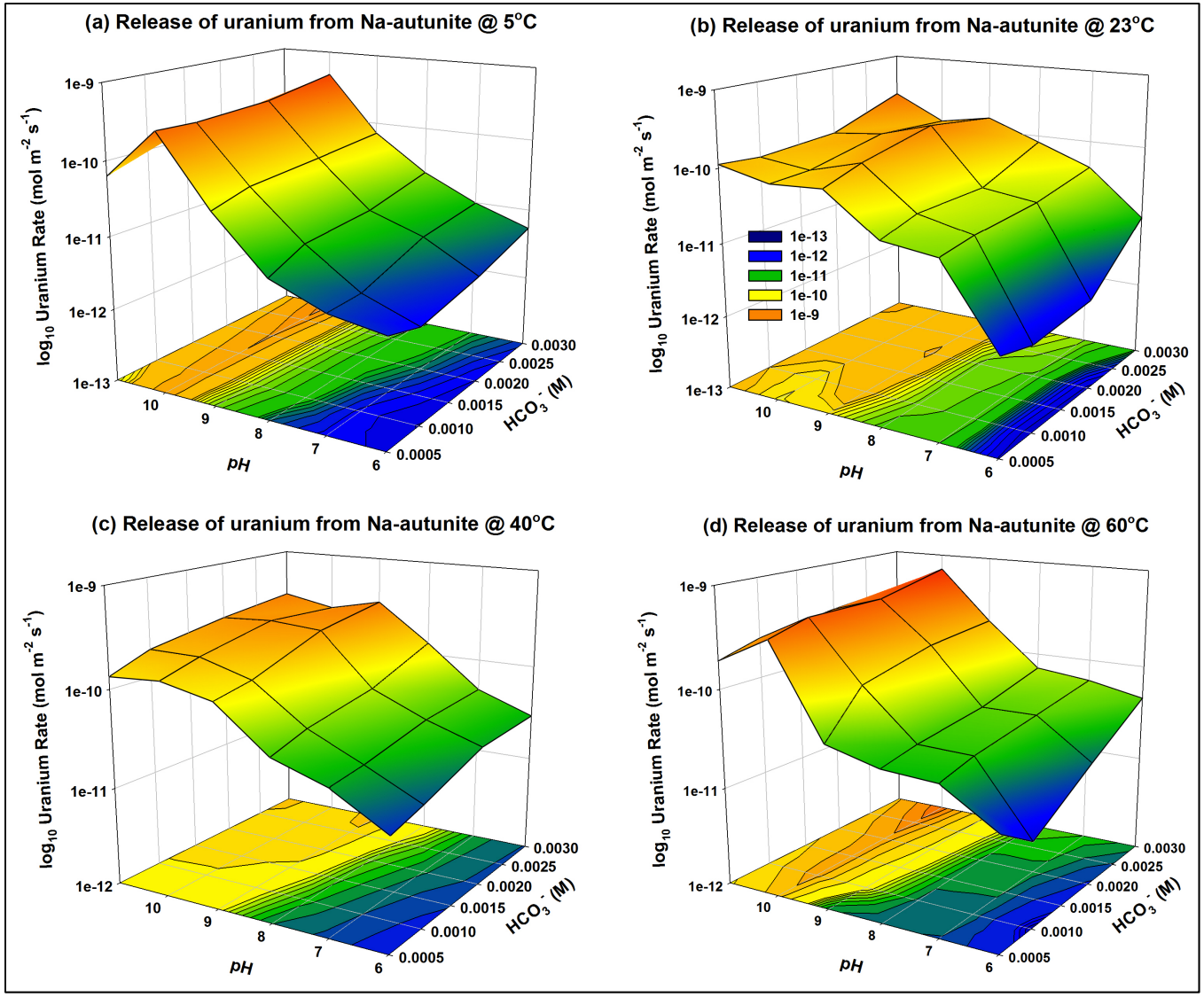


**Figure 24 3D representation of uranium release from Na-autuntie at 5 - 60°C**

Table 9 shows the comparison of the uranium release rates from Na-autunite in the presence and absence of bicarbonate. Literature data presented by Wellman et al., (2006) for uranium release from Na-autunite in the absence of bicarbonate was compared to the current study at 23$^{o}$C in a pH range of 7 - 10. At pH 7, the increase in the bicarbonate concentration caused the increase in the uranium rate of release from Na-autunite in the order of magnitude of 370. However, with the increase in the pH values (8 - 10), the observed increase in the uranium rate of release from Na-autunite was only 30, 25, and 4.0 fold, respectively. At low pH values, bicarbonate concentrations showed higher influence on the system while the effect of bicarbonate was noticed to reduce at higher pH values, consistent with the results showed in 3D plots.

**Table 9 Effect of bicarbonate on the dissolution of uranium from Na-autunite**

| pH | $HCO_3^-$ (M) | Rate of U (mol $m^{-2}$ $s^{-1}$) | Ratio to 0 M $HCO_3^-$ |
|---|---|---|---|
| 7 | 0.0000 | 1.15E-13* | 1.00 |
| | 0.0005 | 2.08E-11 | 181.59 |
| | 0.0010 | 2.48E-11 | 215.91 |
| | 0.0020 | 2.86E-11 | 249.13 |
| | 0.0030 | 4.23E-11 | 368.52 |
| 8 | 0.0000 | 2.79E-12* | 1.00 |
| | 0.0005 | 2.54E-11 | 9.10 |
| | 0.0010 | 3.58E-11 | 12.85 |
| | 0.0020 | 3.59E-11 | 12.88 |
| | 0.0030 | 8.13E-11 | 29.18 |
| 9 | 0.0000 | 8.75E-12* | 1.00 |
| | 0.0005 | 8.56E-11 | 9.77 |
| | 0.0010 | 1.27E-10 | 14.50 |
| | 0.0020 | 2.13E-10 | 24.30 |
| | 0.0030 | 1.55E-10 | 17.66 |
| 10 | 0.0000 | 3.48E-11* | 1.00 |
| | 0.0005 | 7.83E-11 | 2.25 |
| | 0.0010 | 8.23E-11 | 2.37 |
| | 0.0020 | 1.35E-10 | 3.89 |
| | 0.0030 | 1.27E-10 | 3.66 |

* Indicates uranium release date from (Wellman et al., 2006).

Figure 25 depict the dissolution rate of sodium and phosphorus from Na-autunite at pH 6 and pH 11 across bicarbonate concentrations of 0.0005 to 0.003 M and across a temperature range of 5 to 60$^{o}$C. Sodium release from Na-autunite exhibits on deviation with the increase in the temperature (5 - 60$^{o}$C) and bicarbonate concentration (0.0005 - 0.003 M). Interlayer cations (i.e., $Na^{+}$) release from minerals is generally subjected to two separate reactions: matrix dissolution and alkali-hydrogen exchange. The mechanism that may contribute to the release of interlayer cations from the structure depends on the saturation state of the system. When the system is near saturation, the activities of dissolved species near and/or in contact with the solid phase increase, resulting in a decrease in the matrix dissolution rate. Concurrently, the chemical potential difference between autunite and solution will be the driving force for cation diffusion. Dissolution of the autunite matrix will also contribute to the concentration of dissolved cations in solution, therefore, two distinct mechanisms, ion exchange and matrix dissolution, account for $Na^{+}$.

Phosphorus release from Na-autunite showed no differentiable change with the change in temperature and bicarbonate concentration. Geochemical modeling data suggested that the possible secondary minerals containing phosphorus are saturated, limiting the amount of phosphorus available for dissolution.

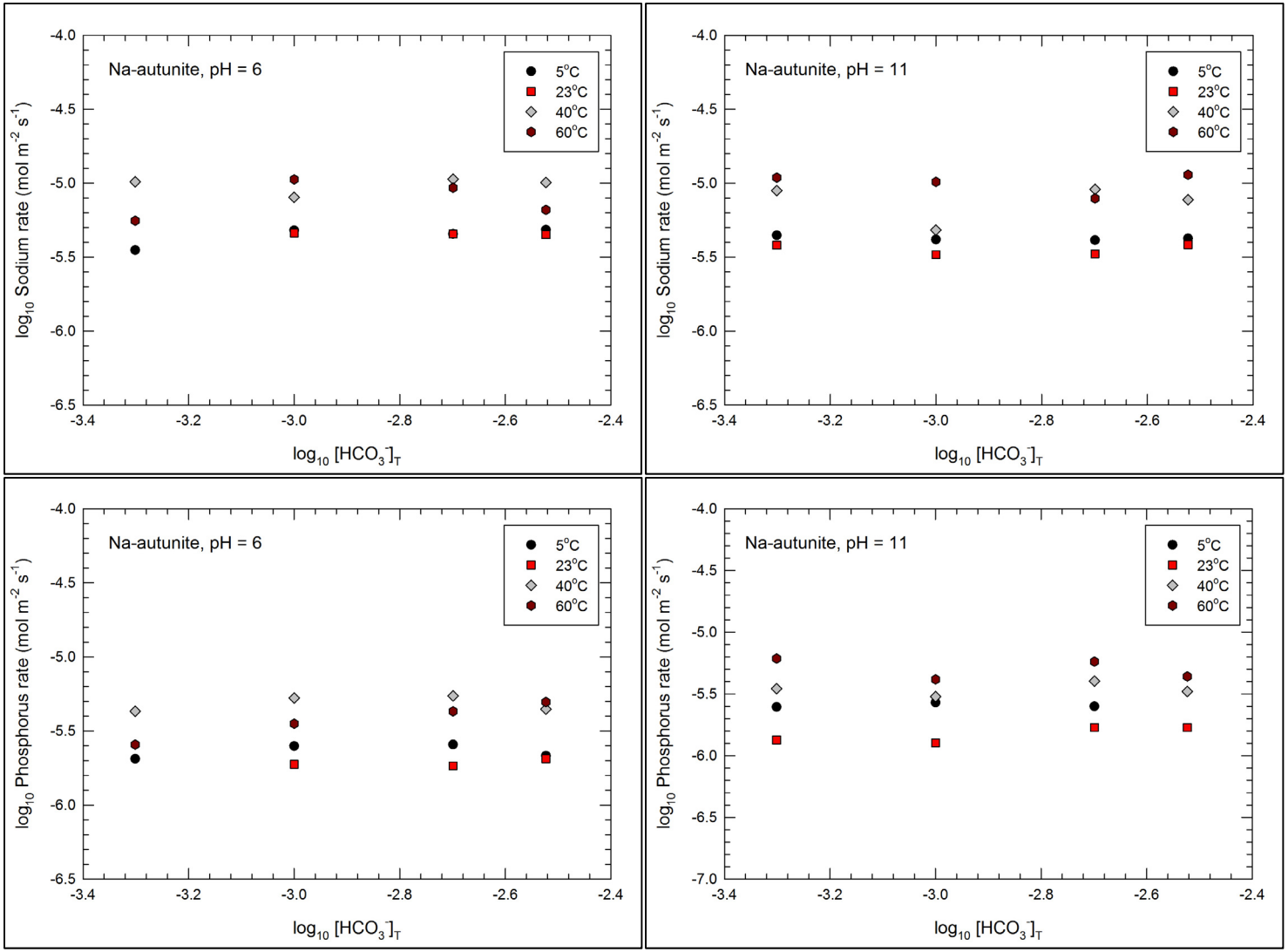


**Figure 25 Sodium and Phosphate rate of release as a function of bicarbonate concentration at pH 6 and pH 11**

The change in the rate of release of sodium (Na) from Na-autunite with respect to bicarbonate concentration (0.0005 - 0.003M) and pH (6 - 11) at a temperature of 5, 23, 40, and 60$^{o}$C are shown in appendix (Figure A1 - A4) respectively. It is evident from the graphs that the change in the rate of release of sodium from Na-autunite with the increase in pH and bicarbonate concentration is invariant. The rate of release of phosphorus from Na-autunite at varying bicarbonate concentrations (0.0005 - 0.003M) and pH (6 - 11) and at a temperature of 5, 23, 40, and 60$^{o}$C is shown in appendix (Figure A5 - A8). The phosphorus rate of release is not affected by the increase in the pH as well as the increase in the bicarbonate concentration.

# CONCLUSIONS

The rate of dissolution of Na-autunite was evaluated under different bicarbonate concentrations ranging from 0.0005 to 0.003 M via single-pass flow-through cell experiments, which provide insight to the geochemical cycle of the uranium system, the hydro-geochemical parameters that affect the mobility of uranium. The experiments conducted were designed to evaluate the effects of pH (6 - 11) and temperature (5 to 60$^{o}$C) on the carbonate promoted dissolution of synthetic Na-autunite.

The rate of release of uranium from Na-autunite is directly correlated to the concentration of bicarbonate. The bicarbonate ion has a tendency to form soluble complexes with uranium, thus releasing uranium from Na-autunite. Results from the experiments showed that the rate of uranium release increased with an increase in the bicarbonate concentrations at lower pH and the effect of bicarbonate was higher at high bicarbonate concentrations (0.003 M) tested. As the pH of the system increased, the effect of bicarbonate reduced due to the dominance of the pH effect. The increase in the uranium release was in the order of 1.5 - 5.0 times with an increase in the bicarbonate concentration at pH of 6 - 11 and temperature of 5 - 60$^{o}$C.

The geochemical modeling data from Visual MINTEQ showed that, at low pH (pH 6 and pH 7), some of the possible secondary phases that contain uranium are saturated and some are unsaturated. At pH 8 and pH 9, the system became mostly unsaturated, suggesting an increase in the rate of release of uranium from Na-autunite and secondary phase minerals. At pH 10 and 11, the system is saturated with respect to Schoepite and β-$UO_2(OH)_2$, resulting in the lower release of uranium at high pH.

The rate of release of sodium and phosphate shows no differentiable change with change in the concentration of bicarbonate. The geochemical modeling data showed that the amount of sodium and phosphate dissolved is much lower than the amount of sodium and phosphate precipitated.

REFERENCES

**Arey S., Seaman J., and Bertsch P.,** Immobilization of Uranium in Contaminated Sediments by Hydroxyapatite Addition - Aiken: Environmental Science & Technology, 1999: Vol. 33, pp. 337 - 342.

**Bostick W. D., Stevenson R. J., Harris L. A., Peery D., Hall J.R., Shoemaker J. L., Jarabek R. J., and Munday E. B.,** Use of Apatite for Chemical Stabilization of Subsurface Contaminants, Oak Ridge: Materials and Chemistry Laboratory, Inc., 2003.

**Brunauer S., Emmett P. H., and Teller E.,** Adsorption of Gases in Multimolecular Layers, Journal of the American Chemical Society, 1938: Vol. 60, pp. 309 - 319.

**Clark D. L., Hobart D. E., and Neu M. P.,** Actinide Carbonte Complexes and Their Importance in Actinide Environmental Chemistry, Chemical Reviews, 1995: Vol. 95, pp. 25 - 48.

**Corbridge D. E. C.,** Phosphorus: An Outline of Its Chemistry, Biochemistry, and Technology, Amsterdam: Elsevier, 1990.

**Curtis G. P., Fox P., Kohler M., and Davis J.,** A Comparison of in situ uranium KD values with a laboratory determined surface complexation model, Applied Geochemistry, 2004: pp. 1643 - 1653.

**Davis J. A., and Curtis G. P.,** Application of Surface Complexation Modeling to Describe Uranium(VI) Adsorption and Retardation at the Uranium Mill Tailings Site at Naturita, Colorado: US Nuclear Regulatory Commission, 2003.

**Davis J. A., Meece D. E., Kohler M., and Curtis, G. P.,** Approaches to surface complexation modeling of uranium(VI) adsorption on aquifer sediments, Geochimica et Cosmochimica Acta, 2004. pp. 3621 - 3641.

**Eisenbud M., and Gesell T. F.**, Environmental Radioactivity from Natural, Industrial & Military Sources, Fourth Edition: From Natural, Industrial and Military Sources, San Diego, Adademic Press, 1997.

**Ejnik J. W., Hamilton M. M., Adams P. R., and Carmichael A. J,**, Optimal sample preparation conditions for the determination of uranium in biological samples by kinetic phosphorescence analysis (KPA), Bethesda: Journal of Pharmaceutical and Biomedical Analysis, 2000, pp. 227 - 235.

**Elless M. P., and Lee S. Y.**, Uranium Solubility of Carbonate-Rich Uranium-Contaminated Soils, Water, Air, and Soil Pollution, Springer, 1998, Vol. 107, pp. 147 - 162.

**EPA Radiation Protection**, EPA, July 2011, http://www.epa.gov/radiation/radionuclides/uranium.html.

**EPA Recovery Act of 2009**, Hanford, 2011, http://www.hanford.gov/page.cfm/FAQ.

**EVS**, Environmental Science Division Argonne National Laboratory, 2011, http://web.ead.anl.gov/uranium/guide/ucompound/health/index.cfm.

**Finch R., and Burns P. C.,** Uranium: Mineralogy, Geochemistry and the Environment, Washington D.C., Mineralogical Society of America, 1999.

**Gascoyne M.,** Geochemistry of the actinides and their daughters. In Uranium-series Disequilibrium: Applications to Earth, Marine, and Environmental Science (eds. M. Ivanovich and R.S. Harmon), Clarendon Press, 1992.

**Giammar D. E., and Hering J. G.,** Time Scales for Sorption-Desorption and Surface Precipitation of Uranyl on Goethite, Pasadena: Environmental Science and Technology, 2001, pp. 3332 - 3337.

**Giammar D.,** Geochemistry of Uranium at Mineral - Water interfaces: Rates of Sorption - Desorption and dissolution-Precipitation Reactions, Pasadena, 2001.

**Gorman - Lewis D., Shavreva T., Karrie-Ann K., Burns P. C., Wellman D. M., Bruce M., Szymanowski J. E., Navrotsky A., and Fein J. B.,** Thermodynamic Properties of Autunite, Uranyl Hydrogen Phosphate, and Uranyl Orthophosphate from Solubility and Calorimetric Measurements, Environmental Science & Technology, 2009, Vol. 43, pp. 7416 - 7422.

**Grenthe I., Fuger J., Konings rjm, Lemire rj, Muller ab, Nguyen-Trung C., and Wanner H.**, Chemical Thermodynamics of Uranium, New York, North - Holland, 1992.

**Gudavalli R.,** Effect of pH and Temperature on the Carbonate Promoted Dissolution of Synthetic Sodium Meta-autunite, Student Poster, Waste Management Symposium, Phoenix, 2010.

**Gudavalli R.,** Investigation of Effects of pH and Temperature on the Carbonate Promoted Dissolution of Meta-autunite, Student Poster, Waste Management Symposium, Phoenix, 2009.

**Gudavalli R., Katsenovich Y., Lagos L., and Tansel B.,** Investigation of the Effect of Water Quality Parameters on Dissolution of Sodium Meta-autunite, Student Poster, Waste Management Symposium, Phoenix, 2012.

**Habib D. C., and Taub S.,** The Environmental Legacy of Nuclear Weapons Production in The United States, Waste Management Symposium, 1997.

**Henk-Jan D. J., and Anton M. H.,** Study of the Hydrolysis of Sodium Polyphosphate in Water Using Raman Spectroscopy, Applied Spectroscopy, 1998, Vol. 52, pp. 808 - 814.

**IEER**, Uranium: Its Uses and Hazards, Institute for Energy and Environmental Research, 2005 (http://www.ieer.org/fctsheet/uranium.html).

**Keith S., Faroon O., Roney N., Scinicariello F., and Wilbur S.,** Toxicological Profile for Uranium, 2011.

**Knox A. S., Brigmon R. L., Kaplan D. I., and Paller M. H.**, Interactions among phosphate amendments, microbes and uranium mobility in contaminated sediments, Science of the Total Environment, 2008, pp. 63 - 71.

**Krupka K. M., and Serne R. J.**, Geochemical Factors Affecting the Behavior of Antimony, Cobalt, Europium, Technetium, and Uranium in Vadose Sediments, Richland: PNNL, 2002.

**Lagos L., Katsenovich P., Gudavalli R.,** Rapid Deployment of Engineered Solutions for Environmental Problems at Hanford, Yearend Technical Report, 2012.

**Lagos L., Katsenovich Y., Pant P., Gudavalli R., Carvajal D. A.**, Rapid Deployment of Engineered Solutions for Environmental Problems at Hanford, 2011.

**Lagos L., Katsenovich Y., Pant P., Gudavalli R., Banerjee R.**, Rapid Deployment of Engineered Solutions for Environmental Problems at Hanford, 2010.

**Langmuir D.,** Aqueous environmental geochemistry, Prentice Hall, 1997.

**Lemire R. J., and Tremaine P. R.,** Uranium and plutonium equilibriums in aqueous solutions to 200 degree C, Journal of Chemical Engineering Data, 1980, pp. 361 - 370.

**Makhijani A., Chalmers L., and Smith B.**, Uranium Enrichment Just Plain Facts to Fuel an Informed Debate on Nuclear Proliferation and Nuclear Power, Institute for Energy and Environmental Research, 2004.

**Manson C. F., Turney W. R., Thomson B. M., Lu N., and Longmire P. A.**, Carbonate Leaching of Uranium from Contaminated Soils, Environmental Science & Technology, 1997, pp. 2707 - 2711.

**McGrail B. P., Ebert W. L., Bakel A. J., and Peeler, D. K.**, Measurement of kinetic rate law parameters on a Na-Ca-Al borosilicate glass for low-activity waste, Journal of Nuclear Materials, 1997, pp. 175 - 189.

**Merkel B. J., and Hasche-Berger A.,** Uranium in the Environment: Mining Impact and Consequences, Springer, 2005.

**Osmond J. K., and Cowart J. B.**, Geochemistry of the actinides and their daughters. In Uranium-series Disequilibrium: Applications to Earth, Marine, and Environmental Science (eds. M. Ivanovich and R. S. Harmon), Clarendon Press, 1992.

**Pekarek V., and Vesely V.,** A study on uranyl phosphates - II sorption properties of some 1- to 4-valent cations on uranyl hydrogen phosphate heated to various temperatures, Journal of Inorganic and Nuclear Chemistry, 1965, Vol. 27, pp. 1151 - 1158.

**Sandino A., and Bruno J.,** The solubility of $(UO_2)_3(PO_4)_2{\cdot}4H_2O(s)$ and the formation of U(VI) phosphate complexes: Their influence in uranium speciation in natural waters, Geochimica et Cosmochimica Acta, Geochimica et Cosmochimica Acta, 1992, pp. 4135 - 4145.

**Schalla R., Webber W. D., and Smith R. M.**, Selection of Sampling Pumps Used for Groundwater Monitoring at the Hanfordsite, Pacific Northwest National Laboratory, 2001.

**Serne R.J., Brown C. F., Schaef H. T., Pierce E. M., Lindberg J., Wang Z., Gassman P., and Catalano J.**, 300 Area Uranium Leach and Adsorption Project, Richland : Pacific Northwest National Laboratory, 2002.

**Settle F.,** Nuclear Chemistry Reprocessing Spent Fuel, 2009, http://chemcases.com/nuclear/nc-08.html.

**Shen C. Y., and Morgan F. W.,** Hydrolysis of Phosphorous Compounds, Environmental Phosphorous Handbook / book author: Griffith Edward. - New York: John Wiley & Sons, 1973.

**Shi Z., Liu C., Zachara J. M., Wang Z., and Deng B.,** Inhibition Effect of Secondary Phosphate Mineral Precipitation on Uranium Release from Contaminated Sediments, Environmental Science & Technology, 2009, Vol. 43, pp. 8344 - 8349.

**Sowder A. G.**, The formation, transformation, and stability of environmentally relevant uranyl mineral phases, 1998.

**Sowder A. G., Clark S. B., and Fjeld R. A.**, Dehydration of Synthetic Autunite Hydrates, Radiochimica Acta., 2000, pp. 533 - 538.

**Sparks D. L.,** Kinetics and Mechanisms of Chemical Reactions at the Soil Mineral/Water Interface, Soil Physical Chemistry, CRC Press, 1999.

**Stumm W., and Wollast R.,** Coordination chemistry of weathering: Kinetics of the surface-controlled dissolution of oxide minerals,Rev. Geophys., 1990, pp. 53 - 69.

**Stumm W., and Morgan J. J.,** Aquatic Chemistry: Chemical Equilibria and Rates in Natural Waters, New York: John Wiley & Sons, 1996.

**Takeno N.,** Atlas of Eh-pH Diagrams - Intercomparison of Thermodynamic Databases, 2005.

**Vermeul V. R., Fruchter J. S., Fritz B. G., Mackley R. D., Mendoza D. P., Wellman D. M., and Williams M. D.,** In-Situ Uranium Stabilization Through Polyphosphate Injection: Pilot-Scale Treatability Test at the 300 Area, Hanford Site, Waste Management, Phoenix, 2008.

**Vochten R., and Deliens M.**, Transformation of curite into metaautunite paragenesis and electrokinetic properties, Physics and Chemistry of Minerals, 1980, pp. 129 - 143.

**Wellman D. M., Gunderson K. M., Icenhower J. P., and Forrester S. W.**, Dissolution kinetics of synthetic and natural meta-autunite minerals, $X_{3-n}^{(n)+}[(UO_2)(PO_4)]_2 \bullet xH_2O$, under acidic conditions, Geochem. Geophys. Geosyst., 2007, pp. 16.

**Wellman D. M., Catalano J. G., Icenhower J. P., and Gamerdinger A. P.**, Synthesis and characterization of sodium meta-autunite, $Na[UO_2PO_4] \bullet 3H_2O$, Radiochimica Acta., 2005, pp. 393 - 399.

**Wellman D. M., McNamara B. K., Bacon D. H., Cordova E. A., Ermi R. M., and Top L. M.**, Dissolution kinetics of meta-torbernite under circum-neutral to alkaline conditions, Environmental Chemistry, 2009, pp. 551 - 560.

**Wellman D. M., Pierce E. M., Richards E. L., Butler B. C., Parker K. E., Glovack J. N., Burton S. D., Baum S. R., Clayton E. T., and Rodriguez E. A.**, Uranium Stabilization Through Polyphosphate Injection 300 Area Uranium Plume Treatability Demonstration Project, Richland: PNNL, 2007.

**Wellman D. M., Pierce E. M., Richards E. L., Fruchter J. S., and Vermeul V. R.**, Uranium Plume Treatability Demonstration at the Hanford Site 300 Area: Development of Polyphosphate Remediation Technology for In Situ Stabilization of Uranium, Waste Management, Phoenix, 2008.

**Wellman Dawn M., Icenhower Jonathan P., Gamerdinger Amy P., and Forrester Steven W.,** Effects of pH, temperature, and aqueous organic material on the dissolution kinetics of meta-autunite minerals, $(Na, Ca)_{2-1}[(UO_2)(PO_4)]_2 \bullet 3H_2O$, American Mineralogist, 2006, pp. 143 - 158.

**Xin D., Benjaporn B., Wei-Min W., Fendorf S., Bargar J., and Craig S. C.,** Reduction of Uranium (VI) by Soluble Iron (II) Conforms with Thermodynamic Predictions, Environmental Science and Technology, 2011, Vol. 45, pp. 4718 - 4725.

**Zachara J., Liu C., Brown C., Kelly S., and Christensen J.**, A Site-Wide Perspective on Uranium Geochemistry at the Hanford Site, Richland: Pacific Northwest National Laboratory, 2007.

**Zachara J.M., Davis, J.A., McKinley, J.P., Wellman, D.M., Liu, C., Qafoku, N., and Yabusaki, S.B.**, Uranium Geochemistry in Vadose Zone and Aquifer Sediments from the 300 Area Uranium Plume, Richland: Pacific Northwest National Laboratory, 2005.

**Zhang Peng-Chu, and Brady Michael V.,** Geochemistry of Soil Radionuclides, Soil Science Society of America, 2002.

**Zheng Z., Wan J., Song X., and Tokunaga T. K.,** Sodium meta-autunite colloids: Synthesis, characterization, and stability, Colloids and Surfaces A: Physicochemical and Engineering Aspects, 2006, pp. 48 - 55.

CHAPTER TWO

## Quantification of kinetic rate law parameters for the dissolution of sodium meta-autunite as a function of aqueous bicarbonate concentration


ABSTRACT

Singe-pass flow-through (SPFT) experiments were used to quantify the dissolution of synthetic Na-autunite and calculate kinetic rate law parameters under bicarbonate concentrations ranging from 0.0005 to 0.003 M, pH 6 to 11 and temperature variations from 5 to 60$^{o}$C. Results indicate the activation energies were unaffected by temperature and bicarbonate concentration variations, but were strongly dependent on pH conditions. As pH increased from 6 to 11, activation energy values were observed to decrease from 29.94 kJ mol$^{-1}$ to 13.07 kJ mol$^{-1}$. The calculated activation energies suggest a surface controlled dissolution mechanism, as previously suggested. Geochemical modeling results supported an increased dominance of aqueous uranyl hydroxide and bicarbonate complexes as a function of pH. The presence of these complexes decreases the chemical affinity of uranium within the system and concurrent increase in the dissolution rate of synthetic sodium autunite.

# INTRODUCTION

Uranium (VI) is a key contaminant of concern at several of DOE sites in the United States, where large quantities of radioactive waste was released into the environment from the past operations of nuclear weapon production. Once released, uranium persists in the environment and can have toxic effects on living organisms. The behavior of uranium in the environment, especially in the groundwater, is influenced by many environmental factors such as temperature, pH and the presence of various ligands. Common ligands in the environment that form stable uranyl solid phases include hydroxyl, phosphate, carbonate, silicate and organic substances (Burns et al., 1996; Lenhart et al., 2000; Davis, 2001). Uranyl ion- ligand complexation reactions often result in the precipitation of U-bearing minerals or formation of mobile aqueous species (Finch et al., 1999).

The presence of phosphate in groundwater promotes the formation of sparingly insoluble autunite minerals, $X_{3-n}^{(n)+}[(UO_2)_2(PO_4)_2]\cdot xH_2O$, greatly limiting the mobility of the uranyl cation ($UO_2^{2+}$) in the subsurface (Wellman et al., 2006). Information on the stability of uranyl- phosphate phases is limited to conditions involving pH, temperature, and a few aqueous organic materials (Wellman et al., 2006). Kinetic dissolution studies of autunite conducted in a wide range of pH and temperatures in flow-through and batch experiments illustrated a strong linear dependency of dissolution rates on pH but were relatively insensitive to temperature variations (Wellman et al., 2006 & 2007; Zheng et al., 2006).

A literature investigation on uranium geochemistry indicates that bicarbonate anion is an important complexing agent for U(VI) and in an oxidized environment is one of the main

variables that affect the dissolution of actinides and facilitate uranium desorption reactions from soil and sediments (Langmuir, 1997; Casas et al., 1998; Perez et al., 2000). Under circumneutral pH conditions, the formation of highly soluble and stable uranyl carbonate complexes, $UO_2CO_3^0$, $UO_2(CO_3)_2^{2-}$ and $UO_2(CO_3)_3^{4-}$, explains the mobility of uranyl ions (Langmuir, 1978; Guillaumont et al., 2003). The strength of uranyl carbonate complexes makes bicarbonate the most effective extractant in terms of dissolution rate and extent for recovery of U from uranyl - bearing mineral phases (Sowder et al., 2001; Perez et al., 2000). Ilton et al. (2006) evaluated the solubility of a synthetic Na-boltwoodite over a range of bicarbonate concentrations representative for pore water compositions at Hanford. They found that U dissolution rates as well as solubility were increased with increasing bicarbonate concentration and pH values from 7.9 to 9.5 and indicated that both factors related to surface reactions controlled the dissolution kinetics. The surface- controlled dissolution is described as fast attachment of the reactants to the mineral surface and then slow detachment of metal species from the surface into solution (Sparks, 1999). Uranyl ions release from autunite proceeds by a two steps process: surface coordination of $HCO_3^-$ on U(VI) mineral surface and then detachment of uranyl carbonate species (Pablo et al., 1999; Liu et al., 2004).

Considering that literature dealing with the effect of bicarbonate ions on the dissolution of uranium-bearing minerals is limited, the release of uranium during the autunite dissolution experiments was quantified as a function of aqueous bicarbonate concentrations under various pH and temperature conditions. The goal of this study was to experimentally determine rate law parameters for the dissolution kinetics of synthetic Na-autunite. Measurements were conducted via a single-pass flow-through (SPFT)

apparatus using bicarbonate TRIS (tris hydroxymethyl aminomethane)-buffered solutions for autunite dissolution experiments.

## MATERIALS AND METHODS

### 1.15 Synthesis of Sodium Meta-autunite

Sodium meta-autunite was synthesized by following the direct precipitation method described by Wellman et al. (2005), which involves mixing 110 mM of uranyl nitrate with 15 mM of sodium phosphate dibasic in 1 to 7.5 volumetric ratios at 70$^{o}$C while stirring. A rapid yellowish green precipitate indicated the formation of sodium meta-autunite; at this time, heating was terminated while stirring was continued until the solution reached room temperature. The precipitate was cured at room temperature for about 24 hours; the precipitate was filtered using vacuum filtration with a 0.45 μm disposable Nalgene filter and was washed with DI water heated to 70$^{o}$C followed by rinsing with isopropyl alcohol.

$$UO_2(NO_3)_2 \cdot 6H_2O + Na_2HPO_4 \cdot 7H_2O \rightarrow Na[(UO_2)(PO_4)] \cdot nH_2O + HNO_3 + NaNO_3 \quad (11)$$

The synthesized autunite solids were characterized by JSM-5900-LV low vacuum scanning electron microscope (SEM) at 15kV for identification of particle size. The composition and purity of the solids was determined via a Noran System Six Model 200SEM energy dispersive x-ray spectroscopy (EDS). The atomic molar ratios of sodium, oxygen, phosphorus and uranium determined by means of EDS analysis were correlated to an ideal empirical formula of Na [$UO_2PO_4$]. Pre-experimental surface area analysis was conducted following the $N_2$-adsorbtion BET method (Brunauer et al., 1938)

by using a Micromeritics ASAP 2020 surface and porosity analyzer at Pacific Northwest National Laboratory (PNNL). A Bruker 5000D XRD instrument was used for compositional analysis.

### 1.16 Single-Pass Flow-Through (SPFT) Experiments

The prediction of the effect of bicarbonate on the long-term stability of autunite minerals requires detailed knowledge of the kinetic rate law and associated parameter values on the dissolution process. A general kinetic rate equation can be used to describe the dissolution reaction of autunite and compute the flux of elements released into the aqueous phase. The equation is based on the Transition State Theory (TST) of chemical kinetics, in which the overall reaction rate is governed by the slowest elementary reaction (Aagaard, 1982; McGrail et al., 1997) and is given by

$$r = k\,\nu_i\, a_{H^+}^{\pm\eta}\, \exp\left(\frac{-E_a}{RT}\right)\left[1-\frac{Q}{K_g}\right]^{\sigma}\prod_j a_j^{n_i}, i = 1,2,....N \qquad (12)$$

Where

$r$ = the dissolution rate (g $m^{-2}$ $d^{-1}$),

$k$ = the intrinsic rate constant (g $m^{-2}$ $d^{-1}$),

$\nu_i$ = the stoichiometric coefficient of element $i$,

$a_j$ = the activity of the $j$-th aqueous species that acts as an inhibitor or catalyst,

$E_a$ = the activation energy (kJ $mol^{-1}$),

R = the gas constant (kJ $mol^{-1}$ $K^{-1}$),

T = the temperature ($^oK$),

Q = the ion activity product,

$K_g$ = the pseudo equilibrium constant,

$Q/K_g$ = chemical affinity term,

$\eta$ = the power law coefficient, and

$\sigma$ = the Temkin coefficient

The dissolution of the Na-autunite mineral was determined using a single-pass flow-through (SPFT) apparatus over a temperature range of 5 to 60$^{o}$C and a controlled pH from 6 to 11. Bicarbonate -bearing solutions prepared in the range of 0.0005 to 0.003 M were buffered with 0.05 M *tris hydroxymethyl aminomethane* (TRIS). 0.1 M hydrochloric acid and potassium hydroxide were used to adjust the pH, ranging from 6 to 11 (Table 7). The SPFT test was designed to limit the accumulation of reaction products using a sufficient ratio of the flow rate to the surface area of the mineral sample (q/S) to ensure the maximum dissolution rate or forward rate was achieved. These conditions allow maintaining the chemical affinity term, Q/K, at a value near zero in Equation 12. By observing changes in the dissolution rate over the range of experimental parameters tested, $k$, $E_a$, and $\eta$ can be easily obtained by means of standard non-linear regression. The schematic and detailed procedures of the experiments are presented in Wellman et al. (2006, 2007).

Surface area of the autunite solids was determined using a micromeritics surface and porosity analyzer by $N_2$-adsorption BET method. Samples analysis for U(VI) followed John et al. (2000) for wet/ashing procedures to completely convert the organic matter into inorganic. The details of sample preparation and analysis are presented in Section 4.6. The concentrations of sodium (Na) and phosphorus (P) were determined with an Optima

7300 ICP-OES (Perkin Elmer). For all samples, three replicate intensities were recorded from which the average and standard deviation were calculated. The total uranium concentrations were measured using a kinetic phosphorescence analyzer (KPA-11) (Chemcheck Instruments, Richland, WA).

### 1.17 Dissolution Rate Calculations

The normalized dissolution rate equation described by Equation 6 was used to determine the experimental rate of dissolution of sodium meta-autunite. Concentrations used to calculate the dissolution rates were obtained when the system reached equilibrium. The steady-state conditions were achieved after approximately six reactor volumes and the concentrations of uranium released from natural Na-autunite became invariant with respect to time for all pH and bicarbonate ranges tested.

Uncertainty associated with each parameter was considered when calculating the dissolution rate; relative errors included are final concentration (10%), background concentration (10%), mass distribution (5%), surface area (15%), and flow rate (5%). Detailed procedures for error calculations are presented in Wellman et al. (2006, 2009). The experimental results were correlated by linear regression using SigmaPlot-11.2 (Systat Software Inc.).

### 1.18 Groundwater Modeling

Steady state elemental concentrations in the effluent solution after the system reached equilibrium were used to identify the predominant uranium species in aqueous solution. The speciation modeling was performed by means of geochemical modeling software Visual MINTEQ v. 3.0 [maintained by J.Gustafsson at KTH, Sweden, available at

http://www.lwr.kth.se/English/OurSoftware/vminteq/ updated with the Nuclear Energy Agency's thermodynamic database for uranium (Guillaumont et al., 2003)].

## RESULTS AND DISCUSSION

### 1.19 Effect of Bicarbonate

The effect of bicarbonate on the dissolution of Na-autunite from experimental results was evaluated by applying common logarithm to Equation 6, resulting equation 13:

$$\log r = \log k + \eta \log\left[HCO_3^-\right] \qquad (13)$$

Where:

R = the dissolution rate (mol $m^{-2}$ $s^{-1}$),

$k$ = the intrinsic rate constant (mol $m^{-2}$ $s^{-1}$),

$HCO_3^-$ = the bicarbonate concentration (mol $L^{-1}$), and

$\eta$ = the power law coefficient (dimensionless).

A non-linear regression was performed for each temperature with dissolution rates as a function of bicarbonate concentration to determine slope and the power law coefficient, $\eta$. The resulting regression coefficient over the entire data helped to determine the intrinsic rate constant, k (mol $m^{-2}$ $s^{-1}$).

### 1.20 Estimation of thermodynamic parameters (Activation Energy of dissolution)

Activation energy, $E_a$, is an important parameter affecting the dissolution rate constants. It depends on the nature of the chemical reaction and usually "fast" reactions have a small $E_a$; those with a large $E_a$ proceed slowly. $E_a$ is independent of temperature and concentrations; however, $E_a$ has exhibited pronounced pH dependence (Zhang et al.,

2001). The activation energy can help to explain the rate-controlling process. In the case of transport-controlled dissolution, the activation energy of the dissolution process with values lower than 20 kJ $mol^{-1}$ stands for surface diffusion as the rate-controlling process (Bemer, 1978; Jordan et al., 1996). Surface controlled dissolution usually results in high activation energy; Lasaga (1984) reported that the surface controlled dissolution of silicates have activation energies in the range of 60 - 80 kJ $mol^{-1}$ and similar activation energy values (72 - 86 kJ $mol^{-1}$) were reported by various authors for alkaline earth flourides whose dissolution rates are believed to be surface controlled. The effect of bicarbonate ions in the wide range of pH and temperature variations on the activation energy of the dissolution reactions of uranyl- phosphate minerals has not been studied before. The previous studies on uranium-bearing materials suggested a surface controlled dissolution mechanism for estimated activation energies ranging between 12 - 60 $kJmol^{-1}$ (Scott et al., 1977; Zhang et al., 2001; Pablo et al., 1999).

Activation energy values for this study of a bicarbonate - promoted dissolution reaction of autunite were estimated using a modified Equation 12 describing the rate of reaction as a function of pH, temperature, saturation state of the system, and the activities of the rate enhancing or inhibiting species (McGrail, 1997), which can be described as:

$$r = k\, e^{\frac{-E_a}{RT}} \left[HCO_3^-\right]^{\eta} \qquad (14)$$

Where

r = the dissolution rate (mol $m^{-2}$ $s^{-1}$) experimentally determined from SPTF tests,

$k$ = the intrinsic rate constant (mol $m^{-2}$ $s^{-1}$),

$[HCO_3^-]$ = the bicarbonate concentration (mol $L^{-1}$),

$\square$ = the power law coefficient (dimensionless),

$E_a$ = activation energy (kJ $mol^{-1}$),

R = the universal gas constant (J $mol^{-1}$ $K^{-1}$), and

T = temperature ($^oK$).

At constant bicarbonate concentrations, the normal logarithmic values of the rate of dissolution (ln r) were plotted against the values of inverse temperature (1/T) (Figure 26). The slope of the linear regression line at each pH value was calculated and the data is presented in Table 10; values are in agreement with estimates reported by Heisbourg et al. (2003) for thorium-uranium complexes. These values also revealed a weak dependency of the dissolution rate on the temperature. The average activation energy at pH 6 and 7 was estimated to be 29.94 kJ $mol^{-1}$ and 26.87 kJ $mol^{-1}$, respectively. These values are higher than the average activation energy observed at higher pH values, suggesting that the dissolution is faster at high pH. The activation energy observed at pH 6 and 7 also suggests that the dissolution process is surface controlled; whereas at higher pH values, the transfer of uranium may be due to adsorption or ion exchange. The calculated activation energies are in good agreement with that reported in the literature for similar materials (Zhang et al., 2001, Heisbourg et al., 2003).

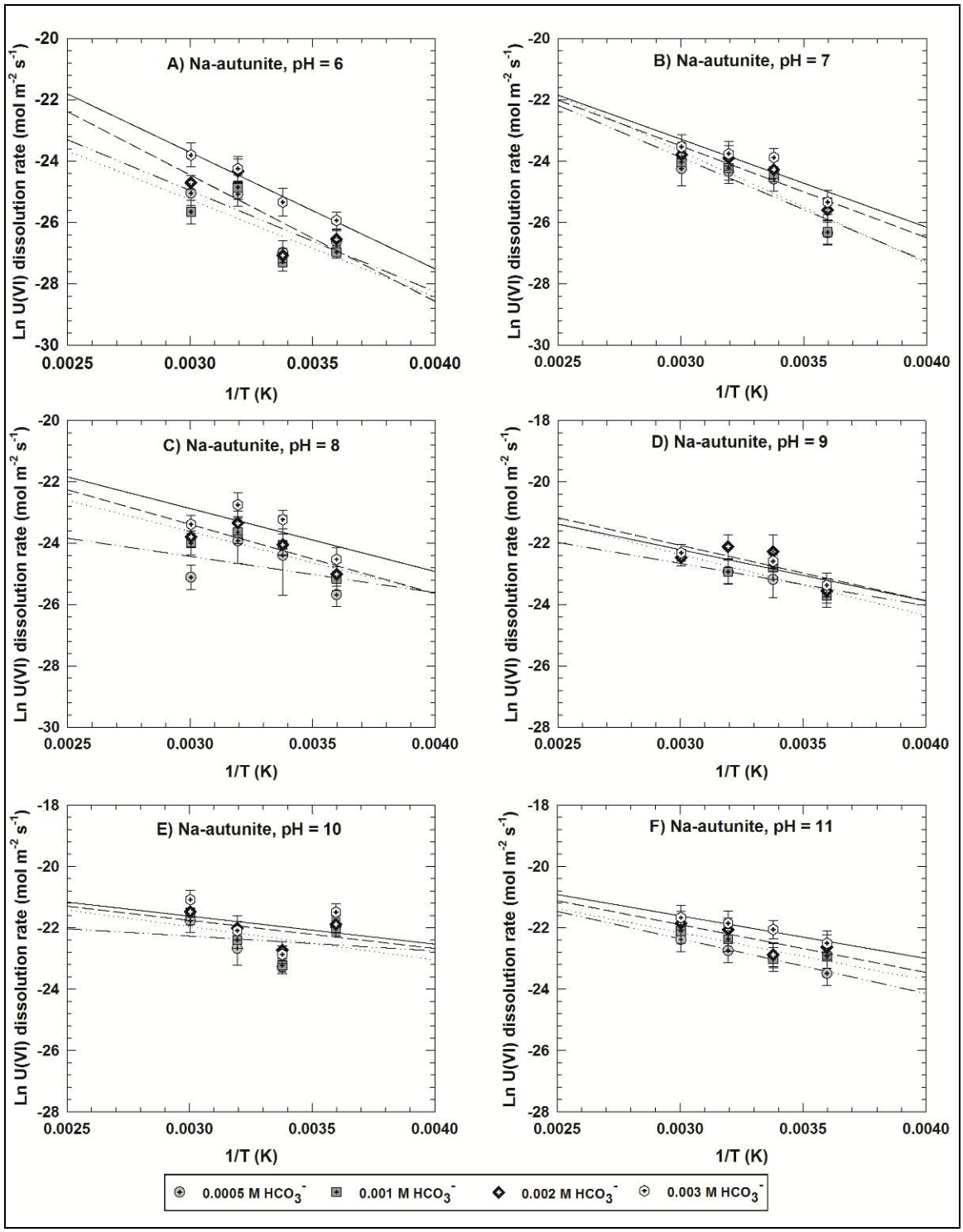


**Figure 26 Activation energies of the Na-autunite dissolution at various pH values**

**Table 10 Activation energies of sodium autunite dissolution**

| $[HCO_3^-]$ (M) | 0.0005 | 0.001 | 0.002 | 0.003 |
|---|---|---|---|---|
| **pH** | **$E_a$ (kJ mol$^{-1}$)** | | | |
| 6 | 27.465 | 26.387 | 34.295 | 31.61 |
| 7 | 28.285 | 30.426 | 24.872 | 23.882 |
| 8 | 9.824 | 16.872 | 18.751 | 17.091 |
| 9 | 11.417 | 16.553 | 14.983 | 13.863 |
| 10 | 4.031 | 9.028 | 7.627 | 7.579 |
| 11 | 14.831 | 12.947 | 12.955 | 11.511 |

The pseudo equilibrium constant, Kg, was estimated using Equation 15, based on the assumption that the concentration of bicarbonate is the rate limiting factor that controls the reaction.

$$r = K_g \left[ HCO_3^- \right] \tag{15}$$

Where:

r = the rate of dissolution (g m$^{-2}$ d$^{-1}$), and

$[HCO^-_3]$ = the total bicarbonate concentration (M).

The values of U(VI) rate dissolution (Y-axis) at different pH values were plotted against variations of bicarbonate concentrations (X-axis) (Figure 27). The resulting slopes of the regression lines provided values of $K_g$ and are listed in Table 11.

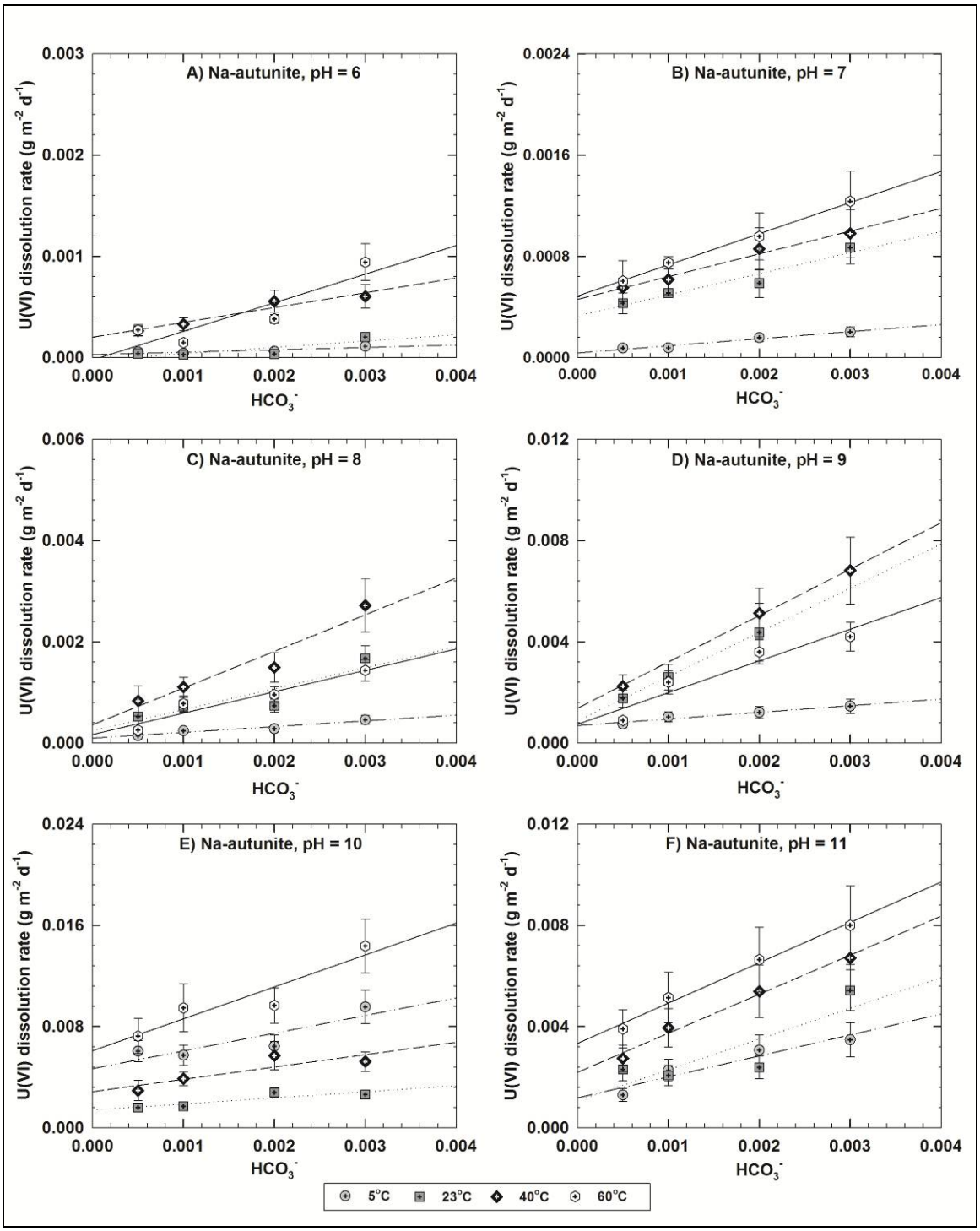


**Figure 27 Changes in the U(VI) release as a function of bicarbonate**

**Table 11 Pseudo equilibrium constants and enthalpy values at various temperatures**

| Temp ($^oC$) | $K_g$ | | | | | |
|---|---|---|---|---|---|---|
| | **pH 6** | **pH 7** | **pH 8** | **pH 9** | **pH 10** | **pH 11** |
| 5 | 0.024 | 0.056 | 0.114 | 0.261 | 1.395 | 0.828 |
| 23 | 0.063 | 0.167 | 0.415 | 1.746 | 0.481 | 1.245 |
| 40 | 0.146 | 0.179 | 0.432 | 1.833 | 1.836 | 1.544 |
| 60 | 0.282 | 0.246 | 0.422 | 1.252 | 2.523 | 1.595 |
| **ΔH (kJ mol$^{-1}$)** | 34.85 | 19.39 | 17.24 | 24.80 | 12.44 | 9.41 |

We next examined the relationship between the pseudo equilibrium constant, $K_g$, and the temperature to estimate the enthalpy of the system:

$$\Delta H = -RT \ln K_g \tag{16}$$

Where:

ΔH = the enthalpy (kJ mol$^{-1}$),

R = the universal gas constant (J mol$^{-1}$ K$^{-1}$), and

T = temperature ($^o$K).

The plot of normal logarithmic Kg values on the Y-axis and the variation of inverse temperature (1/T) on the X-axis is presented on Figure 28; the resulting slope of the regression lines at each pH provided the enthalpy values. These values represent a change in enthalpy for the endothermic reactions that absorb energy to break U(VI) bonds during autunite dissolution. Calculations showed that $K_g$ parameter is increased at larger pH and temperature, which invokes a chemical affinity term, $Q/K_g$, to decrease. The change in

affinity term caused by the presence of ligands has been previously suggested to affect the dissolution rate (Kraemer et al., 1997).

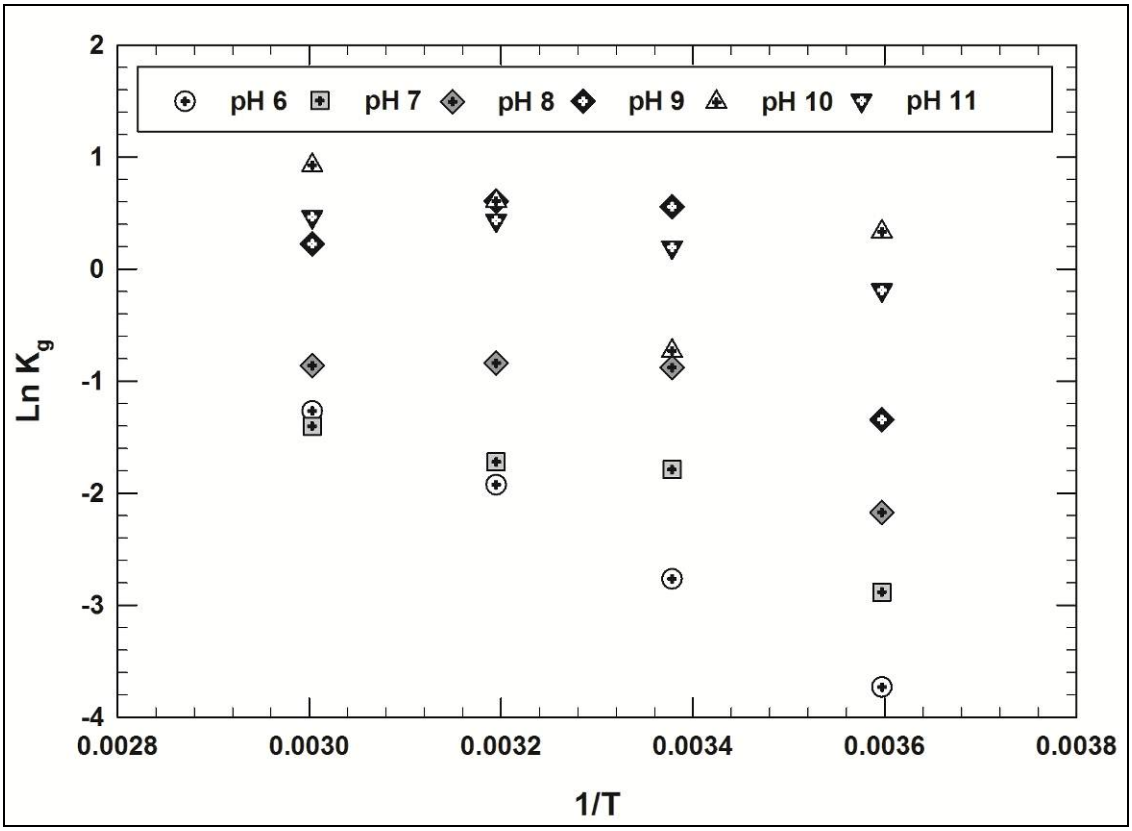


**Figure 28 Changes in the pseudo equilibrium constant as a function of inverse temperature for Na-autunite**

The theoretical rate of uranium release was calculated taking into account experimentally determined parameters associated with Equation 12, including estimated activation energies and $K_g$ values. The theoretically determined rate of U(VI) release differs from the experimentally determined values within an error range of ±10%.

### 1.21 Visual MINTEQ speciation modeling

Geochemical modeling suggests that uranyl speciation is strongly dependent on pH and the concentration of carbonate ions in the solution (Figures 29, 30). At pH 6 and a

concentration of bicarbonate in the solution of 0.0005 M $HCO_3^-$, uranium-carbonate complexes, $UO_2(CO_3)_2^{-2}$, $UO_2CO_3$ (aq), are found as the predominant species. At bicarbonate concentration of 0.0005 M and between pH 7 and 10, uranyl tri-carbonate [$UO_2(CO_3)_3^{-4}$] is a prevailing aqueous U species in the test effluent solution; though, at pH 11, negative hydroxide species, $(UO_2)_3(OH)_7^-$ and uranyl di-carbonate [$UO_2(CO_3)_2^{2-}$] are observed at the highest concentrations. When bicarbonate concentration increases to 0.003 M, $UO_2(CO_3)_3^{-4}$ governs the speciation at any pH; however, at pH 10 and 11, negative hydroxide species, $(UO_2)_3(OH)_7^-$ and $UO_2(CO_3)_2^{2-}$, were found to increase to noticeable amounts. At 0.003 M of $HCO_3$ and pH 11, the dominance of uranyl bicarbonate species in the solution was found at 57%; yet, the total sum of hydroxide species is comparable to uranyl bicarbonate, just slightly less at 43%. These changes in the predominant uranyl species confirmed that dissolution of uranyl phosphate phases is a function of the solution composition (Sowder, 2001), which can explain the mechanism of autunite dissolution and the reduction in activation energy values noted at pH $\geq$ 8. At higher pH conditions in the presence of dissolved bicarbonate ions, uranyl carbonates and uranyl hydroxide species play a role as two main activated complexes. The existence of those two powerful complexes on the surface of autunite induces the reduction in both chemical affinity term, ($Q/K_g$), and the activation energies determined at basic pH regions, which decreases the cohesion of uranium ions present at the surface of autunite and accelerates the dissolution reaction. Likely, at high pH, the surface is saturated with hydroxide and bicarbonate complexes that facilitate release of uranium from the autunite structure. Enhanced dissolution attributed to complexation of ligands on the mineral

surface induces a change in bond strengths weakening the crystal structure (Stumm, 1992).

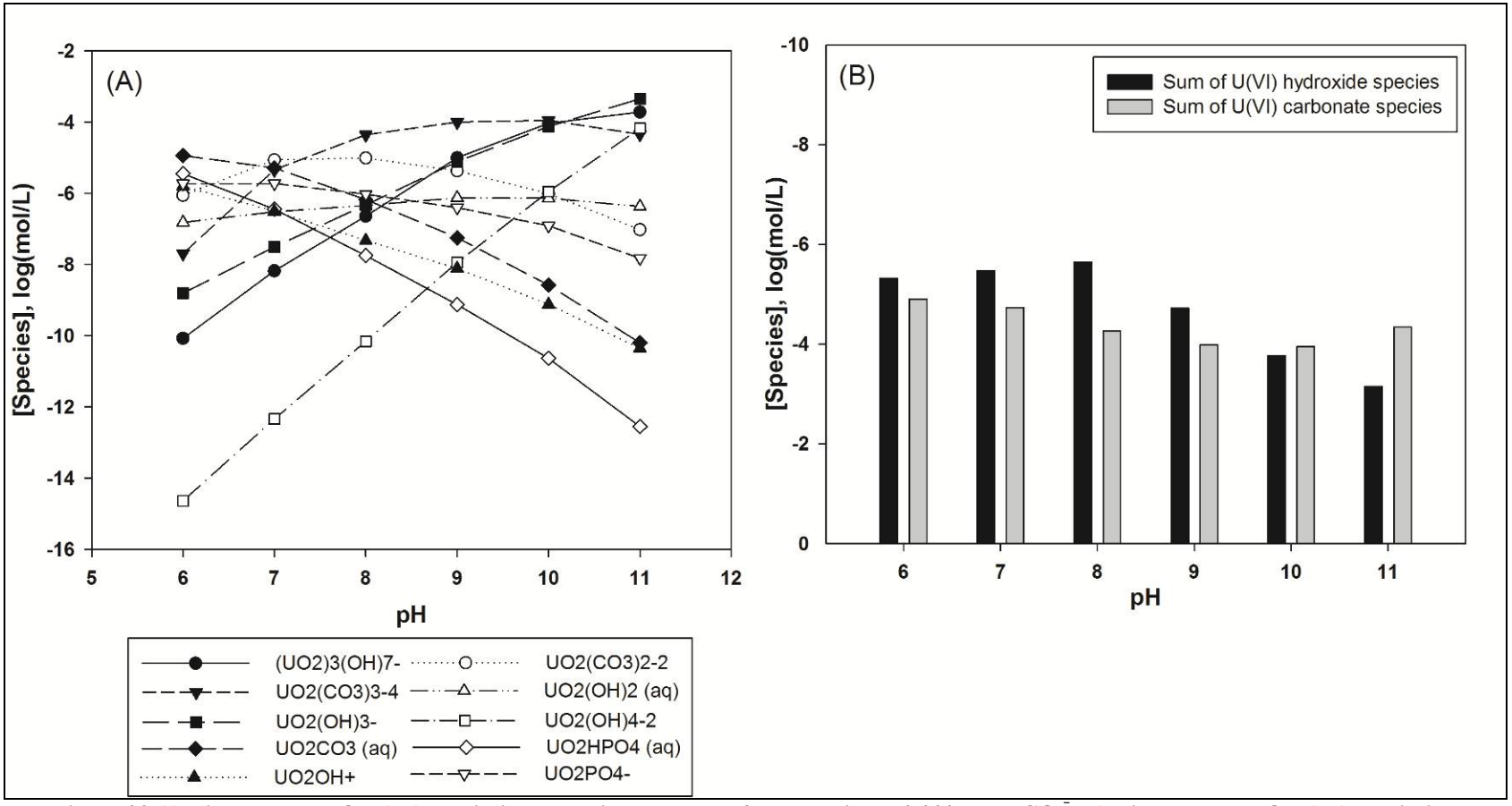


**Figure 29 A) Visual MINTEQ U(VI) speciation modeling summary for U species at 0.0005 M $HCO_3^-$; B) Visual MINTEQ U(VI) speciation modeling summary of the total hydroxide and carbonate U(VI) species at 0.0005 M $HCO_3^-$.**

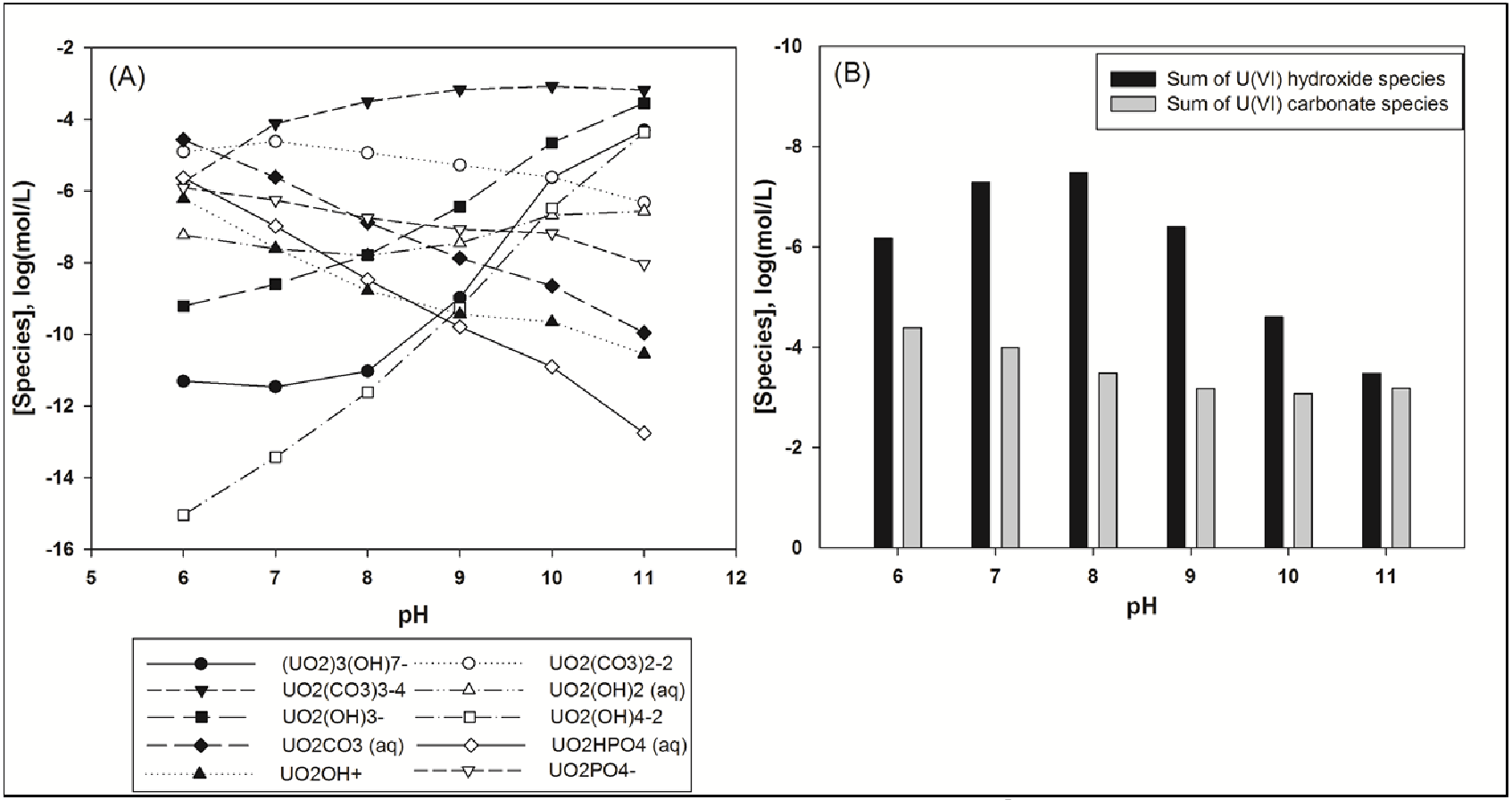


**Figure 30 A) Visual MINTEQ U(VI) speciation modeling summary for U species at 0.003 M $HCO_3^-$; B) Visual MINTEQ U(VI) speciation modeling summary of the total hydroxide and carbonate U(VI) species at 0.003 M $HCO_3^-$.**

# CONCLUSIONS

The rate of dissolution of Na-autunite was evaluated under bicarbonate concentrations ranging from 0.0005 to 0.003 M, pH 6 to 11 and temperature variations from 5 to 60$^{o}$C via single-pass flow-through cell experiments.

The study confirmed a strong influence of bicarbonate ligands on the autunite dissolution rates, which is probably due to the high values of carbonate species thermodynamic constants relative to actinides. In the range of bicarbonate concentrations tested, the intrinsic rate constant of autunite dissolution was increased about 12 times from 4.54 x $10^{-10}$ to 5.51 x $10^{-09}$ as pH rose from 6 to 11. The overall increase in the U(VI) rate of release was found to be 16.7 times when comparing the U(VI) rates of release obtained at 0.0005 M, 5$^{o}$C and 0.003 M, 60$^{o}$C. The activation energy values were unaffected by temperature and bicarbonate concentration variations but were strongly dependent on pH conditions. The activation energy averaged 29.94 kJ mol$^{-1}$ and 26.87 kJ mol$^{-1}$ for pH 6 and 7, respectively. In the pH range 8 - 11, activation energies ranged from 15.6 to 13.1 kJ mol$^{-1}$. Geochemical modeling suggested that uranyl speciation is strongly dependent on pH and the concentration of carbonate ions in the solution. At high pH, the mineral surface is saturated with hydroxide and carbonate uranyl complexes that accelerate the release of U(VI) ions out of the autunite structure. The calculated theoretical and experimental values of U(VI) rate of release differ within a ±10% error range. To the best of our knowledge, this is the first investigation that has quantified the kinetic rate law parameters of Na-autunite in bicarbonate-bearing solutions under these temperatures and pH ranges.

# REFERENCES

**Aagaard P., and Helgeson H.C.,** Thermodynamic and Kinetic Constraints on Reaction Rates among Minerals and Aqueous Solutions. I. Theoretical Considerations. Amer. J. Sci., 1982, Vol. 282(3), pp. 237 - 285.

**Bemer R. A.,** Rate control of mineral dissolution under earthsurface conditions. Amer. J. Sci., 1978, Vol. 278, pp. 1235 - 1252.

**Brunauer S., Emmett P. H., and Teller E.,** Adsorption of Gases in Multimolecular Layers. Journal of the American Chemical Society, 1938, Vol. 60(2), pp. 309 - 319.

**Burns P.C., Miller M.L., and Ewing R.C.,** U6+ minerals and inorganic phases: acomparison and hierarchy of crystal structures, The Canadian Mineralogist, 1996, Vol. 34, pp. 845 - 880.

**Casas I., De Pablo J., Gimenez J., Torrero M. E., Bruno J., Cera E., Finch R.J., and Ewing R. C.,** The role of pe, pH, and carbonate on the solubility of $UO_2$ and uraninite under nominally reducing conditions. Geochemica et Cosmochimica Acta, 1998, Vol. 62, pp. 2223 - 2231.

**Davis J. A.,** Surface Complexation Modeling of Uranium (VI) Adsorption on Natural Mineral Assemblages. Report NUREG/CR- 6708. U. S. Nuclear Regulatory Commission, Rockville, MD, 2001.

**Finch R.J., and Murakami T.,** Systematics and paragenesis of uranium minerals. in" Uranium: Mineralogy, Geochemistry and the Environment", PC Burns & B. Finch, eds," Rev. Mineral. Geochem, 1999, Vol. 38, pp. 91 - 179.

**Gudavalli R.,** Effect of pH and Temperature on the Carbonate Promoted Dissolution of Synthetic Sodium Meta-autunite, Student Poster, Waste Management Symposium, Phoenix, 2010.

**Gudavalli R.,** Investigation of Effects of pH and Temperature on the Carbonate Promoted Dissolution of Meta-autunite, Student Poster, Waste Management Symposium, Phoenix, 2009.

**Gudavalli R., Katsenovich Y., Lagos L., and Tansel B.,** Investigation of the Effect of Water Quality Parameters on Dissolution of Sodium Meta-autunite, Student Poster, Waste Management Symposium, Phoenix, 2012.

**Gudavalli R., Katsenovich Y., Wellman D., Lagos L., and Tansel B.,** Effect of bicarbonate on the dissolution of sodium meta-autunite. Geochimica et Cosmochimica Acta, (under review).

**Guillaumont R., Fanhänel T., Fuger J., Grenthe I., Neck V., Palmer D. A. and Rand M.H.,** Chemical Thermodynamics, OECD Nuclear Energy Agency, 2003, Vol. 5, Elsevier.

**Heisbourg G., Hubert S., Dacheux N., and Ritt J.,** The kinetics of dissolution of $Th_{1-x}U_xO_2$ solid solutions in nitric media. Journal of Nuclear Materials, 2003, Vol. 321 (2-3), pp. 141 - 151.

**Ilton E S., Liu C., Yantasee W., Wang Z., Moore D.A., Felmy A.R., and Zachara J. M.,** The dissolution of synthetic Na-boltwoodite in sodium carbonate solutions. Geochimica et Cosmochimica Acta, 2006, Vol. 70, pp. 4836 - 4849.

**John W. E., Matthew M. H., Philip R. A., and Alasdair J. C.,** Optimal sample preparation conditions for the determination of uranium in biological samples by kinetic phosphorescence analysis (KPA), Journal of Pharmaceutical and Biomedical Analysis, 2000, Vol. 24(2), pp. 227 - 235.

**Jordan G., and Rammensee W.,** Dissolution rates and activation energy for dissolution of brucite (001): A new method based on the microtopography of crystal surfaces. Geochemica et Cosmochimica Acta, 1996, Vol. 60(24), pp. 5055 - 5062.

**Kraemer S. M., and Hering J. G.,** Influence of solution saturation state on the kinetics of ligand-controlled dissolution of aluminum oxide. Geochimica etCosmochimica Acta, 1997, Vol. 61, pp. 2855 - 2866.

**Langmuir D.,** Uranium solution-mineral equilibria at low temperatures with applications to sedimentary ore deposits. Geochimica et Cosmochimica Acta, 1978, Vol. 42, pp. 547 - 569.

**Langmuir D.,** Aqueous environmental geochemistry Prentice Hall. Upper Saddle River, NJ, 1997.

**Lasaga A. C.,** Chemical kinetics of water-rock interactions. J. Geophys., Res. 1984, pp. 4009 - 4025.

**Lenhart J. J., Cabaniss S. E., MacCarthy P., and Honeyman B. D.,** Uranium(VI) complexation with citric, humic and fulvic acids, Radiochim Acta, 2000, Vol. 88, pp. 345 - 353.

**Liu C, Zachara JM., Qafoku O., Mckinley J. P., Heald S. M., and Wang Z.,** Dissolution of uranyl microprecipitates in subsurface sediments at Hanford Site, USA, Geochimica et Cosmochimica Acta, 2004, Vol. 68(22), pp. 4519 - 4537,

**McGrail B. P., Ebert W. L., Bakel A. J., and Peeler D. K.,** Measurement of kinetic rate law parameters on a Na- Ca- Al borosilicate glass for low-activity waste, Journal of Nuclear Materials, 1997, Vol. 249 (2), pp. 175 - 189.

**Pablo J. D., Casas I., Gimenez J., Molera M., Rovira M., and Duro L.,** The oxidative dissolution mechanism of uranium dioxide. I. The effect of temperature in hydrogen carbonate medium, Geochemica et Cosmochimica Acta, 1999, Vol. 63, pp. 3097 - 3103.

**Perez I., Casas I., Martin M., and Bruno J.,** The thermodynamics and kinetics of uranophane dissolution in bicarbonate test solutions, Geochemica et Cosmochimica Acta, 2000, Vol. 64, pp. 603 - 608.

**Scott P.D., Glasser D., and Nicol M.J.,** Kinetics of dissolution of β-uranium trioxide in acid and carbonate solutions, Journal of the Chemical Society, 1977, Vol. 20, pp. 1939 - 1946.

**Sowder A. G., Clark S. B., and Fjeld R.A.,** The impact of mineralogy in the U(VI)-Ca-$PO_4$ system on the environmental availability of uranium. Journal of Radioanalytical and Nuclear Chemistry, 2001, Vol. 248 (3), pp. 517 - 524.

**Sparks D. L.,** Kinetics and Mechanisms of Chemical Reactions at the Soil Mineral/Water Interface, Soil Physical Chemistry, 1999, CRC Press.

**Stumm W.,** Chemistry of the Solid-Water Interface: Processes at the Mineral - Water and Particle-Water Interface in Natural Systems, J. Wiley & Sons., New Jersey, 1992.

**Wellman D. M., Catalano J. G., Icenhower J. P., and Gamerdinger A. P.,** Synthesis and characterization of sodium meta-autunite, $Na[UO_2PO_4]\bullet 3H_2O$, Radiochimica Acta, 2005, Vol. 93, pp. 393 - 399.

**Wellman D. M., Icenhower J. P., Gamerdinger A. P., and Forrester S. W.,** Effects of pH, temperature, and aqueous organic material on the dissolution kinetics of meta-autunite minerals, $(Na, Ca)_{2-1}[(UO_2)(PO_4)]_2\bullet 3H_2O$, American Mineralogist, 2006, Vol. 91, pp. 143 - 158.

**Wellman D. M., Gunderson K. M., Icenhower J. P., and Forrester S. W.,** Dissolution kinetics of synthetic and natural meta-autunite minerals, $X_{3-n}^{(n)+}[(UO_2)(PO_4)]_2\bullet xH_2O$, under acidic conditions, Geochem. Geophys. Geosyst., 2007, Vol. 8, pp. 16.

**Wellman D. M., McNamara B. K., Bacon D. H., Cordova, E. A., Ermi R. M., and Top L. M.,** Dissolution kinetics of meta-torbernite under circum-neutral to alkaline conditions, Environmental Chemistry, 2009, Vol. 6(6), pp. 551 - 560.

**Zhang Y., Hart K.P., Bourcier W.L., Day R.A., Colella M., Thomas B., Aly Z., and Jostsons A.,** Kinetics of uranium release from Synroc phases, Journal of Nuclear Materials, 2001, Vol. 289 (3), pp. 254 - 262.

**Zheng Z., Wan J., Song X., and Tokunaga T. K.,** Sodium meta-autunite colloids: Synthesis, characterization, and stability, Colloids and Surfaces A: Physicochemical and Engineering Aspects, 2006, Vol. 274, pp. 48 - 55.

CHAPTER THREE

## Comparison of the kinetic rate law parameters for the dissolution of natural and synthetic autunite in the presence of bicarbonate ions


ABSTRACT

This research evaluated the effect of aqueous bicarbonate on the uranium rate of release from natural Ca-autunite and quantified the process kinetic rate law for better prediction of the stability of autunite-group minerals. Testing was accomplished via a single-pass flow-through (SPFT) apparatus using buffered aqueous bicarbonate (0.0005 to 0.003M) at temperatures of 23° - 90°C and pH values of 7 - 11. The release rate of uranium from Ca-autunite was directly correlated to increasing bicarbonate concentrations and showed strong pH dependency. Ca-autunite kinetic rate law parameters were compared to the values obtained for synthetic Na-autunite. The power law coefficient and intrinsic rate constant were higher at pH 9 - 11 for Ca-autunite than for Na-autunite. The lower stability of Ca-autunite was attributed to the high Ca-autunite surface cracking, fractures and basal plane cleavages as compared to Na-autunite and the formation of aqueous calcium uranium species, altering the solution saturation state.

# INTRODUCTION

Globally, uranium (U) occurs as an essential component in different minerals and the majority of naturally occurring uranium deposits are oxides, silicates, vanadates, and phosphate minerals such as autunite (Burns, 1999). Uranium is one of the most frequently found radionuclides in groundwater as a result of reactor operations, nuclear fuel production and waste reprocessing (Riley, 1992). Autunite minerals $\{(X^m)_{2/m}[(UO_2)(PO4)]_2 \cdot xH_2O\}$ are an important group known for their low solubility that largely controls the mobility of U in the subsurface. The autunite-group is very diverse, permits a wide range of cation and anion substitutions, and varying degrees of hydration (Burns, 1999). Many arid and semi-arid environments, including areas used for the storage of high-level radioactive waste at the U.S. Department of Energy (DOE) sites, contain elevated concentrations of sodium that in the presence of phosphorus (P) and uranium U(VI) rapidly form sodium uranyl phosphate phases. Chernikov et al. (1957) conducted characterization of the hydrated sodium meta-autunite discovered in the Kuruk uranium deposit of northern Tajikistan and found that it is similar in properties to the autunite group. Mills et al., (2012) reported that metanatroautunite from the Lake Boga granite, Victoria, Australia, was similar to synthetic $Na[(UO_2)(PO_4)] \cdot (H_2O)_3$ and featured identical corrugated polyhedral sheets as the meta-autunite-group minerals, consisting of corner-sharing uranyl square pyramids and phosphate tetrahedra.

Calcium, as one of most abundant metals in the earth's crust, promotes the formation of calcium-autunite, $Ca[(UO_2)(PO4)]_2 \cdot (H_2O)_{11}$. This phase has been recognized as the dominant form of autunite (Burns, 1999). The crystal structure contains the well-known autunite type sheet with composition $[(UO_2)(PO_4)]^-$, resulting from the sharing of

equatorial vertices of the uranyl square bipyramids with the phosphate tetrahedra. The calcium atom in the interlayer is coordinated by seven $H_2O$ groups and two longer distances from uranyl ion oxygen atoms (Locock et al., 2003).

Fairchild (1929) showed that in artificial autunites sodium was replaced by calcium and the exchange reactions take place rapidly with compounds of the autunite type. According to Anthony et al. (2000), two distinct changes occur during the exchange of sodium for calcium in the autunite structure. Primarily, two sodium cations are exchanged for the calcium ion to maintain the charge balance of the structure. The exchange of sodium for calcium is also associated with an increase in waters of hydration (Wellman et al., 2005). These changes in the chemical and structural composition of autunite raise questions on the impact of environmental factors on the stability of autunite-group minerals.

Literature data suggest the low solubility and high stability of many uranyl-phosphate minerals (Felmy et al., 2003; Gorman - Lewis et al., 2009). The solubility constant of the calcium form of autunite, log $K_{sp}$, has been measured as - 44.7 (Grenthe et al., 1992; Langmuir, 1997). A recent solubility study on natural Ca-U-P stability constant values for aqueous complexes yielded a log $K_{sp}$ value of - 48.36 with 2σ uncertainty values of ±0.03 (Gorman - Lewis et al., 2009). Associated solubility products are shown in Equation 17.

$$Ca(UO_2)_2(PO_4)_2 \cdot 3H_2O \rightarrow 3H_2O + Ca^{2+} + 2PO_4^{3-} + 2UO_2^{2+} \quad (17)$$

Different environmental variables including temperature and pH have been extensively investigated (Wellman et al., 2006) on the dissolution of synthetic Na meta-autunite (herein designated as Na-autunite) and natural Ca meta-autunite minerals (herein designated as Ca-autunite). Their results indicated that meta-autunite dissolution kinetics

is strongly dependent on pH and independent of temperature variation (Wellman et al., 2006; Wellman et al., 2007). Ca-rich carbonate-bearing subsurface environments, typical for the arid areas of the western U.S., afford the formation of aqueous calcium uranyl-carbonate and hydroxide complexes, which are mobile and promote U(VI) migration in natural waters (Clark et al., 1995; Kalmykov et al., 2000; Bernhard et al., 2001). The strength of uranyl carbonate complexes makes bicarbonate the most effective extractant in terms of the dissolution rate and the extent of recovery of U from uranyl - bearing mineral phases (Sowder et al., 2001; Perez et al., 2000). Single-pass flow-through (SPFT) experiments, investigated the rate of U(VI) release from Na-autunite, $Na_2[(UO_2)_2(PO_4)_2]\cdot 3H_2O$, as a function of bicarbonate concentrations ranging from 0.5 mM to 3.0 mM in the pH range of 6-11 and temperature between 5 - 60$^{o}$C. They noted that the rate of U(VI) release from Na-autunite in the presence of low bicarbonate concentrations was increased over 300 fold when compared to the rate of U(VI) release in the absence of bicarbonate. Quantification of kinetic rate law parameters for the dissolution reaction of sodium meta-autunite suggested that activation energies were unaffected by temperature and bicarbonate concentrations but strongly depended on pH conditions. Considering rapid exchange reactions of sodium for calcium in the autunite structure, the study of the effect of aqueous bicarbonate concentrations on the rate of U(VI) release from Ca-autunite can be extended to better understand U(VI) mobilization in groundwater.

The objectives of this research were (i) to investigate the effect of low concentrations of bicarbonate on the dissolution of U(VI) from Ca-autunite via SPFT experiments and determine the U(VI) rate of release, (ii) to quantify the kinetic rate law parameters of Ca-

autunite dissolution, and (iii) to compare the results with the dissolution of Na-autunite for better prediction of the impact of bicarbonate on the release of U(VI) and the dissolution process of the autunite minerals group. This information is critical for the prediction of autunite stability and long-term fate and transport of uranium in the subsurface.

## MATERIALS AND METHODS

### 1.22 Autunite Specimens

Synthesis of Na-autunite, $Na_2[(UO_2)_2(PO_4)_2]\cdot 3H_2O$, was followed by a modified direct precipitation method described by Wellman, et al., (2005). Synthesis procedures and solids composition assessment are presented in detail in Section 4.1. The structure of synthesized autunite solids, characterized by JSM-5900-LV low vacuum scanning electron microscope (SEM) at 15kV, exhibited a smooth surface without distinctive cleavage planes (Figure 31a).

Natural Ca-autunite, $Ca[(UO_2)(PO_4)]_2\cdot 3H_2O$, obtained from Excalibur Mineral Corporation (Peekskill, New York), was previously characterized using ICP-OES, ICP-MS analyses, X-ray diffraction and SEM/EDS to confirm the mineral composition, structure, and morphology as 98-99% pure autunite (Wellman et al., 2006). Scanning electron micrographs (SEM) of Ca-autunite illustrate the multilayer structure resulting from the negatively charged $[(UO_2)(PO_4)]_2^{2-}$ layers. The morphology features perfect (001) basal, cleavage producing planes characteristic of autunite minerals (Anthony et al., 2000). As illustrated in the scanning electron micrographs (Figures 31b and 31c), surface cracking, fractures, and basal plane cleavage are greater in Ca-autunite, resulting in a

greater surface area in comparison to the Na-autunite. The autunite sample was powdered to the size fraction of 75 to 150 μm (-100 to + 200 mesh) corresponding to an average surface area of 0.88 $m^2$ $g^{-1}$ (Wellman et al., 2006).

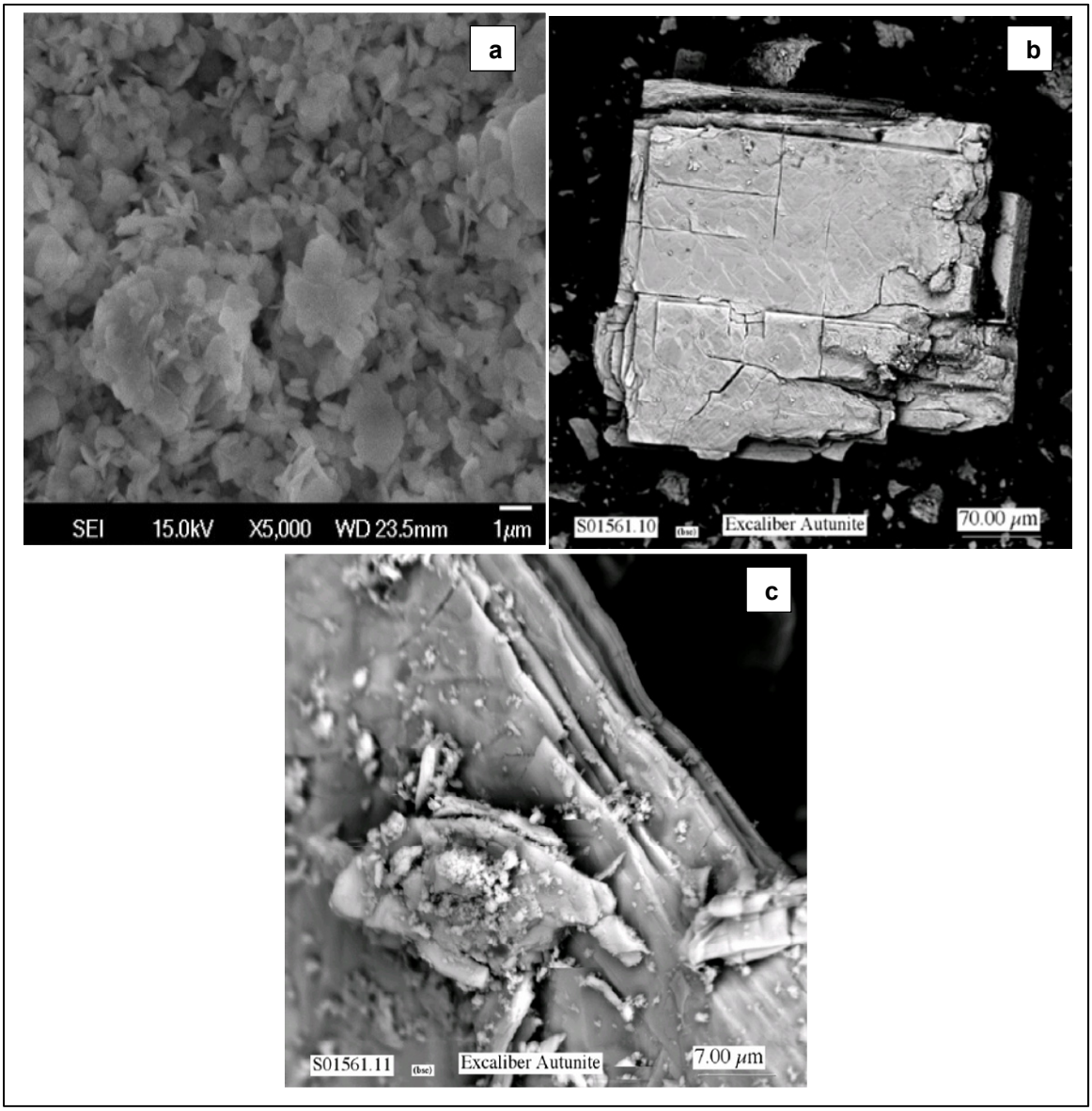


**Figure 31 SEM images of precipitated (a) Na-autunite and natural Ca-autunite sample (b, c)**

## 1.23 Single-Pass Flow-Through (SPFT) Experiments

The release rate of elements from solids into solution is frequently controlled by reaction rates (i.e. kinetics). It has been accepted practice by geochemists to use the transition

state theory (TST) to describe the dissolution reaction of autunite and compute the flux of elements released into the aqueous phase (Nagy, 1995). A general form of rate equation (equation 12) is based on the TST of chemical kinetics, centered on the prediction that the overall reaction rate is governed by the slowest elementary reaction (Aagaard, 1982; McGrail et al., 1997).

The dependence of the dissolution rate of the Ca-autunite mineral on bicarbonate concentration was quantified via single-pass flow-through (SPFT) experiments conducted over a temperature range of $23^{o}$ to $90^{o}$C and a controlled pH range from 7 to 11. The schematic and detailed procedures of the experiments are presented in Wellman et al., (2006, 2007, 2009). A series of buffer compositions, all prepared with distilled, de-ionized water (DDIW), consisting of 0.01 M *tris (hydroxymethyl) aminomethane* (TRIS) buffer and aqueous bicarbonate concentrations ranging from $5 \times 10^{-4}$ to $3 \times 10^{-3}$ M, were used to investigate U(VI) release from natural Ca-autunite mineral over the pH (23°C) interval of 7 to 11. Concentrated spectroscopy-grade nitric acid ($HNO_3$ at 15.8 M) and 5 M lithium hydroxide (LiOH) solutions were used for adjusting the pH of the solutions. The SPFT test was designed to limit the accumulation of reaction products using a sufficient ratio of the flow rate to the surface area of the mineral sample (q/S) to ensure the maximum dissolution rate or forward rate was achieved. These conditions allow maintaining the chemical affinity term, $Q/K_g$, at a value near zero in Equation 12. By observing changes in the dissolution rate over the range of experimental parameters tested, k, Ea, and $\eta$ can be easily obtained by non-linear regression.

### 1.24 Quantification of Dissolution Rate

The normalized dissolution rate of Ca-autunite solids was calculated from Equation 6 when the system reached equilibrium (McGrail et al., 1997). The steady-state conditions were achieved after approximately six reactor volumes and the concentrations of uranium released from natural Na-autunite became invariant with respect to time for all pH and bicarbonate ranges tested.

Uncertainty associated with each parameter was considered when calculating the dissolution rate; relative errors included are final concentration (10%), background concentration (10%), mass distribution (5%), surface area (15%), and flow rate (5%). The error analysis determining the standard deviations of the dissolution rates was performed by following the procedures described in Wellman et al. (2009). The experimental results were correlated by linear regression using SigmaPlot-11.2 (Systat Software Inc.).

### 1.25 Groundwater Modeling

Steady state elemental concentrations in the effluent solution after the system reached equilibrium were used to identify the predominant uranium species in aqueous solution. The speciation modeling was performed by means of geochemical modeling software Visual MINTEQ v. 3.0 [maintained by J. Gustafsson at KTH, Sweden, available at http://www.lwr.kth.se/English/OurSoftware/vminteq/ and updated with the Nuclear Energy Agency's thermodynamic database for uranium (Guillaumont et al., 2003)].

## 1.26 Effect of Bicarbonate

The effect of bicarbonate on the dissolution of Ca-autunite was estimated from experimental results using Equation 12. Figure 32 illustrates the rate of U(VI) release from Ca-autunite under the range of pH 7 - 11, across the aqueous bicarbonate concentrations tested and the temperature range of 23$^{o}$ to 90$^{o}$C. This figure depicts the strong effect of pH on the uranium rate of release, which is consistent with previous studies on the dissolution rate of autunite minerals (Wellman et al., 2006 & 2007 & 2009). At pH 7, the increase in the rate of U(VI) release was noted to be ~18 fold as the bicarbonate concentration increased from 0.3 mM to 3 mM. The value of the power law coefficient, □, calculated from the slope of U(VI) rate of release as 0.50 ± 0.12 was further used to estimate the intrinsic rate constant, k, of 1.09 x $10^{-09}$ (mol $m^{-2}$ $s^{-1}$). Saturation indexes at pH 7 showed that potential secondary phases such as schoepite and β-$UO_2(OH)_2$ were under-saturated at all bicarbonate concentrations suggesting that the release of U(VI) was solely due to the dissolution of Ca-autunite. At pH 8 and 9, the rate of U(VI) release was observed to increase approximately 6.5 times with an increase in the bicarbonate concentration and by 17 - 65 fold, correspondingly, with respect to the rate of release at pH 7. The power law coefficients calculated from the slope of U(VI) release rate and the resulting intrinsic rate constant, *k*, at pH 8 and 9 are presented in comparison with similar parameters obtained for Na-autunite in Table 12. Calculations showed that at pH 9 values of □ and *k* were 1.6 and 19 times higher for the Ca-autunite, compared to Na-autunite, respectively (Table 12). The rate of U(VI) release at pH 10 and 11 over the

aqueous bicarbonate concentration interval tested was higher by approximately 18.5 fold and 14 fold, respectively, and by 300 - 400 fold with respect to the rate of U(VI) release at pH 7. For the same pH range, values of □ and *k* were higher for the Ca-autunite by 1.8 - 2.8 and 126 - 484 times, correspondingly, compared to Na-autunite, indicative of the greater stability of Na-autunite. The values of the power law coefficient were observed to be unvarying over the temperature interval, indicating that the dissolution process within experimental error is independent of temperature (Figure 32).

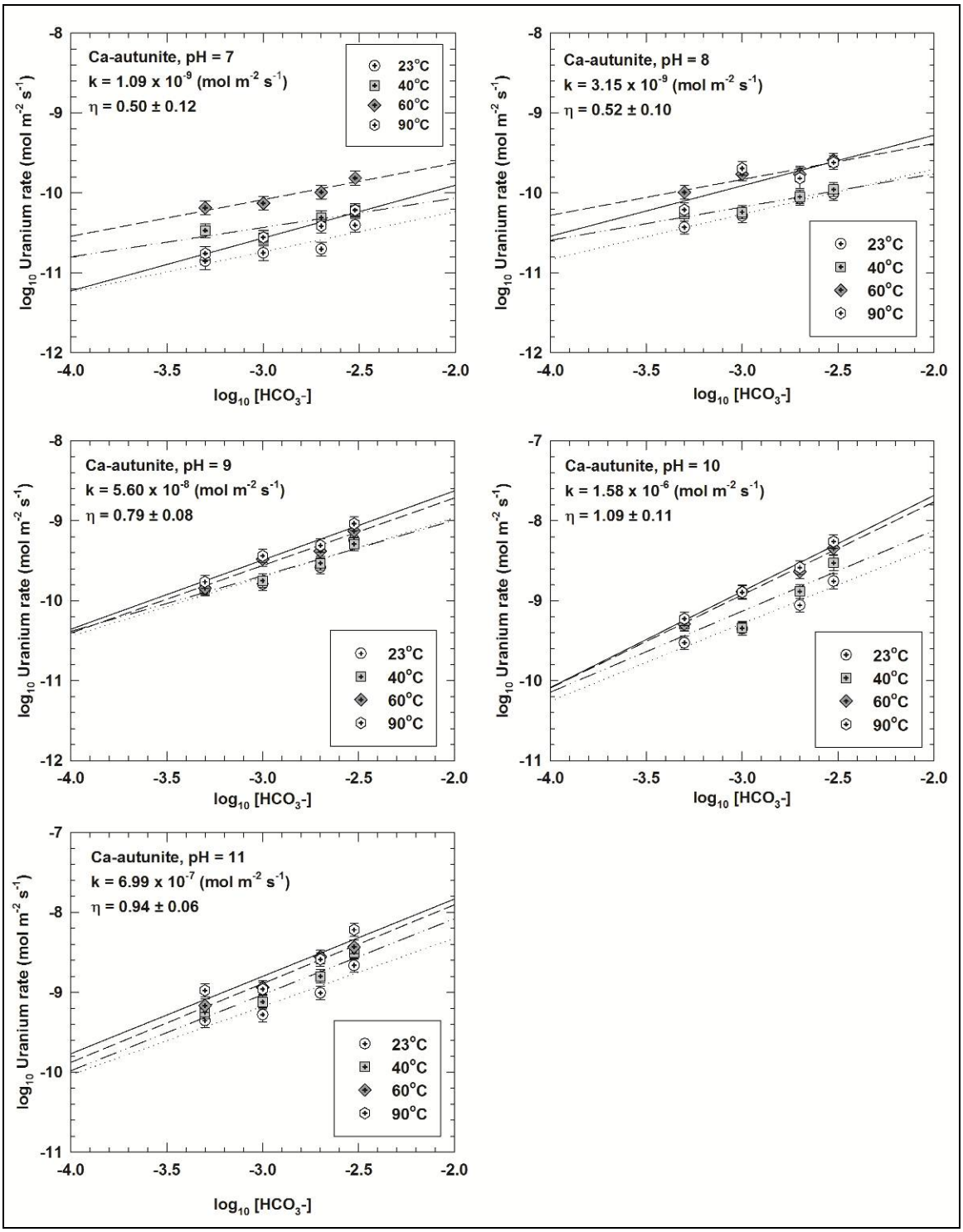


**Figure 32 Change in U(VI) release rate from Ca-autunite as a function of bicarbonate concentration**

**Table 12 Power law coefficients and intrinsic rate constants**

| pH | Ca-autunite | | Na-autunite | |
|---|---|---|---|---|
| | η | k (mol $m^{-2}$ $s^{-1}$) | η | k (mol $m^{-2}$ $s^{-1}$) |
| 7 | 0.50 ± 0.12 | $1.09 \times 10^{-09}$ | 0.42 ± 0.13 | $3.62 \times 10^{-10}$ |
| 8 | 0.52 ± 0.10 | $3.15 \times 10^{-09}$ | 0.57 ± 0.04 | $1.48 \times 10^{-09}$ |
| 9 | 0.79 ± 0.08 | $5.60 \times 10^{-08}$ | 0.48 ± 0.12 | $2.86 \times 10^{-09}$ |
| 10 | 1.09 ± 0.11 | $1.58 \times 10^{-06}$ | 0.39 ± 0.03 | $3.26 \times 10^{-09}$ |
| 11 | 0.94 ± 0.06 | $6.99 \times 10^{-07}$ | 0.51 ± 0.02 | $5.51 \times 10^{-09}$ |

It was previously determined that the dissolution kinetics of Ca and Na autunite minerals is a surface-mediated reaction with the uranium polyhedral (Wellman et al., 2006, 2007). This reaction is described by fast sorption of the reactants to the mineral surface and then slow detachment of metal species from the surface into solution (Sparks, 1999). Uranyl ions release from autunite under the influence of bicarbonate ions proceeds by a two-step process: surface coordination of $HCO_3^-$ on the U(VI) mineral surface and then detachment of the uranyl carbonate species back in to solution (Pablo et al., 1999; Liu et al., 2004). The autunite minerals structure is characterized by the relatively weak forces holding successive sheets together (Wellman et al., 2009). The liberation of U(VI) influences congruent reactions to release Ca and P from the mineral structure and their presence in the aqueous solution profoundly effect the system . An increase in the aqueous bicarbonate concentrations at pH 8 - 9 correlated with a decrease in the saturation indices of potential secondary phases as schoepite and β-$UO_2(OH)_2$, suggesting a faster release of U(VI) from autunite under these conditions. Starting from pH 9, hydroxyapatite was super saturated at all bicarbonate concentrations; besides, the speciation modeling indicated that at pH 10 and 11, the system was potentially saturated

with respect to various secondary Ca-P phases (Table 13). At pH interval 7-11, highly soluble and stable uranyl-carbonate and calcium uranyl carbonate complexes, $UO_2(CO_3)_3^{4-}$ and $CaUO_2(CO_3)_3^{2-}$, became predominate species. The percentage of Ca-U-$CO_3$ species increased to about 10%-27.7% in the pH range 9-11, while U-$CO_3$ species were ranging between 52-76%. Aqueous Ca and P release into solution during Ca-autunite dissolution was noted to increase as a function of pH. The concentration of Ca and P-bearing species increased 26 fold from $1.18 \times 10^{-05}$ mol $L^{-1}$ and $2.36 \times 10^{-05}$ mol $L^{-1}$ at pH 7 to $3.02 \times 10^{-04}$ mol $L^{-1}$ and $6.06 \times 10^{-04}$ mol $L^{-1}$ at pH 11, respectively. As predicted by speciation modeling, the formation of secondary Ca-P, uranyl phosphate secondary phases and Ca-U-$CO_3$ aqueous species can control the net release of uranium. Similar observations were noted in the bio-enhanced release of U(VI) from Ca-autunite in the presence of aqueous bicarbonate (Katsenovich et al., 2012).

**Table 13 Species distribution data for Ca-autunite**

| pH | $HCO_3^-$ (M) | Schoepite | β-$UO_2(OH)_2$ | Hydroxyapatite | β-$Ca_3(PO_4)_2$ | $Ca_3(PO_4)_2$ (am2) | $Ca_3(PO_4)_2$ (am1) | $Ca_4H(PO_4)_3 \cdot 3H_2O$(s) |
|---|---|---|---|---|---|---|---|---|
| 7 | 0.0005 | 0.028 | -0.202 | | | | | |
| | 0.001 | -0.2 | -0.43 | | | | | |
| | 0.002 | -0.522 | -0.752 | | | | | |
| | 0.003 | -0.735 | -0.965 | | | | | |
| 8 | 0.0005 | 0.335 | 0.105 | -0.948 | | | | |
| | 0.001 | -0.016 | -0.245 | 0.279 | | | | |
| | 0.002 | -0.428 | -0.657 | 1.744 | | | | |
| | 0.003 | -0.678 | -0.908 | 2.658 | | | | |
| 9 | 0.0005 | 0.575 | 0.346 | 5.996 | | | | |
| | 0.001 | 0.381 | 0.151 | 6.231 | | | | |
| | 0.002 | 0.039 | -0.191 | 7.48 | | | | |
| | 0.003 | -0.382 | -0.611 | 8.195 | | | | |
| 10 | 0.0005 | 0.659 | 0.429 | 14.6 | 3.979 | 3.142 | 0.384 | 2.543 |
| | 0.001 | 0.605 | 0.375 | 13.485 | 3.318 | 2.481 | -0.277 | 1.675 |
| | 0.002 | 0.351 | 0.121 | 11.948 | 2.398 | 1.561 | -1.197 | 0.452 |
| | 0.003 | -0.826 | -1.055 | 11.653 | 2.218 | 1.382 | -1.377 | 0.209 |
| 11 | 0.0005 | 0.25 | 0.02 | 15.121 | 3.86 | 3.023 | 0.265 | 1.665 |
| | 0.001 | 0.209 | -0.021 | 14.78 | 3.66 | 2.823 | 0.065 | 1.406 |
| | 0.002 | 0.06 | -0.17 | 14.223 | 3.33 | 2.494 | -0.265 | 0.975 |
| | 0.003 | -0.257 | -0.487 | 13.915 | 3.146 | 2.309 | -0.449 | 0.729 |

Evaluation of the solid phase's surface morphology suggested that the synthetic Na-autunite did not exhibit cleavage planes prior to dissolution (Figure 31). SEM images of reacted synthetic minerals have only revealed the minor formation of cleavage planes during the dissolution process, showing generally undisturbed post-experimental uranyl-phosphate sheets in the Na-autunite structure (Figure 33). Comparably, the crystals structure of post-reacted Ca-autunite showed a dramatic degree of distortion and layers separation (Wellman et al., 2006).

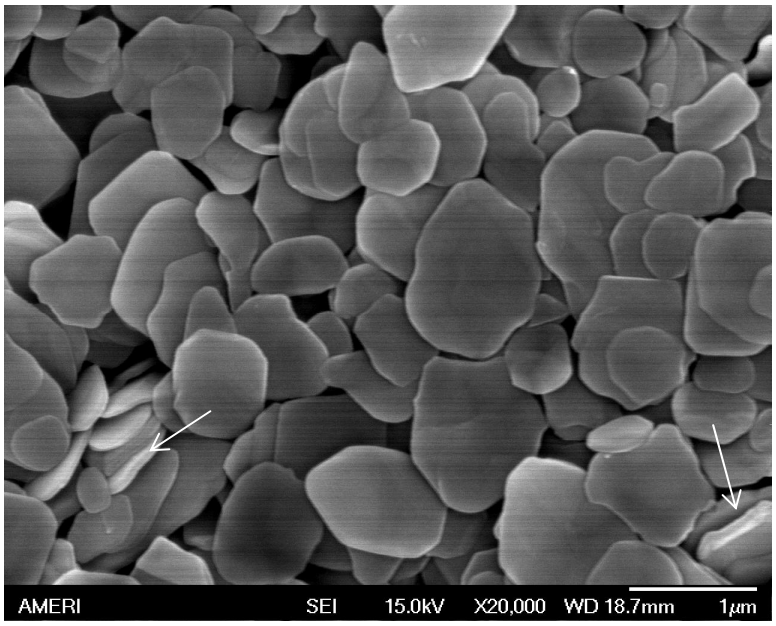


**Figure 33 SEM image of post-reacted Na-autunite**

Perhaps surface structural differences between Na and Ca autunite minerals along with the formation of secondary uranyl phosphate phases and Ca-U-$CO_3$ aqueous species contribute to the increased rate of U(VI) dissolution observed via SPFT Ca-autunite dissolution experiments. The separation of the sheet structure within the natural Ca-autunite minerals increases the probability that dissolution could occur through attack by aqueous bicarbonate ions on the surface structural defects.

### 1.27 Estimation of Thermodynamic Parameters (Activation Energy of Dissolution)

An important factor affecting the dissolution rate is activation energy, $E_a$, which depends on the nature of chemical reactions. Fast reactions have small activation energy and those with large activation energy usually progress slowly. Previous studies showed that pH has a pronounced effect on activation energy (Zhang et al., 2001). Bemer (1978) and Jordan (1996) reported that the activation energy can help identify the rate-controlling process of dissolution: activation energy values lower than 20 kJ $mol^{-1}$ represent surface diffusion as the rate-controlling process. Surface controlled dissolution usually results in higher activation energy; Lasaga (1984) reported that the surface controlled dissolution of silicates have activation energies in the range of 60 - 80 kJ $mol^{-1}$, and similar activation energy values (72 - 86 kJ $mol^{-1}$) were reported by various authors for alkaline earth fluorides whose dissolution rates are believed to be surface controlled. Previous studies on uranium-bearing materials suggested a surface controlled dissolution mechanism for measured activation energies calculated in the range of 12 - 60 kJ$mol^{-1}$ (Scott et al., 1977; Zhang et al., 2001; Pablo et al., 1999). In this study, the effect of bicarbonate ions on the activation energy of the dissolution reactions of Ca-autunite in a wide range of pH and temperatures is conducted by comparison with $E_a$ values for Na-autunite dissolution.

Activation energy values were estimated using a modified transition state theory equation describing the rate of reaction as a function of pH, temperature, and the activities of the rate enhancing or inhibiting species, described by Equation 15.

At constant bicarbonate concentrations, the normal logarithmic values of the dissolution rate (Ln r) were plotted against inverse temperature values (1/T). The slope of the linear

regression line at each pH value was calculated and the data is presented in Table 14. Data comparison for Ca-autunite with estimates obtained for Na-autunite revealed a weak dependency of the dissolution rate on the temperature for both materials. The average activation energy at pH 7 for Ca-autunite was estimated to be 25.50 kJ $mol^{-1}$, suggesting that the dissolution process is surface controlled, which is also in agreement with the average activation energy value reported for Na-autunite at pH 7 (26.86 kJ $mol^{-1}$). The average values of activation energy for Ca-autunite at pH 8 - 11 were estimated in the range of 8 - 18 kJ $mol^{-1}$, suggesting that the dissolution is faster at high pH. These values are similar to ones reported for Na-autunite, indicating that the transfer of uranium may be due to adsorption or ion exchange. The calculated activation energies for both Ca and Na autunite are in good agreement with that reported in the literature for similar materials (Zhang et al., 2001; Heisbourg et al., 2003).

**Table 14 Changes in activation energies of autunite dissolution**

| **$[HCO_3^-]$ (M)** | **Ca-autunite** | | | | **Na-autunite** | | | |
|---|---|---|---|---|---|---|---|---|
| | 0.0005 | 0.001 | 0.002 | 0.003 | 0.0005 | 0.001 | 0.002 | 0.003 |
| **pH** | **$E_a$ (kJ $mol^{-1}$)** | | | | **$E_a$ (kJ $mol^{-1}$)** | | | |
| 7 | 21.87 | 26.39 | 27.72 | 26.00 | 28.285 | 30.426 | 24.872 | 23.882 |
| 8 | 22.41 | 20.72 | 15.57 | 13.95 | 9.824 | 16.872 | 18.751 | 17.091 |
| 9 | 2.63 | 13.07 | 8.95 | 7.32 | 11.417 | 16.553 | 14.983 | 13.863 |
| 10 | 8.17 | 16.68 | 15.05 | 15.17 | 4.031 | 9.028 | 7.627 | 7.579 |
| 11 | 11.39 | 10.19 | 12.23 | 11.78 | 14.831 | 12.947 | 12.955 | 11.511 |

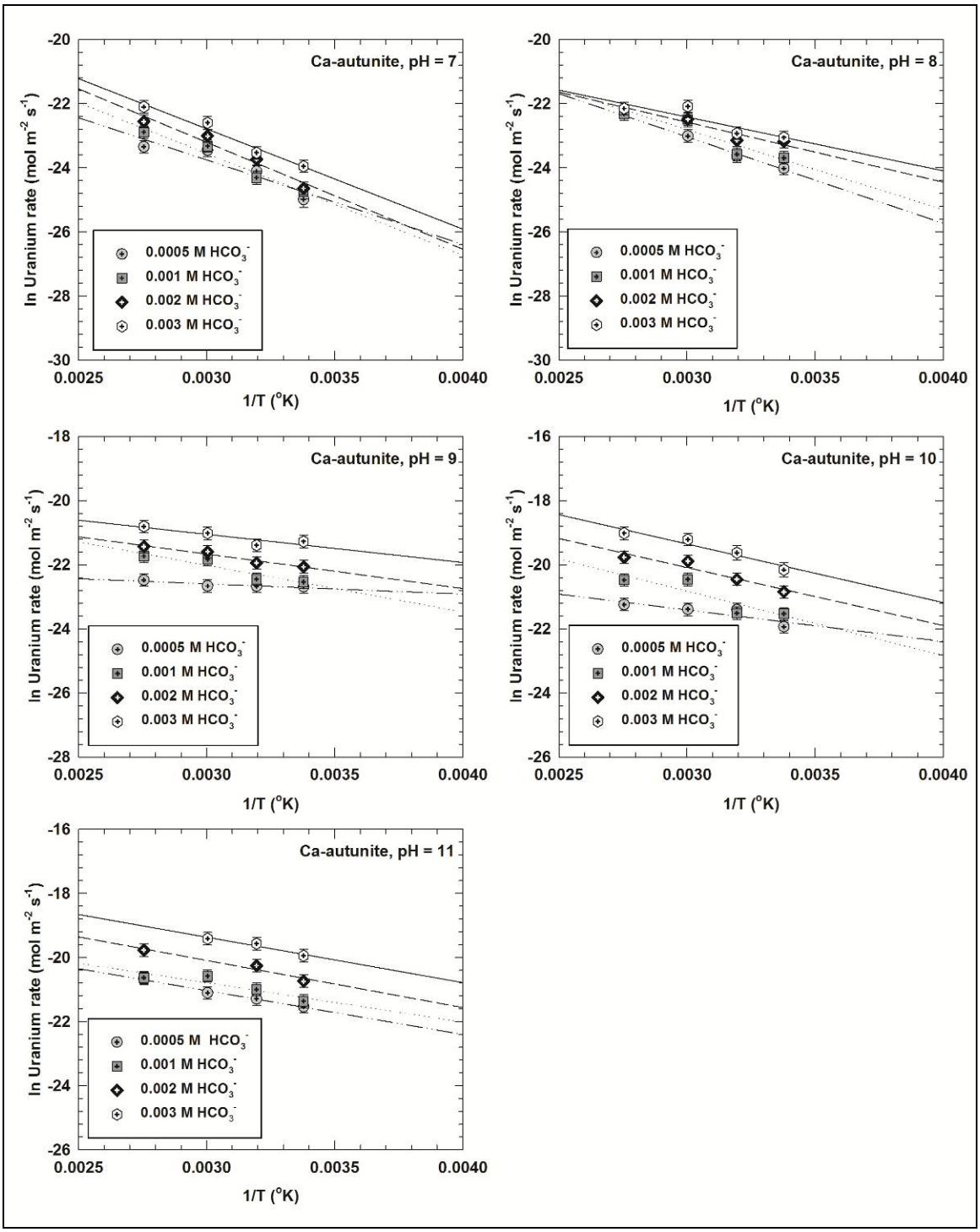


**Figure 34 Activation energy of the Ca-autunite dissolution at various pH values**

The pseudo equilibrium constant, $K_g$, was estimated using Equation 14, based on the assumption that the concentration of bicarbonate is the rate limiting factor that controls

the reaction. The values of U(VI) rate dissolution (Y-axis) at different pH values were plotted against variations of bicarbonate concentrations (X-axis). The resulting slopes of the regression lines (Figure 35) provided values of $K_g$ and are listed in Table 15.

Enthalpy of the system was evaluated using the correlation between the pseudo equilibrium constant, enthalpy, and the temperature of the system, described by Equation 17. A slope of a linear graph (Figure 36) with inverse temperature (1/T) on the X-axis and the normal logarithmic values of pseudo equilibrium constant, Ln $K_g$, on the Y-axis were used to estimate the enthalpy of the system at various pH values (Table 15).

The pseudo equilibrium rate constant values pertaining to Ca-autunite were found to be 4 times higher at low pH values (7 - 9) and 21 times higher at high pH values (10 - 11) than that for Na-autunite (Table 15). This data suggests that the reaction occurred slowly at low pH values and significantly faster at high pH values. A similar trend was shown by the intrinsic rate constant values. The change in enthalpy of Ca-autunite was found to be 0.5 - 1.5 times higher compared to the value of Na-autunite (Table 15).

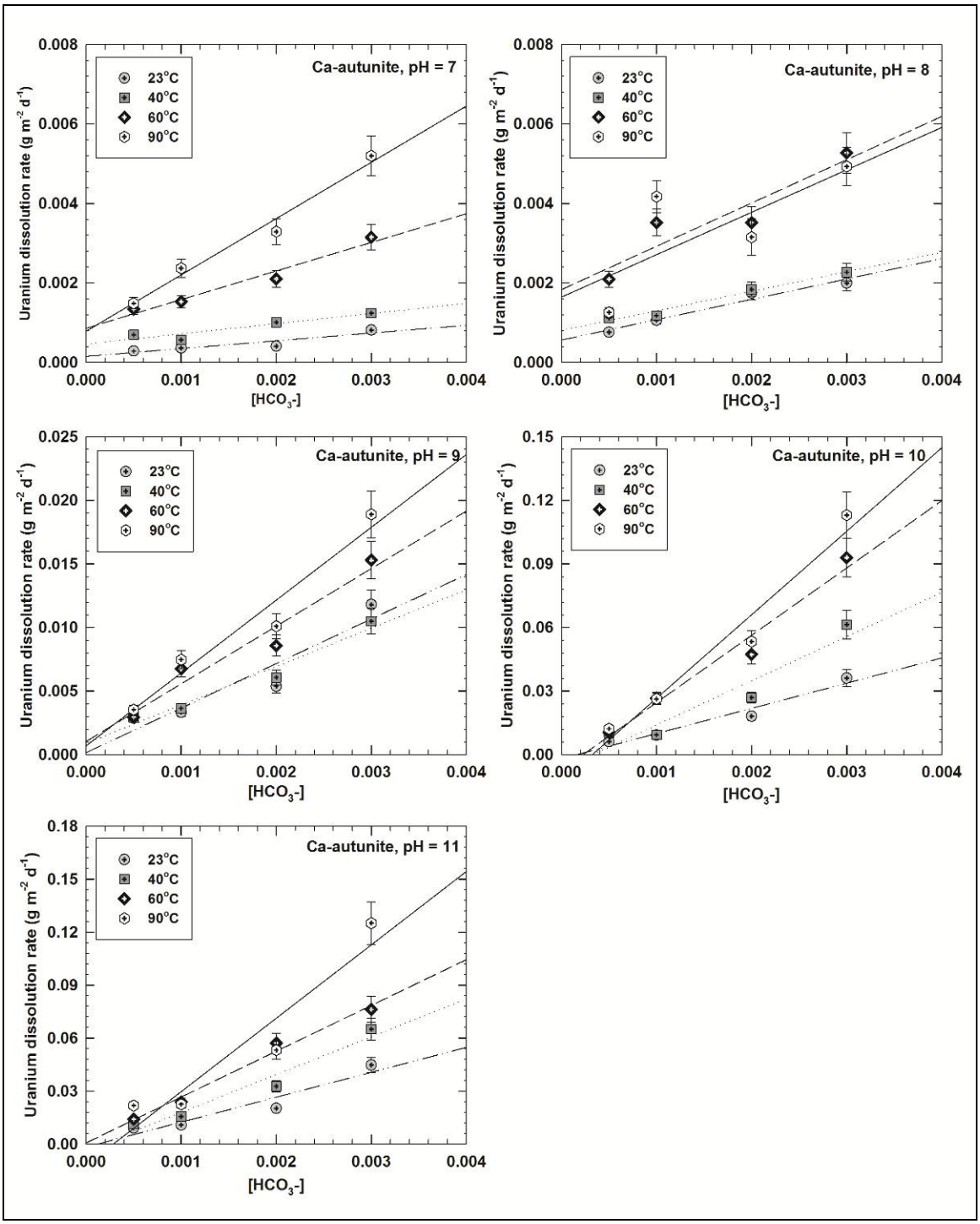


**Figure 35 Variations in the uranium dissolution as a function of bicarbonate concentration**

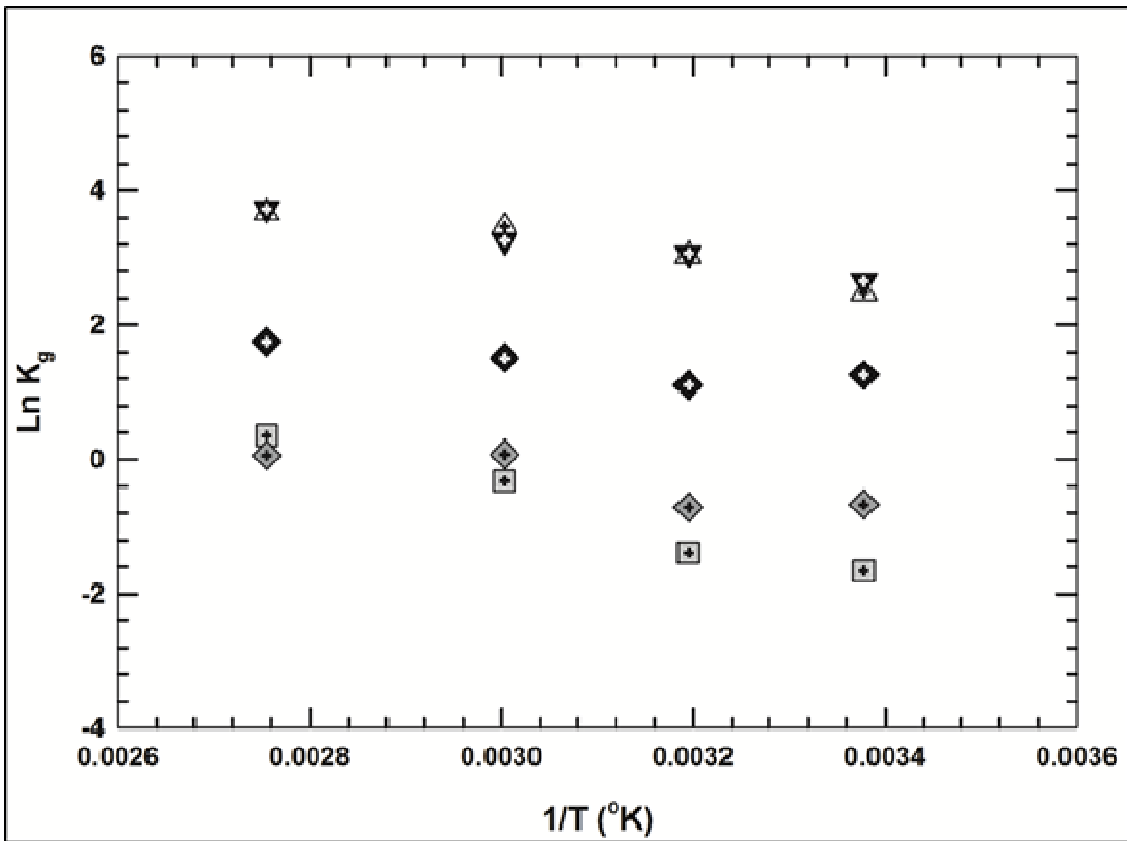


**Figure 36 Pseudo equilibrium constant for uranium release from Ca-autunite at different temperatures**

**Table 15 Pseudo equilibrium constants and enthalpy values at various pH for Ca-autunite and Na-autunite**

| pH | Ca-autunite | | Na-autunite | |
|---|---|---|---|---|
| | $K_g$ | ΔH (kJ $mol^{-1}$) | $K_g$ | ΔH (kJ $mol^{-1}$) |
| 7 | 0.65 | 28.58 | 0.16 | 19.39 |
| 8 | 0.79 | 11.83 | 0.35 | 17.24 |
| 9 | 4.20 | 11.90 | 1.39 | 24.80 |
| 10 | 25.97 | 15.88 | 1.34 | 12.44 |
| 11 | 27.75 | 13.84 | 1.30 | 9.41 |

The theoretical rate of uranium release was calculated, taking into account experimentally determined parameters associated with Equation 12, including estimated activation

energies and $K_g$ values. The theoretically determined rate of U(VI) release differs from the experimentally determined values within an error range ±10%.

## CONCLUSIONS

The rate of dissolution of Ca-autunite was evaluated under bicarbonate concentrations ranging from 0.0005 to 0.003 M, pH 7 to 11 and temperature variations from 23 to 90$^{o}$C via single-pass flow-through cell experiments. The power law coefficient (□) for Ca-autunite in the range of the experimental parameters tested was observed between 0.5 and 1.0. Similar to Na-autunite, there was no quantifiable dependency of Ca-autunite dissolution on temperature. The activation energy ($E_a$) data at pH 7 showed that the rate of dissolution was surface controlled while, at pH 8 - 11, the rate of dissolution was achieved by mass transfer, which is consistent with Na-autunite behavior. Pseudo equilibrium and enthalpy data showed that the dissolution process is slower at pH 7-8 and at higher pH the speed of dissolution increased. The kinetic rate law parameters for Ca-autunite were found to be higher than that for Na-autunite, suggesting a higher stability of Na-autunite. These differences were due to the active surface features of Ca-autunite and the formation of calcium uranium species, altering the solution saturation state. The dissolution rate data indicates that a low concentration of bicarbonate in the subsurface environments can impact the stability of the uranyl phosphate minerals. The information presented here provides necessary fundamental data to refine the bulk kinetic parameters currently being used to predict the fate of uranium in the subsurface.

REFERENCES

**Aagaard P., and Helgeson H. C.,** Thermodynamic and Kinetic Constraints on Reaction Rates among Minerals and Aqueous Solutions. I. Theoretical Considerations, American Journal of Science, 1982, Vol. 282, pp. 237 - 285.

**Anthony J. W., Bideaux R. A., Bladh K. W., and Nichols M. C.,** Arsenates, Phosphates, Vanadates. Mineral Data Publishing, 2000, pp. 680.

**Bemer R. A.,** Rate control of mineral dissolution under earth surface conditions, Amer. J. Sci., 1978, Vol. 278, pp. 1235 - 1252.

**Bernhard G., Geipel G., Riech T., Brendler V., Amayri S. and Nitsche H.,** Uranyl(VI) carbonate complex formation: Validation of the $Ca_2UO_2(CO_3)_3$ (aq) species, Radiochimica Acta, 2001, Vol. 89, pp. 511.

**Burns P. C.,** The crystal chemistry of uranium, Rev. Mineral. Geochem, 1999, Vol. 38, pp. 23 - 90.

**Chernikov A. A., Krutetskaya O. V., and Organova N. I.,** Natroautunite, Atomic Energy, 1957, pp. 901 - 905. DOI: 10.1007/BF01480073

**Clark D. L., Hobart D. E., and Neu M. P.,** Actinide carbonate complexes and their importance in actinide environmental chemistry, Chemical Reviews**,** 1995, Vol. 95, pp. 25.

**Fairchild J.G.,** Base exchange in artificial autunites. American Mineralogist, 1929,Vol. 4, pp. 265 - 275.

**Felmy A. R., Xia Y., and Wang Z.,** The solubility product of $NaUO_2PO_4*H_2O$ determined on phosphate and carbonate solutions, Radiochim. Acta, 2003, Vol. 93, pp. 401 - 408.

**Gorman - Lewis D., Shvareva T., Kubatko K., Burns P., Wellman D. M., Amara B., Szymanowski J.S., Navrotsky A., and Fein J B.,** Thermodynamic properties of autunite, uranyl hydrogen phosphate, and uranyl orthophosphate from solubility and calorimetric measurements, Environ. Sci. Technol. 2009, Vol. 43, pp. 7416 - 7422.

**Grenthe I., Fuger J., Konings R. J. M., Lemire R. J., Muller A. J., Nguyen-Trung C., and Wanner H.,** Chemical Thermodynamics of Uranium, Elsevier, Amsterdam, 1992.

**Gudavalli R.**, Effect of pH and Temperature on the Carbonate Promoted Dissolution of Synthetic Sodium Meta-autunite, Student Poster, Waste Management Symposium, Phoenix, 2010.

**Gudavalli R.**, Investigation of Effects of pH and Temperature on the Carbonate Promoted Dissolution of Meta-autunite, Student Poster, Waste Management Symposium, Phoenix, 2009.

**Gudavalli R., Katsenovich Y., Wellman D., Lagos L., and Tansel B.,** Investigation of the Effect of Water Quality Parameters on Dissolution of Sodium Meta-autunite, Student Poster, Waste Management Symposium, Phoenix, 2012.

**Gudavalli R., Katsenovich Y., Wellman D., Lagos L., and Tansel B.,** Effect of bicarbonate on the dissolution of sodium meta-autunite, Geochim. Cosmochim. Acta., (under review).

**Gudavalli R., Katsenovich Y., Wellman D., Lagos L., and Tansel B.,** Quantification of kinetic rate law parameters for the dissolution of sodium meta-autunite as a function of aqueous bicarbonate concentration, Geochim. Cosmochim. Acta., (under review).

**Guillaumont, R., Fanhänel, T., Fuger, J., Grenthe, I., Neck, V., Palmer D.A. and Rand M.H.,** Chemical Thermodynamics, OECD Nuclear Energy Agency, vol. 5, Elsevier, 2003.

**Heisbourg G., Hubert S., Dacheux N., Ritt J.,** The kinetics of dissolution of Th1-xUxO2 solid solutions in nitric media, Journal of Nuclear Materials, 2003, Vol. 321 (2-3), pp. 141 - 151.

**Jordan G., and Rammensee W.,** Dissolution rates and activation energy for dissolution of brucite (001): A new method based on the microtopography of crystal surfaces, Geochemica et Cosmochimica Acta, 1996, Vol. 60(24), pp. 5055 - 5062.

**Kalmykov S. N., and Choppin G. R.,** Mixed $Ca^{2+}/UO_2^{2+}/CO_3^{2-}$ complex formation at different ionic strengths, Radiochimica Acta, 2000, Vol. 88, pp. 603 - 606.

**Katsenovich Y. P., Carvajal D.A., Wellman D.M., Lagos E.L.,** Enhanced U(VI) release from autunite mineral by aerobic Arthrobacter sp. in the presence of aqueous bicarbonate, Chemical Geology, 2012, Vol. 308 - 309, pp. 1 - 9.

**Langmuir D.,** Aqueous environmental geochemistry. Prentice-Hall Inc., 1997.

**Lasaga A. C.,** Chemical kinetics of water-rock interactions, J. Geophys., 1984, Vol. 89 (B6), pp. 4009 - 4025.

**Lasaga A.C.,** Fundamental approaches in discibing mineral dissolution and precipitation rates, In A.F.White and S.L.Brantley (eds.): Chemical Weathering Rates of Silicate Minerals, Mineralogical Society of America, Washington, D.C., 1995, pp. 23 - 86.

**Liu C., Zachara J. M., Qafoku O., Mckinley J. P., Heald S. M., and Wang Z.,** Dissolution of uranyl microprecipitates in subsurface sediments at Hanford Site, USA, Geochimica et Cosmochimica Acta, 2004, Vol. 68(22), pp. 4519 - 4537.

**Locock A. J., and Burns P. C.,** The crystal structure of synthetic autunite, $Ca[(UO_2)(PO_4)]_2(H_2O)_{11}$, American Mineralogist, 2003, Vol. 88, pp. 240 - 244.

**McGrail B. P., Ebert W. L., Bakel A. J., and Peeler D. K.,** Measurement of kinetic rate law parameters on a Na- Ca- Al borosilicate glass for low-activity waste. Journal of Nuclear Materials, 1997, Vol. 249 (2), pp. 175-189.

**Mills, S. J., Kamp, A. R., and Birch W. D.,** The crystal structure of metanatroautunite, $Na[(UO_2)(PO_4)](H_2O)_3$, from the Lake Boga Granite, Victoria, Australia, American Mineralogist, 2012. Vol. 97, pp. 735 - 738.

**Nagy K.L.,** Dissolution and precipitation kinetics of sheet silicates, 1995: In A.F.White and S.L. Brantley (eds): Chemical Weathering Rates of Silicate Minerals, Mineralogical Society of America, Washington, D. C., pp. 173 - 233.

**Pablo J. D., Casas I., Gimenez J., Molera M., Rovira M., and Duro L.,** The oxidative dissolution mechanism of uranium dioxide. I. The effect of temperature in hydrogen carbonate medium, Geochemica et Cosmochimica Acta, 1999, vol. 63, pp. 3097-3103.

**Perez I., Casas I., Martin M., and Bruno J.,** The thermodynamics and kinetics of uranophane dissolution in bicarbonate test solutions, Geochemica et Cosmochimica Acta, 2000, Vol. 64, pp. 603 - 608.

**Riley R.G., Zachara J.M., and Wobber F.J.** Chemical Contaminants on DOE Lands and Selection of Contaminant Mixtures for Subsurface Science Research, Washington D. C., U.S. Department of Energy, Office of Energy Research, 1992.

**Scott P.D., Glasser D., and Nicol M.J.,** Kinetics of dissolution of β-uranium trioxide in acid and carbonate solutions, Journal of the Chemical Society, Dalton Transactions, 1997, Vol. 20, pp. 1939 - 1946.

**Sowder A. G., Clark S. B., and Fjeld R.A.,** The impact of mineralogy in the U(VI)-Ca-$PO_4$ system on the environmental availability of uranium, Journal of Radioanalytical and Nuclear Chemistry, 2001, Vol. 248 (3), pp. 517 - 524.

**Sparks D. L.,** Kinetics and Mechanisms of Chemical Reactions at the Soil Mineral/Water Interface, Soil Physical Chemistry. CRC Press, 1999.

**Wellman D. M., Gunderson K. M., Icenhower J. P., and Forrester S. W.,** Dissolution kinetics of synthetic and natural meta-autunite minerals, $X_{3-n}^{(n)+}[(UO_2)(PO_4)]_2 \bullet xH_2O$, under acidic conditions.,Geochem. Geophys. Geosyst., 2007, Vol. 8, pp. 16.

**Wellman D. M., Icenhower J. P., Gamerdinger A.P., and Forrester S. W.,** Effects of pH, temperature and aqueous organic material on the dissolution kinetics of meta-autunite minerals, $(Na, Ca)_{2-1}[(UO_2)(PO_4)]_2 \cdot 3H_2O$, American Mineralogist, 2006, Vol. 91, pp. 143- 158.

**Wellman D. M., McNamara B. K., Bacon D. H., Cordova E. A., Ermi R. M. and Laken M. T.,** Dissolution kinetics of meta-torbernite under circum-neutral to alkaline conditions, Environmental Chemistry, 2009, Vol. 6(6), pp. 551-560.

**Wellman D. M., Catalano J. G., Icenhower J. P., Gamerdinger A. P.,** Synthesis and characterization of sodium meta-autunite, $Na[UO_2PO_4]\cdot 3H_2O$, Radiochim. Acta, 2005, Vol. 93, pp. 393 - 399.

**Zhang Y., Hart K.P., Bourcier W.L., Day R.A., Colella M., Thomas B., Aly Z., and Jostsons A.,** Kinetics of uranium release from Synroc phases, Journal of Nuclear Materials, 2001, Vol. 289(3), pp. 254 - 262

**Zheng Z., Wan J., Song X., and Tokunaga T. K.,** Sodium meta-autunite colloids: Synthesis, characterization, and stability, Colloids and Surfaces A: Physicochem. Eng. Aspects, 2006, Vol. 274, pp. 48 - 55.

# APPENDIX

**Table A1. Single-pass flow-through experimental conditions and dissolution rates of Na-autunite**

| Sample ID | Surface Area ($m^2$) | Temp ($^oC$) | pH ($23^oC$) | Flow Rate ($mL\ d^{-1}$) | U ($\mu g\ L^{-1}$) | U Release ($mol\ m^{-2}\ s^{-1}$) |
|---|---|---|---|---|---|---|
| | | | 0.0005M $HCO_3^-$ | | | |
| SAUT-01 | 1.07 | 5 | 6 | 1014 | 24.3 | 2.74E-12 (5.31E-13) |
| SAUT-02 | 1.09 | 5 | 7 | 1021 | 41.2 | 3.600E-12 (6.98E-13) |
| SAUT-03 | 1.03 | 5 | 8 | 1022 | 79.5 | 7.02E-12 (1.36E-12) |
| SAUT-04 | 0.97 | 5 | 9 | 976 | 404.8 | 3.66E-11 (7.10E-12) |
| SAUT-05 | 0.65 | 5 | 10 | 1020 | 2057.8 | 2.94E-10 (4.09E-11) |
| SAUT-06 | 0.59 | 5 | 11 | 1003 | 414.7 | 6.30E-11 (1.22E-11) |
| SAUT-07 | 1.59 | 23 | 6 | 1016 | 245.9 | 1.90E-12 (3.69E-13) |
| SAUT-08 | 1.18 | 23 | 7 | 976 | 279.4 | 2.084E-11 (4.036E-12) |
| SAUT-09 | 1.59 | 23 | 8 | 952 | 1025.2 | 2.54E-11 (1.45E-11) |
| SAUT-10 | 1.18 | 23 | 9 | 1030 | 1075.8 | 8.55E-11 (2.46E-11) |
| SAUT-11 | 1.60 | 23 | 10 | 822 | 2070.4 | 7.83E-11 (8.77E-12) |
| SAUT-12 | 1.59 | 23 | 11 | 997 | 2799.0 | 1.12E-10 (2.17E-11) |
| SAUT-13 | 0.89 | 40 | 6 | 1483 | 85.6 | 1.28E-11 (2.49E-12) |
| SAUT-14 | 0.89 | 40 | 7 | 1500 | 177.7 | 2.685E-11 (5.19E-12) |
| SAUT-15 | 1.63 | 40 | 8 | 1474 | 496.0 | 4.06E-11 (1.43E-11) |
| SAUT-16 | 0.88 | 40 | 9 | 1513 | 706.7 | 1.10E-10 (2.12E-11) |
| SAUT-17 | 1.58 | 40 | 10 | 1512 | 1652.9 | 1.43E-10 (3.84E-11) |
| SAUT-18 | 1.12 | 40 | 11 | 1508 | 1161.0 | 1.33E-10 (2.58E-11) |
| SAUT-19 | 0.88 | 60 | 6 | 1910 | 68.6 | 1.32E-11 (2.55E-12) |
| SAUT-20 | 1.61 | 60 | 7 | 2429 | 214.9 | 2.94E-11 (7.92E-12) |
| SAUT-21 | 1.14 | 60 | 8 | 2448 | 640.7 | 1.24E-11 (2.41E-12) |
| SAUT-22 | 0.89 | 60 | 9 | 2425 | 1766.7 | 4.35E-11 (6.46E-12) |
| SAUT-23 | 1.16 | 60 | 10 | 2442 | 1816.2 | 3.52E-10 (6.81E-11) |
| SAUT-24 | 0.89 | 60 | 11 | 2435 | 681.9 | 1.90E-10 (3.68E-11) |

**Table A1 - Continued**

| Sample ID | Surface Area ($m^2$) | Temp ($^oC$) | pH ($23^oC$) | Flow Rate ($mL\ d^{-1}$) | U ($\mu g\ L^{-1}$) | U Release ($mol\ m^{-2}\ s^{-1}$) |
|---|---|---|---|---|---|---|
| | | | 0.001M $HCO_3^-$ | | | |
| SAUT-25 | 0.46 | 5 | 6 | 990 | 9.573 | 1.94E-12 (1.98E-13) |
| SAUT-26 | 0.77 | 5 | 7 | 989 | 32.123 | 3.70E-12 (7.16E-13) |
| SAUT-27 | 0.77 | 5 | 8 | 1003 | 99.458 | 1.18E-11 (2.28E-12) |
| SAUT-28 | 0.76 | 5 | 9 | 1021 | 414.558 | 5.04E-11 (9.76E-12) |
| SAUT-29 | 0.69 | 5 | 10 | 1002 | 2131.330 | 2.79E-10 (3.88E-11) |
| SAUT-30 | 0.55 | 5 | 11 | 986 | 683.31 | 1.10E-10 (2.12E-11) |
| SAUT-31 | 1.17 | 23 | 6 | 976 | 14.4 | 1.4E-12 (2.1E-13) |
| SAUT-32 | 0.88 | 23 | 7 | 973 | 48.5 | 2.47E-11 (6.99E-13) |
| SAUT-33 | 1.18 | 23 | 8 | 980 | 654.0 | 3.58E-11 (5.98E-12) |
| SAUT-34 | 1.18 | 23 | 9 | 971 | 1605.6 | 1.27E-10 (2.46E-11) |
| SAUT-35 | 0.88 | 23 | 10 | 1001 | 799.9 | 8.23E-11 (8.77E-12) |
| SAUT-36 | 1.14 | 23 | 11 | 1000 | 1303.3 | 1.00E-10 (1.94E-11) |
| SAUT-37 | 0.88 | 40 | 6 | 1509 | 102.6 | 1.59E-11 (3.09E-12) |
| SAUT-38 | 0.88 | 40 | 7 | 1514 | 191.4 | 2.99E-11 (5.80E-12) |
| SAUT-39 | 0.88 | 40 | 8 | 1518 | 315.4 | 5.36E-11 (9.54E-12) |
| SAUT-40 | 0.89 | 40 | 9 | 1528 | 832.0 | 1.09E-10 (2.12E-11) |
| SAUT-41 | 1.59 | 40 | 10 | 1495 | 1589.8 | 1.88E-10 (2.61E-11) |
| SAUT-42 | 1.13 | 40 | 11 | 1507 | 1548.1 | 1.92E-10 (3.71E-11) |
| SAUT-43 | 0.89 | 60 | 6 | 2430 | 21.2 | 7.15E-12 (1.35E-12) |
| SAUT-44 | 0.87 | 60 | 7 | 2443 | 64.9 | 3.64E-11 (2.44E-12) |
| SAUT-45 | 1.12 | 60 | 8 | 2412 | 194.3 | 3.78E-11 (7.33E-12) |
| SAUT-46 | 1.16 | 60 | 9 | 2452 | 615.2 | 1.17E-10 (2.26E-11) |
| SAUT-47 | 1.13 | 60 | 10 | 2442 | 2433.2 | 4.60E-10 (9.21E-11) |
| SAUT-48 | 1.55 | 60 | 11 | 2447 | 1757.6 | 2.50E-10 (4.85E-11) |

**Table A1 - Continued**

| Sample ID | Surface Area ($m^2$) | Temp ($^oC$) | pH ($23^oC$) | Flow Rate ($mL\ d^{-1}$) | U ($\mu g\ L^{-1}$) | U Release ($mol\ m^{-2}\ s^{-1}$) |
|---|---|---|---|---|---|---|
| | | | 0.002M $HCO_3^-$ | | | |
| SAUT-49 | 0.61 | 5 | 6 | 977 | 20.3 | 2.95E-12 (4.11E-13) |
| SAUT-50 | 0.84 | 5 | 7 | 1037 | 68.2 | 7.65E-12 (1.48E-12) |
| SAUT-51 | 1.03 | 5 | 8 | 1019 | 152.6 | 1.37E-11 (2.65E-12) |
| SAUT-52 | 0.82 | 5 | 9 | 976 | 551.1 | 5.90E-11 (1.14E-11) |
| SAUT-53 | 0.59 | 5 | 10 | 1003 | 2060 | 3.13E-10 (4.36E-11) |
| SAUT-54 | 0.59 | 5 | 11 | 1004 | 946.1 | 1.49E-10 (2.89E-11) |
| SAUT-55 | 0.88 | 23 | 6 | 994 | 13.9 | 1.73E-12 (2.08E-13) |
| SAUT-56 | 1.18 | 23 | 7 | 961 | 388.2 | 2.86E-11 (5.54E-12) |
| SAUT-57 | 1.18 | 23 | 8 | 966 | 393.1 | 3.59E-11 (6.34E-12) |
| SAUT-58 | 1.59 | 23 | 9 | 955 | 3851.3 | 2.12E-10 (5.57E-11) |
| SAUT-59 | 1.12 | 23 | 10 | 976 | 1727.2 | 1.35E-10 (1.88E-11) |
| SAUT-60 | 0.89 | 23 | 11 | 978 | 1154.2 | 1.16E-10 (2.21E-11) |
| SAUT-61 | 0.88 | 40 | 6 | 1492 | 191.4 | 2.70E-11 (5.23E-12) |
| SAUT-62 | 0.86 | 40 | 7 | 1504 | 265.5 | 4.17E-11 (8.09E-12) |
| SAUT-63 | 0.86 | 40 | 8 | 1506 | 460.3 | 7.26E-11 (1.40E-11) |
| SAUT-64 | 0.87 | 40 | 9 | 1517 | 1576.9 | 2.49E-10 (4.83E-11) |
| SAUT-65 | 1.63 | 40 | 10 | 1512 | 3386.3 | 2.77E-10 (5.40E-11) |
| SAUT-66 | 1.14 | 40 | 11 | 1502 | 2196.0 | 2.62E-10 (5.07E-11) |
| SAUT-67 | 0.86 | 60 | 6 | 2432 | 55.7 | 1.86E-11 (2.11E-12) |
| SAUT-68 | 1.15 | 60 | 7 | 2450 | 241.3 | 4.65E-11 (9.01E-12) |
| SAUT-69 | 1.14 | 60 | 8 | 2455 | 203.4 | 4.64E-11 (7.65E-12) |
| SAUT-70 | 0.89 | 60 | 9 | 2440 | 633.5 | 1.75E-10 (2.33E-11) |
| SAUT-71 | 0.88 | 60 | 10 | 2445 | 1833.1 | 4.70E-10 (6.78E-11) |
| SAUT-72 | 1.17 | 60 | 11 | 2430 | 1723.1 | 3.23E-10 (6.26E-11) |

**Table A1 - Continued**

| Sample ID | Surface Area ($m^2$) | Temp ($^oC$) | pH ($23^oC$) | Flow Rate ($mL\ d^{-1}$) | U ($\mu g\ L^{-1}$) | U Release ($mol\ m^{-2}\ s^{-1}$) |
|---|---|---|---|---|---|---|
| | | | 0.003M $HCO_3^-$ | | | |
| SAUT-73 | 0.60 | 5 | 6 | 1016 | 34.7 | 5.41E-12 (7.52E-13) |
| SAUT-74 | 0.83 | 5 | 7 | 990 | 92.8 | 9.85E-12 (1.91E-12) |
| SAUT-75 | 0.82 | 5 | 8 | 994 | 204.2 | 2.22E-11 (4.31E-12) |
| SAUT-76 | 0.88 | 5 | 9 | 973 | 709.5 | 7.08E-11 (1.37E-11) |
| SAUT-77 | 0.64 | 5 | 10 | 973 | 3380.0 | 4.64E-10 (6.45E-11) |
| SAUT-78 | 0.65 | 5 | 11 | 995 | 1218.6 | 1.69E-10 (3.28E-11) |
| SAUT-79 | 1.19 | 23 | 6 | 986 | 150.8 | 9.88E-12 (2.18E-12) |
| SAUT-80 | 1.19 | 23 | 7 | 995 | 427.9 | 4.23E-11 (6.25E-12) |
| SAUT-81 | 0.88 | 23 | 8 | 1001 | 798.8 | 8.13E-11 (1.21E-11) |
| SAUT-82 | 0.89 | 23 | 9 | 982 | 1329.5 | 1.55E-10 (2.57E-11) |
| SAUT-83 | 1.12 | 23 | 10 | 982 | 1487.4 | 1.17E-10 (1.63E-11) |
| SAUT-84 | 0.89 | 23 | 11 | 978 | 2670.8 | 2.64E-10 (3.92E-11) |
| SAUT-85 | 0.87 | 40 | 6 | 1501 | 188.1 | 2.94E-11 (5.69E-12) |
| SAUT-86 | 0.87 | 40 | 7 | 1508 | 305.1 | 4.76E-11 (9.22E-12) |
| SAUT-87 | 1.14 | 40 | 8 | 1501 | 1113.4 | 1.32E-10 (2.56E-11) |
| SAUT-88 | 1.12 | 40 | 9 | 1504 | 2748.5 | 3.31E-10 (6.42E-11) |
| SAUT-89 | 0.87 | 40 | 10 | 1477 | 1665.9 | 2.54E-10 (3.77E-11) |
| SAUT-90 | 1.15 | 40 | 11 | 1512 | 2737.6 | 3.26E-10 (6.31E-11) |
| SAUT-91 | 1.15 | 60 | 6 | 2431 | 238.9 | 4.58E-11 (8.86E-12) |
| SAUT-92 | 1.59 | 60 | 7 | 2442 | 310.8 | 6.00E-11 (1.16E-11) |
| SAUT-93 | 0.86 | 60 | 8 | 2432 | 274.9 | 6.98E-11 (1.03E-11) |
| SAUT-94 | 0.87 | 60 | 9 | 2426 | 743.7 | 2.04E-10 (2.76E-11) |
| SAUT-95 | 0.86 | 60 | 10 | 2429 | 2736.3 | 6.98E-10 (1.03E-10) |
| SAUT-96 | 1.14 | 60 | 11 | 2421 | 2026.7 | 3.89E-10 (7.53E-11) |

**Table A2 Single-Pass flow-through experimental conditions and dissolution rates of Ca-autunite**

| Sample ID | Surface Area ($m^2$) | Temp ($^oC$) | pH ($23^oC$) | Flow Rate ($mL\ d^{-1}$) | U ($\mu g\ L^{-1}$) | U Release ($mol\ m^{-2}\ s^{-1}$) |
|---|---|---|---|---|---|---|
| | | | 0.0005 M $HCO_3^-$ | | | |
| AUT-261 | 0.195 | 23 | 7 | 847 | 48 | 1.40E-11 (1.72E-12) |
| AUT-262 | 0.198 | 23 | 8 | 991 | 88 | 3.70E-11 (3.58E-12) |
| AUT-263 | 0.199 | 23 | 9 | 971 | 341 | 1.40E-10 (1.39E-11) |
| AUT-264 | 0.197 | 23 | 10 | 998 | 696 | 2.97E-10 (2.89E-11) |
| AUT-265 | 0.196 | 23 | 11 | 954 | 1090 | 4.44E-10 (4.43E-11) |
| AUT-266 | 0.197 | 40 | 7 | 1510 | 53 | 3.38E-11 (3.29E-12) |
| AUT-267 | 0.196 | 40 | 8 | 1510 | 84 | 5.45E-11 (5.30E-12) |
| AUT-268 | 0.197 | 40 | 9 | 1500 | 222 | 1.42E-10 (1.38E-11) |
| AUT-269 | 0.196 | 40 | 10 | 1490 | 793 | 5.06E-10 (4.91E-11) |
| AUT-270 | 0.198 | 40 | 11 | 1490 | 889 | 5.64E-10 (5.45E-11) |
| AUT-271 | 0.202 | 60 | 7 | 2290 | 69 | 6.52E-11 (6.32E-12) |
| AUT-272 | 0.197 | 60 | 8 | 2200 | 109 | 1.02E-10 (9.87E-12) |
| AUT-273 | 0.196 | 60 | 9 | 2180 | 153 | 1.43E-10 (1.41E-11) |
| AUT-274 | 0.199 | 60 | 10 | 2380 | 506 | 5.11E-10 (4.96E-11) |
| AUT-275 | 0.202 | 60 | 11 | 2340 | 699 | 6.81E-10 (6.61E-11) |
| AUT-276 | 0.201 | 90 | 7 | 2620 | 66 | 7.25E-11 (7.05E-12) |
| AUT-277 | 0.197 | 90 | 8 | 2620 | 54 | 6.13E-11 (5.93E-12) |
| AUT-278 | 0.197 | 90 | 9 | 2620 | 154 | 1.72E-10 (1.67E-11) |
| AUT-279 | 0.195 | 90 | 10 | 2710 | 507 | 5.93E-10 (5.74E-11) |
| AUT-280 | 0.199 | 90 | 11 | 2690 | 929 | 1.06E-09 (1.03E-10) |

**Table A2 - Continued**

| Sample ID | Surface Area ($m^2$) | Temp ($^oC$) | pH ($23^oC$) | Flow Rate ($mL\ d^{-1}$) | U ($\mu g\ L^{-1}$) | U Release ($mol\ m^{-2}\ s^{-1}$) |
|---|---|---|---|---|---|---|
| | | | 0.001 M $HCO_3^-$ | | | |
| AUT-281 | 0.201 | 23 | 7 | 1090 | 38 | 1.77E-11 (1.85E-12) |
| AUT-282 | 0.199 | 23 | 8 | 1100 | 113 | 5.15E-11 (5.01E-12) |
| AUT-283 | 0.200 | 23 | 9 | 1100 | 362 | 1.62E-10 (1.58E-11) |
| AUT-284 | 0.198 | 23 | 10 | 1110 | 980 | 4.45E-10 (4.32E-11) |
| AUT-285 | 0.199 | 23 | 11 | 1080 | 1110 | 5.25E-10 (5.50E-11) |
| AUT-286 | 0.202 | 40 | 7 | 1340 | 48 | 2.77E-11 (2.81E-12) |
| AUT-287 | 0.198 | 40 | 8 | 1350 | 101 | 5.74E-11 (5.59E-12) |
| AUT-288 | 0.199 | 40 | 9 | 1350 | 315 | 1.77E-10 (1.73E-11) |
| AUT-289 | 0.197 | 40 | 10 | 1340 | 808 | 4.54E-10 (4.43E-11) |
| AUT-290 | 0.198 | 40 | 11 | 1340 | 1300 | 7.59E-10 (7.63E-11) |
| AUT-291 | 0.197 | 60 | 7 | 2310 | 75 | 7.44E-11 (7.20E-12) |
| AUT-292 | 0.197 | 60 | 8 | 2170 | 187 | 1.71E-10 (1.66E-11) |
| AUT-293 | 0.197 | 60 | 9 | 2190 | 354 | 3.29E-10 (3.19E-11) |
| AUT-294 | 0.200 | 60 | 10 | 2330 | 1330 | 1.30E-09 (1.26E-10) |
| AUT-295 | 0.196 | 60 | 11 | 2330 | 1150 | 1.15E-09 (1.12E-10) |
| AUT-296 | 0.202 | 90 | 7 | 2550 | 108 | 1.15E-10 (1.12E-11) |
| AUT-297 | 0.199 | 90 | 8 | 2620 | 183 | 2.03E-10 (1.97E-11) |
| AUT-298 | 0.197 | 90 | 9 | 2660 | 321 | 3.63E-10 (3.53E-11) |
| AUT-299 | 0.201 | 90 | 10 | 2720 | 1120 | 1.28E-09 (1.24E-10) |
| AUT-300 | 0.197 | 90 | 11 | 2660 | 965 | 1.09E-09 (1.07E-10) |

**Table A2 - Continued**

| Sample ID | Surface Area ($m^2$) | Temp ($^oC$) | pH ($23^oC$) | Flow Rate ($mL\ d^{-1}$) | U ($\mu g\ L^{-1}$) | U Release ($mol\ m^{-2}\ s^{-1}$) |
|---|---|---|---|---|---|---|
| | | | 0.002 M $HCO_3^-$ | | | |
| AUT-301 | 0.201 | 23 | 7 | 990 | 48 | 1.99E-11 (1.93E-12) |
| AUT-302 | 0.201 | 23 | 8 | 997 | 203 | 8.51E-11 (8.27E-12) |
| AUT-303 | 0.200 | 23 | 9 | 995 | 623 | 2.62E-10 (2.56E-11) |
| AUT-304 | 0.198 | 23 | 10 | 1030 | 2010 | 8.80E-10 (8.56E-11) |
| AUT-305 | 0.198 | 23 | 11 | 968 | 2380 | 9.82E-10 (9.58E-11) |
| AUT-306 | 0.202 | 40 | 7 | 1500 | 79 | 4.91E-11 (4.86E-12) |
| AUT-307 | 0.197 | 40 | 8 | 1520 | 137 | 8.95E-11 (8.70E-12) |
| AUT-308 | 0.198 | 40 | 9 | 1520 | 456 | 2.95E-10 (2.87E-11) |
| AUT-309 | 0.200 | 40 | 10 | 1520 | 2040 | 1.31E-09 (1.27E-10) |
| AUT-310 | 0.201 | 40 | 11 | 1520 | 2500 | 1.59E-09 (1.54E-10) |
| AUT-311 | 0.202 | 60 | 7 | 2250 | 110 | 1.02E-10 (9.92E-12) |
| AUT-312 | 0.199 | 60 | 8 | 1910 | 247 | 1.71E-10 (1.93E-11) |
| AUT-313 | 0.201 | 60 | 9 | 2450 | 406 | 4.17E-10 (4.04E-11) |
| AUT-314 | 0.196 | 60 | 10 | 2450 | 2180 | 2.30E-09 (2.24E-10) |
| AUT-315 | 0.202 | 60 | 11 | 2440 | 2720 | 2.78E-09 (2.71E-10) |
| AUT-316 | 0.198 | 90 | 7 | 2520 | 150 | 1.60E-10 (1.56E-11) |
| AUT-317 | 0.197 | 90 | 8 | 2390 | 225 | 1.53E-10 (2.26E-11) |
| AUT-318 | 0.202 | 90 | 9 | 2960 | 396 | 4.91E-10 (4.78E-11) |
| AUT-319 | 0.196 | 90 | 10 | 2820 | 2150 | 2.60E-09 (2.52E-10) |
| AUT-320 | 0.199 | 90 | 11 | 2800 | 1740 | 2.59E-09 (2.52E-10) |

**Table A2 - Continued**

| Sample ID | Surface Area ($m^2$) | Temp ($^oC$) | pH ($23^oC$) | Flow Rate ($mL\ d^{-1}$) | U ($\mu g\ L^{-1}$) | U Release ($mol\ m^{-2}\ s^{-1}$) |
|---|---|---|---|---|---|---|
| | | | 0.003 M $HCO_3^-$ | | | |
| AUT-321 | 0.198 | 23 | 7 | 940 | 99 | 3.96E-11 (3.85E-12) |
| AUT-322 | 0.199 | 23 | 8 | 1010 | 227 | 9.73E-11 (9.43E-12) |
| AUT-323 | 0.199 | 23 | 9 | 1030 | 1310 | 5.74E-10 (5.54E-11) |
| AUT-324 | 0.201 | 23 | 10 | 805 | 4130 | 1.76E-09 (1.97E-10) |
| AUT-325 | 0.199 | 23 | 11 | 1010 | 5070 | 2.17E-09 (2.12E-10) |
| AUT-326 | 0.196 | 40 | 7 | 1500 | 94 | 6.03E-11 (5.84E-12) |
| AUT-327 | 0.200 | 40 | 8 | 1560 | 168 | 1.10E-10 (1.07E-11) |
| AUT-328 | 0.197 | 40 | 9 | 1540 | 774 | 5.11E-10 (4.96E-11) |
| AUT-329 | 0.197 | 40 | 10 | 1220 | 5090 | 2.98E-09 (3.34E-10) |
| AUT-330 | 0.197 | 40 | 11 | 1540 | 4840 | 3.17E-09 (3.07E-10) |
| AUT-331 | 0.201 | 60 | 7 | 2400 | 151 | 1.53E-10 (1.55E-11) |
| AUT-332 | 0.201 | 60 | 8 | 2270 | 268 | 2.56E-10 (2.49E-11) |
| AUT-333 | 0.202 | 60 | 9 | 2270 | 791 | 7.44E-10 (7.25E-11) |
| AUT-334 | 0.197 | 60 | 10 | 2260 | 4670 | 4.52E-09 (4.38E-10) |
| AUT-335 | 0.197 | 60 | 11 | 2270 | 3830 | 3.71E-09 (3.59E-10) |
| AUT-336 | 0.201 | 90 | 7 | 2800 | 217 | 2.53E-10 (2.46E-11) |
| AUT-337 | 0.201 | 90 | 8 | 2810 | 204 | 2.40E-10 (2.32E-11) |
| AUT-338 | 0.199 | 90 | 9 | 2790 | 779 | 9.19E-10 (8.90E-11) |
| AUT-339 | 0.196 | 90 | 10 | 2700 | 4740 | 5.50E-09 (5.30E-10) |
| AUT-340 | 0.199 | 90 | 11 | 2640 | 5440 | 6.08E-09 (5.88E-10) |

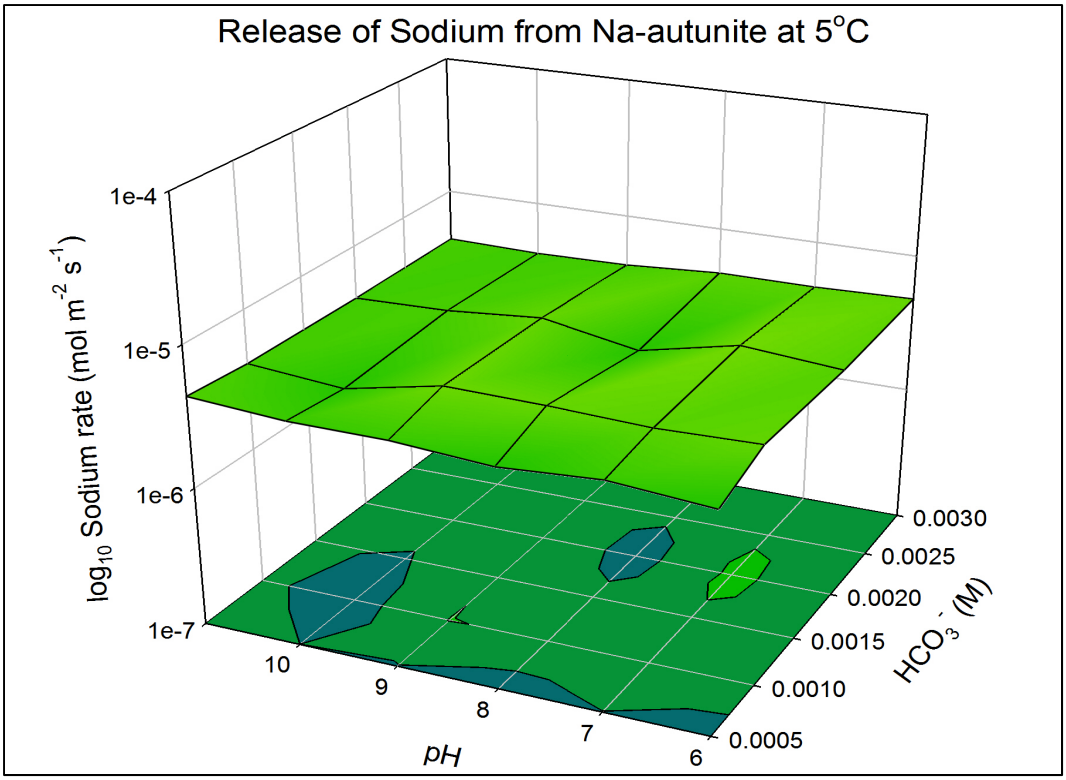


**Figure A1 3D representation of sodium release from Na-autunite at 5°C**

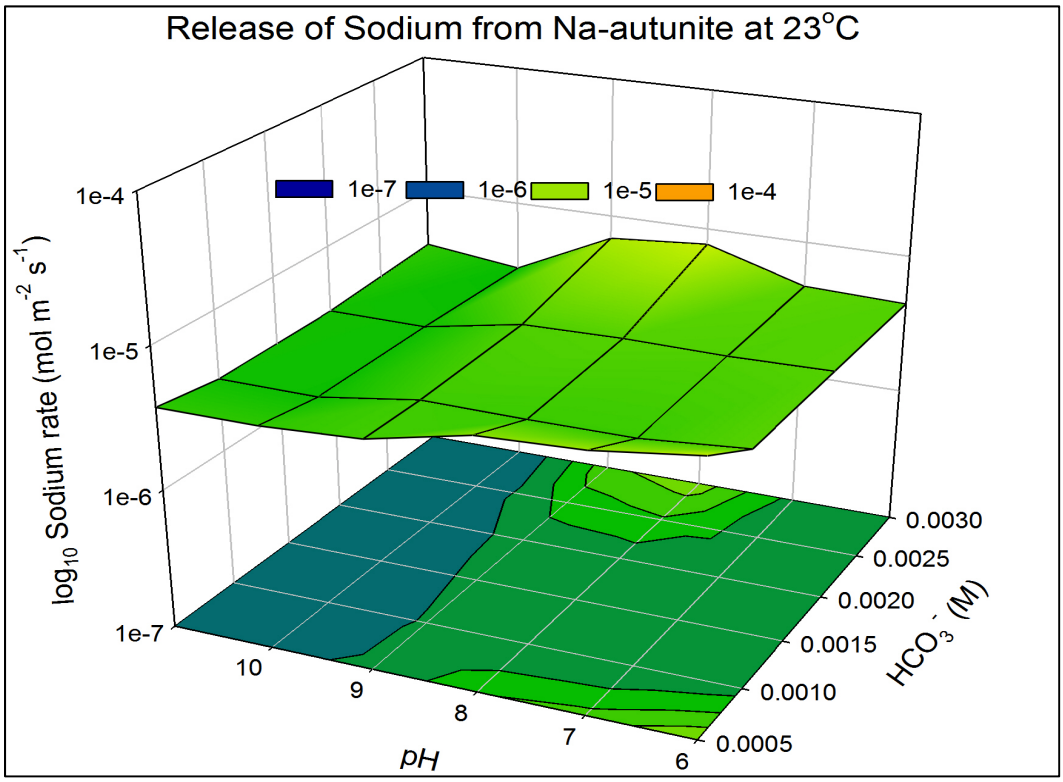


**Figure A2 3D representation of sodium release from Na-autunite at 23°C**

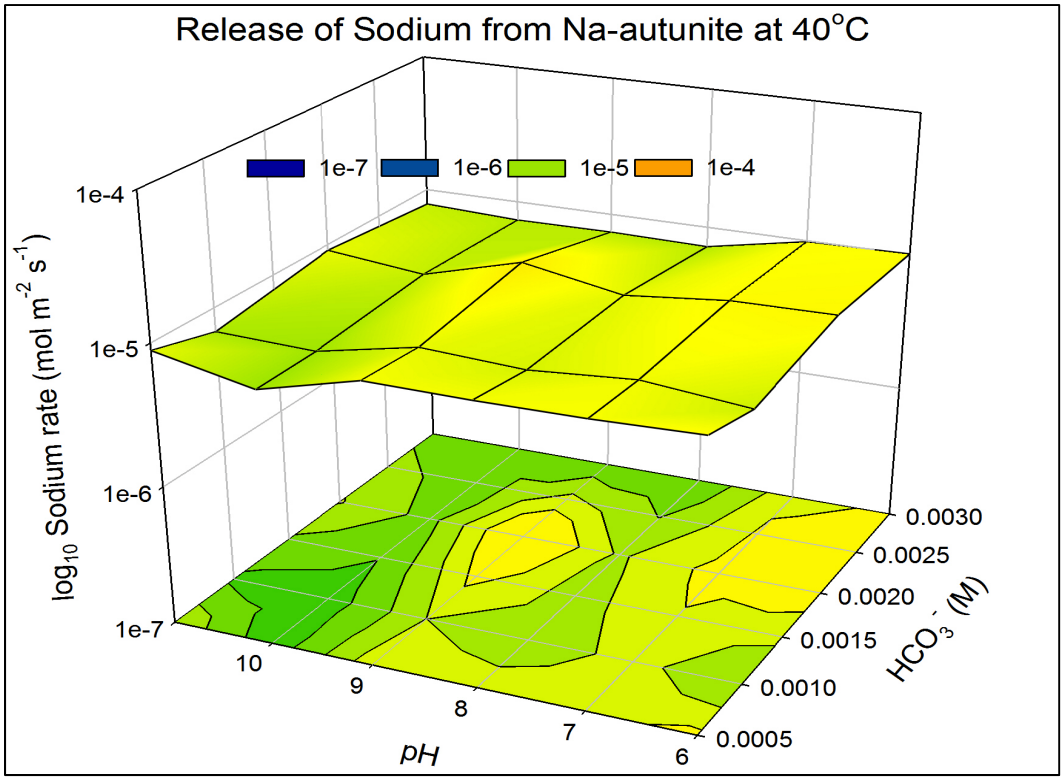


**Figure A3 3D representation of sodium release from Na-autunite at 40°C**

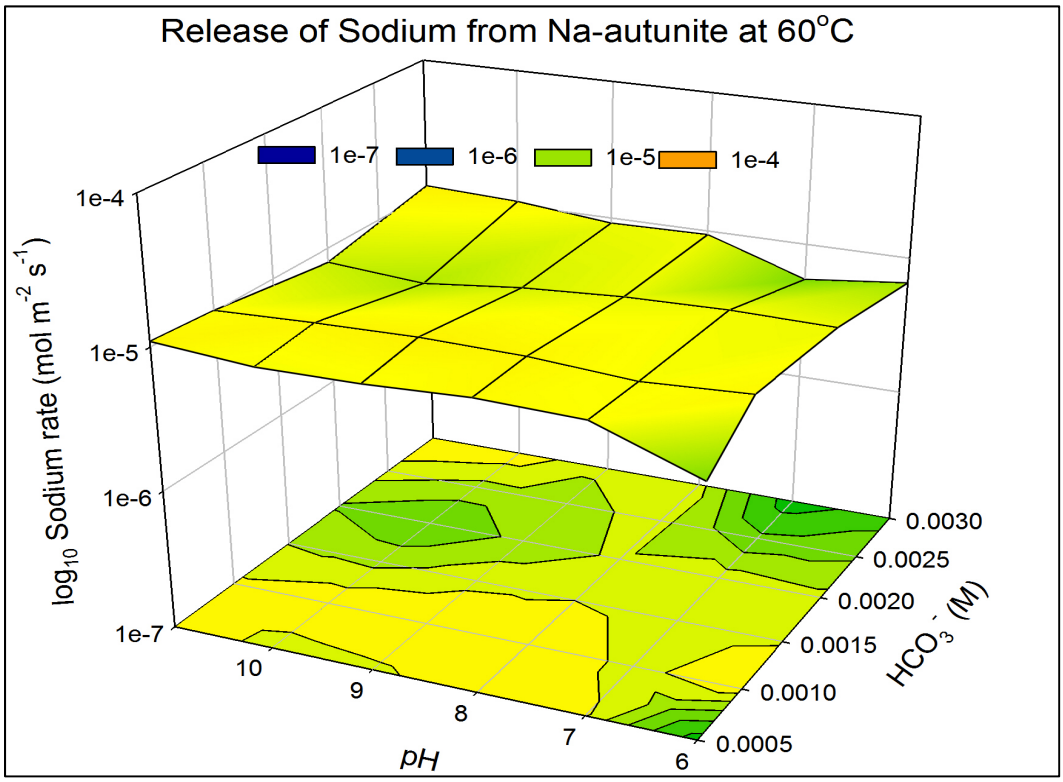


**Figure A4 3D representation of sodium release from Na-autunite at 60°C**

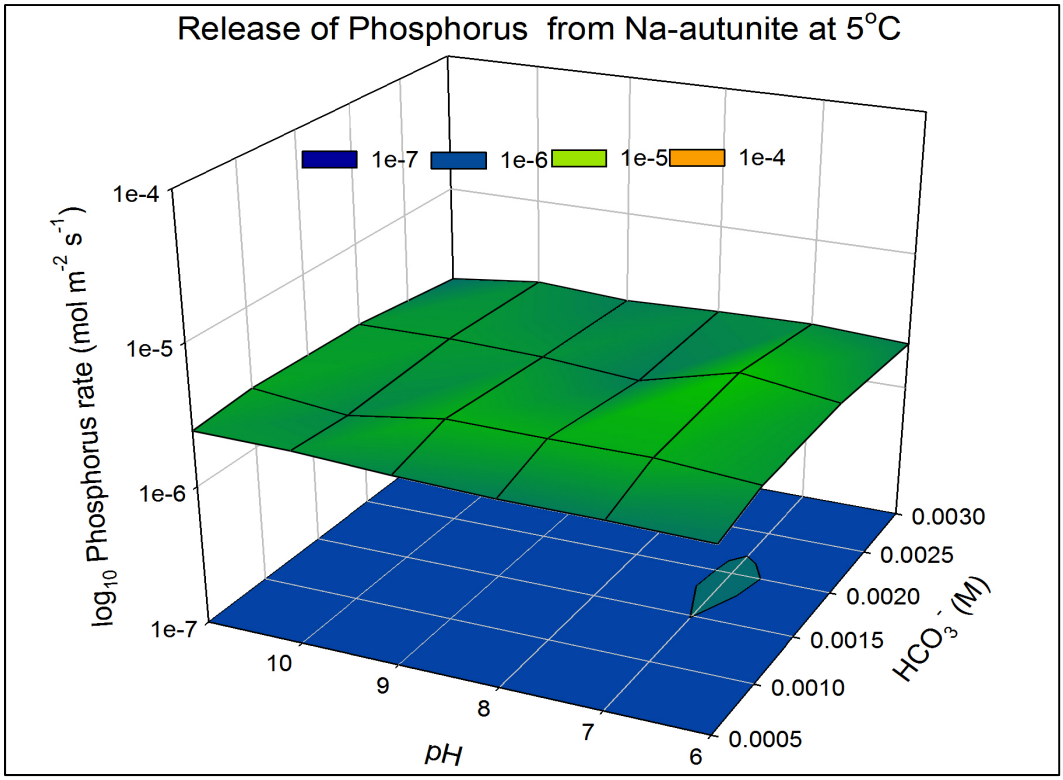


**Figure A5 3D representation of phosphorus release from Na-autunite at 5°C**

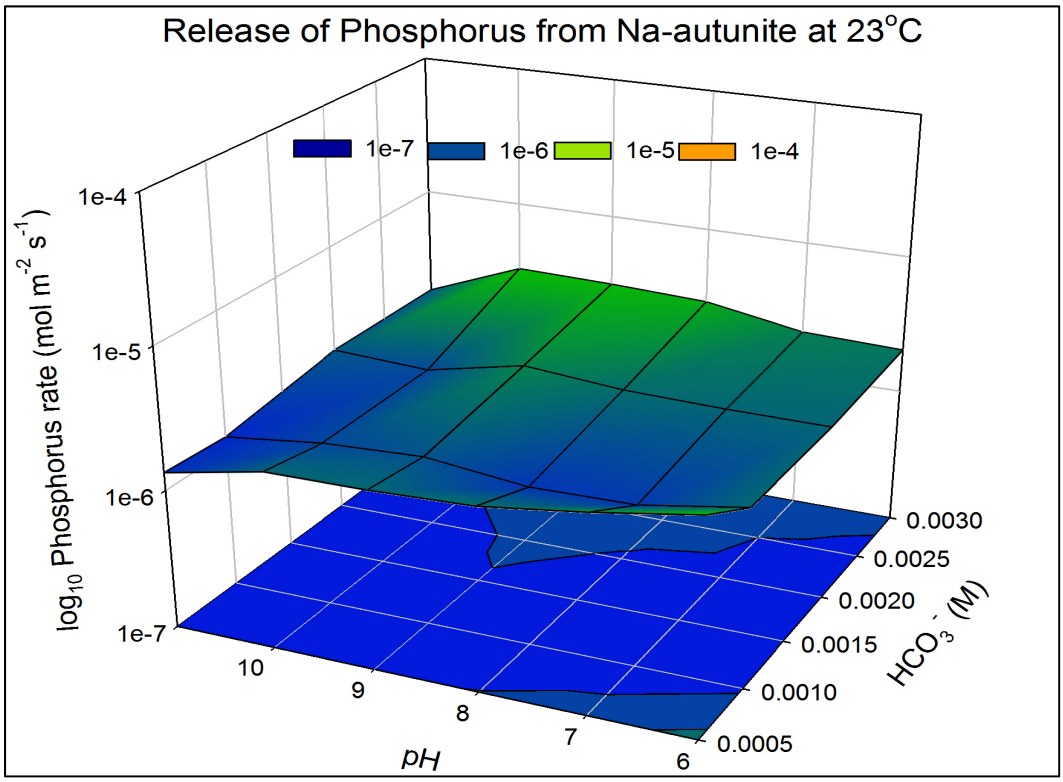


**Figure A6 3D representation of phosphorus release from Na-autunite at 23°C**

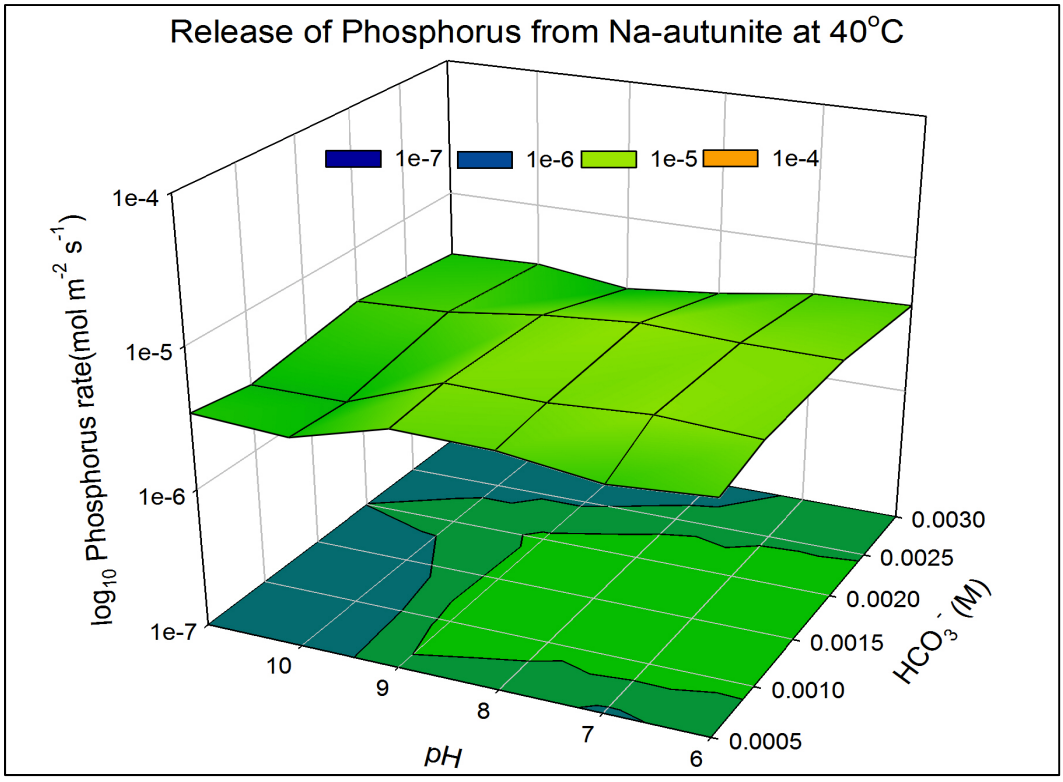


**Figure A7 3D representation of phosphorus release from Na-autunite at 40°C**

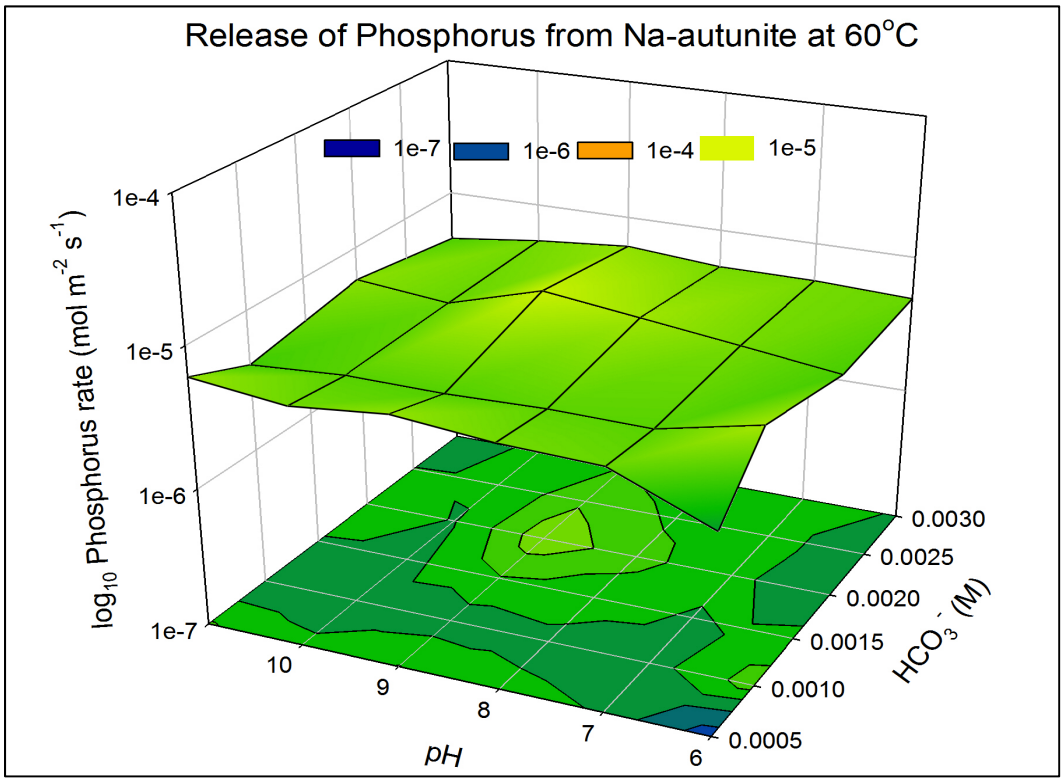


**Figure A8 3D representation of phosphorus release from Na-autunite at 60°C**

# VITA

RAVI KRISHNA PRASANTH GUDAVALLI

| | |
|---|---|
| 2002 | B.Tech., Chemical Engineering<br>Jawaharlal Nehru Technological University,<br>Hydrabad, India |
| 2005 | M.S., Environmental Engineering<br>Florida International University<br>Miami, Florida |
| 2003 - 2005<br>2008 - 2012 | Research Assistant<br>Applied Research Center<br>Florida International University<br>Miami, Florida |
| 2006 | Research Analyst, Assistant Lab Manager<br>Applied Research Center<br>Florida International University<br>Miami, Florida |
| 2007 | Instructor<br>Department of Civil and Environmental Engineering<br>Florida International University<br>Miami, Florida |
| 2008 - 2012 | Doctoral Candidate<br>Florida International University<br>Miami, Florida |

## PUBLICATIONS AND PRESENTATIONS

R. Gudavalli, Y. Katsenovich, D. Wellman, M. Idarraga, L. Lagos, and B. Tansel: "*Comparison of the kinetic rate law parameters for the dissolution of natural and synthetic autunite in the presence of bicarbonate ions*", Chemical Geology., (under review).

R. Gudavalli, Y. Katsenovich, D. Wellman, L. Lagos, and B. Tansel: "*Quantification of kinetic rate law parameters for the dissolution of sodium meta-autunite as a function of aqueous bicarbonate concentration*", Geochim. Cosmochim. Acta., (under review).

R. Gudavalli, Y. Katsenovich, D. Wellman, L. Lagos, and B. Tansel: "*Effect of bicarbonate on the dissolution of sodium meta-autunite*", Geochim. Cosmochim. Acta., (under review).

R. Gudavalli, Y. Katsenovich, L. Lagos, and B. Tansel: "*Investigation of the Effect of*

*Water Quality Parameters on Dissolution of Sodium Meta-Autunite*", Student Poster Competition, Waste Management Symposia, Phoenix, Arizona, February 27 - March 3, 2012.

R. Gudavalli: "*Effect of pH and Temperature on the Carbonate-Promoted Dissolution of Synthetic Sodium Meta-autunite*", Student Poster Competition, Waste Management Symposia, Phoenix, Arizona, March 7 - 11, 2010.

L. Lagos, R Gudavalli, A. Zidan, and B. Tansel: "*Effectiveness of Moisture and Fixatives in Controlling Mobility of Contaminated Soil Particles by Wind Forces*", Pract. Period. Hazard. Toxic Radioact. Waste Manage., 14(3), 215 - 218, 2010.

R. Gudavalli: "*Investigation of Effects of pH and Temperature on the Carbonate Promoted Dissolution of Meta-autunite*", Student Poster Competition, Waste Management Symposia, Phoenix, Arizona, March 1 - 5, 2009.

L. Lagos, and R. Gudavalli: "*Assessment of Soil Moisture and Fixative Performance in Controlling Wind Erosion of Contaminated Soil at the Hanford Site*", Waste Management Symposia, Phoenix, Arizona, February 24 - 28, 2008.

L. Lagos, J. Varona, A. Zidan, R. Gudavalli, and K. Wu: *"Preliminary Experimental Analysis of Soil Stabilizers for Contamination Control"*, ICONE14, International Conference on Nuclear Engineering, Miami, Florida, July 17 - 20, 2006.

L. Lagos, C. Duran, J. Varona, Dr. Y. Katsenovich, R. Gudavalli, and A. Zidan: " Design and Testing of an Improved Field Deplorable System for the Remote Long Term Monitoring of Bromide, pH, and ORP at the Hanford Site", Waste Management Symposia, Tucson, Arizona, February 26 - March 2, 2006.

C. Duran, J. Varona, R. Gudavalli, L. Logos, and M. Allen; "*Long Term Remote Monitoring of TCE Contaminated Groundwater at Savannah River Site*", American Nuclear Energy Symposium, Miami, Florida, October 3 - 6, 2004.